UPPER CRITICAL MAGNETIC FIELD OF SUPERCONDUCTING FILMS WITH MAGNETIC IMPURITIES

BY

THOMAS RICHARD LEMBERGER

B.S., University of Illinois, 1973
M.S., University of Illinois, 1975

THESIS

Submitted in partial fulfillment of the requirements
for the degree of Doctor of Philosophy in Physics
in the Graduate College of the
University of Illinois at Urbana-Champaign, 1978

Urbana, Illinois

DISCLAIMER

UPPER CRITICAL MAGNETIC FIELD OF SUPERCONDUCTING FILMS WITH MAGNETIC IMPURITIES

Thomas Richard Lemberger, Ph.D.
Department of Physics
University of Illinois at Urbana-Champaign, 1978

We have measured the upper critical magnetic field, $H_{c2}(T)$, of In-Mn and Pb-Mn alloy films. H_{c2} was determined from the resistance of the films. The results were compared with the theory of Fulde and Maki. This theory assumes that the electron-phonon coupling is weak, and that the interaction between the impurity spins and the conduction electron spins is weak. The theory predicts that the pair-breaking effect of the magnetic impurities is temperature-independent, and that the pair-breaking effects of the magnetic impurities and the applied magnetic field are additive. Furthermore, it predicts explicitly the temperature dependence of H_{c2}.

The temperature dependence of H_{c2} for the In-Mn alloy films is well described by the Fulde-Maki theory, despite the moderately strong electron-phonon coupling and the strong interaction between the impurity spins and the conduction electron spins. The temperature dependence of H_{c2} for the Pb-Mn alloy films is not well described by the Fulde-Maki theory, probably due to the strong electron-phonon coupling in Pb. However, even without a quantitatively correct theory, one can conclude from the Pb-Mn data that the pair-breaking effect of the magnetic impurities is temperature independent, and that the pair-breaking effects of the magnetic impurities and the applied magnetic field are additive.

For some of the Pb-Mn alloy films, there was a region of positive curvature in $H_{c2}(T)$ near the zero-field transition temperature. This positive curvature is not understood.

ACKNOWLEDGMENTS

The author wishes to thank his advisor, Professor Donald M. Ginsberg, for the patience, guidance, and encouragement which he provided.

He is grateful to the National Science Foundation for financial support under Grant DMR 76-80159, and to the Department of Energy for financial support under Grant EY-76-C-02-1198.

He thanks Jeffrey Willis, Brian Gibson, and John Przybysz for many useful discussions and experimental assistance.

Finally, he thanks his wife Ellen and his parents for their constant support and encouragement.

TABLE OF CONTENTS

Page

LIST OF TABLES

LIST OF FIGURES

I. INTRODUCTION

A. Overview

This experiment is part of a concerted effort in our research group to understand the effects of magnetic impurities on superconductors.[1-10] The thermal conductivities of Pb-Mn, In-Mn, and In-Cr have already been measured. Heat capacity and tunneling experiments on these materials are in progress.

The theory of magnetic impurities in superconductors explains the effects of rare earth impurities quite well because the unpaired, or magnetic, electrons are in the $4f$ shell where they are well shielded from the conduction electrons. Hence they interact only weakly with the conduction electrons. The theory does not explain all of the results of measurements on superconductors containing transition metal impurities, whose unpaired electrons are in the $3d$ shell. Figure 1 shows a comparison of the shielding of the $4f$ shell in Gd, a rare earth, with the shielding of the $3d$ shell in Mn, a transition element.

We hope that by making several different types of measurements on the same systems we can better define the extent of agreement between theory and experiment.

As will be discussed later, measurements of the upper critical magnetic field, H_{c2}, enable one to test some of the basic concepts of the theory, independent of the approximations made in order to perform the actual calculations.

Figure 1. Radial probability function for Gd and Mn. P(r) is the relative probability of finding an electron a distance r away from the nucleus in gadolinium and manganese atoms. These curves were calculated by Charlotte Froese Fischer by using a Hartree-Fock method (unpublished).

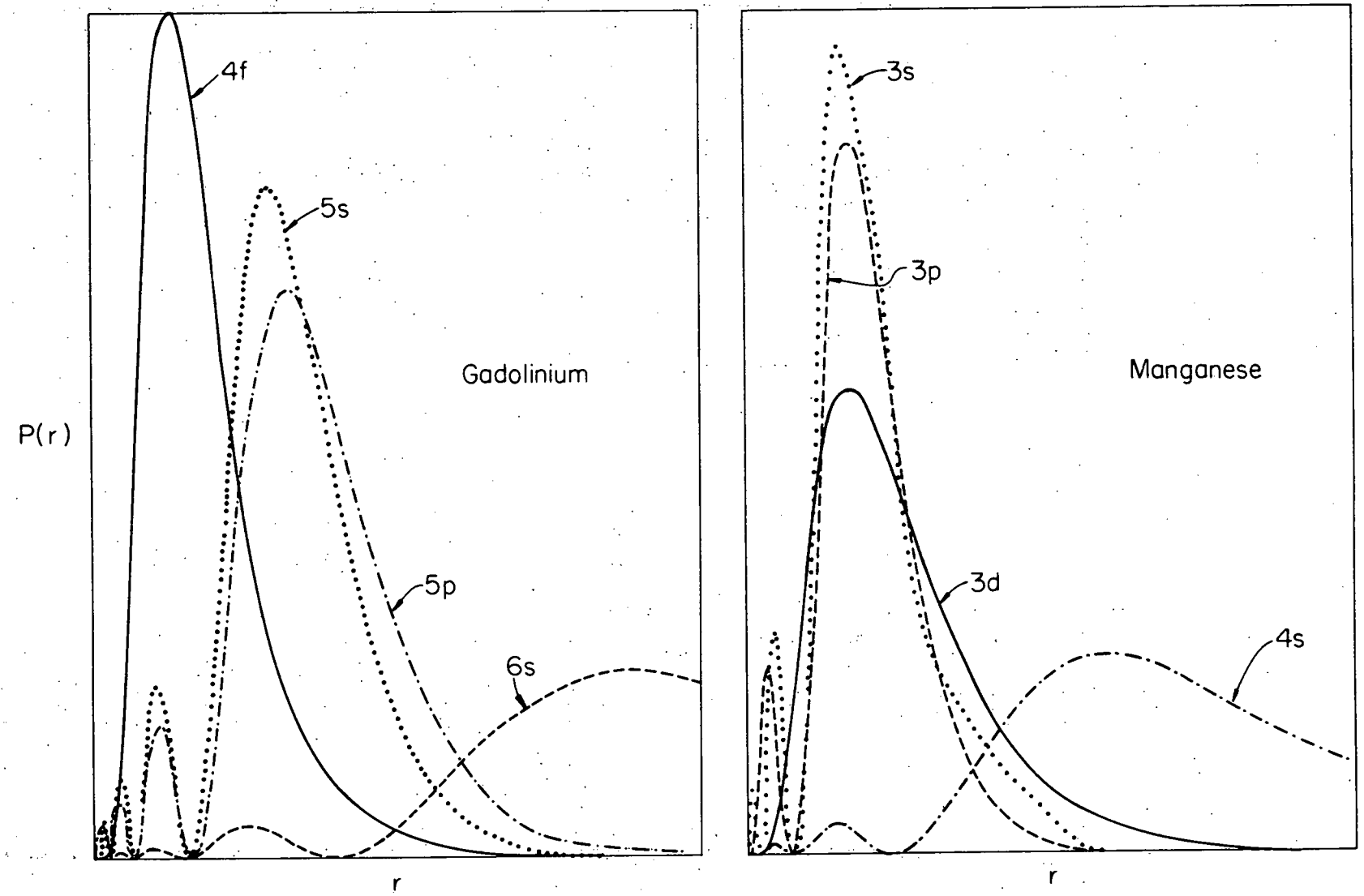
P(r)
4f
5s
5p
6s
Gadolinium
r
3s
3p
3d
4s
Manganese
r

B. Background

The study of magnetic impurities began in the 1950's when it was discovered that small concentrations of magnetic impurities depress the superconducting transition temperature of the host severely.[11,12] The fact that the strength of the depression was correlated with the spin of the impurity, and not with its magnetic moment,[12] led Herring[13] to suggest that the interaction responsible for the effect of the magnetic impurities was the exchange interaction between the impurity spins and the conduction electrons. Abrikosov and Gor'kov (AG)[14] showed how to incorporate this interaction into calculations of superconducting properties. The theory was later developed by Skalski et al,[15] Ambegaokar and Griffin,[16] and by others.[17] Experimental studies of the tunneling characteristics of Pb-Gd by Woolf and Reif,[18] and of the specific heat jump in La-Gd by Finnemore et al,[19] and other studies,[20] verified the basic correctness of the AG theory.

However, it was found that the AG theory worked well for rare earth impurities but not so well for $3d$ shell magnetic impurities. This was shown in measurements of tunneling into In-Fe and Pb-Mn alloys,[18] of far infra-red absorption in Pb-Mn alloys,[21] and of thermal conductivity of In-Mn alloys.[1] The source of the disagreement was thought to be that AG had treated the exchange interaction as a weak interaction; they used the first Born approximation.

An attempt to treat the exchange interaction to higher order was made by Shiba.[22] In fact, by assuming that the impurity spins were classical spins, he was able to treat the impurities exactly.

Calculations based on this theory agreed with the tunneling data on Pb-Mn,[23,24] but not with the tunneling data on In-Fe.[5] Other disagreement between theory and experiment was discussed by Ginsberg.[4]

Müller-Hartmann and Zittartz (M-HZ)[25] constructed a theory in which they included the quantum mechanical nature of the impurity spins. This theory was later extended by Schuh and Müller-Hartmann.[26] Their theory reduced to the AG theory in the limit of zero Kondo temperature. The agreement of the M-HZ theory with experiment has recently been reviewed by Takayanagi and Sugawara.[27]

A calculation of H_{c2} based on the AG theory was performed by Fulde and Maki (FM),[28] and a calculation of H_{c2} based on the M-HZ theory was first performed by Maki[29] and was later improved by Schuh and Müller-Hartmann.[26] These calculations showed that the Kondo effect could cause large qualitative differences in the $H_{c2}(T)$ curve from the FM prediction, if the Kondo temperature were near the superconducting transition temperature of the host.

These theories all assumed that the impurity spins were randomly oriented. However, calculations have been made of some properties of superconductors assuming some order among the impurity spins. In particular, Fischer[30] calculated the effect of paramagnetic impurity spin alignment on the upper critical magnetic field, H_{c2}. Bennemann[31] calculated some of the effects of impurity-impurity interactions. Since these impurity-impurity interactions typically become important only when the impurity concentration is high enough to reduce the transition temperature of the alloy to below half of the transition

temperature of the pure host,[9] we avoided them by keeping the impurity concentration low enough that the transition temperature of the alloyswas greater than half of the transition temperature of the pure host.

These theories are discussed in more detail in the next section. But, details aside, these theories provide at least a qualitative idea of what the temperature dependence of H_{c2} might be. These qualitative aspects should be independent of some of the approximations of the theories, e.g., weak electron-phonon coupling. Even without a quantitatively correct theory, it may be possible to distinguish the Kondo effect from impurity spin alignment, should one of them be present in the data.

C. Theory

This section describes the theories of magnetic impurities in superconductors due to Abrikosov and Gor'kov (AG) and to Shiba. It describes what these theories predicted for the temperature dependence of the upper critical magnetic field, H_{c2}, in superconductors containing magnetic impurities. These theories assumed that the impurity spins were classical, randomly oriented spins, and that the electron-phonon coupling was weak. This section also discusses what effects the quantum nature of the impurity spins, impurity spin alignment, and strong electron-phonon coupling might have on the temperature dependence of H_{c2}.

The first successful theory of magnetic impurities in superconductors was the AG theory. AG assumed that the impurities spins were

randomly distributed, randomly oriented, had an infinite lifetime, and that they interacted weakly with the conduction electrons through the exchange interation

$$H_{ex} = -2J\vec{S}\cdot\vec{s}_e \ , \tag{1}$$

where J is the exchange constant, $\vec{S}$ is the impurity spin, and $\vec{s}_e$ is the conduction electron spin. They treated this interaction in the first Born approximation. Note that the exchange interaction treats the two members of a Cooper pair differently. Hence it is called a 'pair-breaking' interaction.

They obtained an expression for the dependence of the transition temperature of a superconductor with magnetic impurities

$$\ln(T_c/T_{c0}) = \psi(\tfrac{1}{2}) - \psi(\tfrac{1}{2} + \frac{\alpha_i}{2\pi T_c}). \tag{2}$$

Here T_c is the transition temperature of the alloy, T_{c0} is the transition temperature of the pure material, ψ is the digamma function, $k_B = 1$, and α_i is the spin flip scattering rate from the magnetic impurities, given by

$$\alpha_i \equiv \frac{1}{\tau_s} = n_i \pi \, N(0) \, J^2 S(S+1) \tag{3}$$

where n_i is the concentration of the magnetic impurities, and N(0) is the density of electronic states at the Fermi energy for one spin direction. α_i is commonly referred to as a 'pair-breaking' parameter.

Shiba extended this theory by making all of the assumptions of the AG theory plus assuming that the impurity spins were classical and not quantum mechanical. He was then able to treat the exchange interaction exactly. This theory necessarily reduced to the AG theory in the limit of weak exchange coupling. In Shiba's theory, the dependence of T_c on the magnetic impurity concentration was

$$\ln(T_c/T_{c0}) = \psi(\tfrac{1}{2}) - \psi(\tfrac{1}{2} + \frac{\alpha_i}{2\pi T_c}) \ , \tag{4}$$

where α_i is given by

$$\alpha_i = \frac{n_i}{\pi N(0)}(1 - \varepsilon_0^2) \ . \tag{5}$$

ε_0 could be expressed in terms of other constants in the theory as

$$\varepsilon_0 = \left| \frac{1 - [\frac{1}{2}\pi JSN(0)]^2}{1 + [\frac{1}{2}\pi JSN(0)]^2} \right| \ . \tag{6}$$

From Equation (6), it is clear that

$$0 \leq \varepsilon_0 \leq 1 \ ; \tag{7}$$

when ε_0 approached 1, the Shiba theory reduced to the AG theory. A comparison of Equations (2) and (4) shows that the functional dependence of T_c on n_i was the same in the AG and Shiba theories.

According to the AG and Shiba theories, there was a concentration of magnetic impurities which was sufficient to destroy superconductivity

in the alloy at all temperatures. This concentration was called the critical concentration, n_{cr}.

But what do these theories predict about H_{c2}?

First, let's look at the effect of a magnetic field on a superconductor without magnetic impurities. The magnetic field interacts with the conduction electrons through the following terms in the Hamiltonian:

$$H_{int} = \frac{-e}{mc} \vec{p} \cdot \vec{A} \tag{8}$$

and

$$H_{int} = -g\vec{\mu}_B \cdot \vec{H} \quad . \tag{9}$$

Both of these interactions, like the exchange interaction, are pair-breaking interactions because they treat the two members of a Cooper pair differently. The second of these interactions will be discussed later.

Maki[32] calculated the effect which the first of these interactions would have on the superconducting state. He showed that in a dirty, bulk, type II superconductor

$$\ln(T/T_{c0}) = \psi(\tfrac{1}{2}) - \psi(\tfrac{1}{2} + \frac{\alpha_H(T)}{2\pi T_c}) \tag{10}$$

where

$$\alpha_H(T) = \frac{DeH_{c2}(T)}{c} \quad . \tag{11}$$

Here D is the diffusion constant, given by

$$D = \frac{1}{3} v_f \ell, \tag{12}$$

v_f is the Fermi velocity, and ℓ is the electron mean free path. Dirty, bulk, type II superconductors have the properties:

$$\ell << \xi_0 \quad , \tag{13}$$

$$d >> \sqrt{\ell \xi_0} \quad , \tag{14}$$

$$\kappa \geq \frac{1}{\sqrt{2}} \tag{15}$$

where d is the thickness of the sample, ξ_0 is the ideal coherence length, and κ is the Ginzburg-Landau parameter. Equation (10) has the same form as Equation (2), but with a different pair-breaking parameter corresponding to a different pair-breaking interaction.

Fulde and Maki (FM) then showed in the AG theory that in dirty, bulk, type II superconductors containing magnetic impurities, the pair-breaking effects of the field and of the impurities were additive, i.e.,

$$\ln(T/T_{c0}) = \psi(\tfrac{1}{2}) - \psi(\tfrac{1}{2} + \frac{\alpha(T)}{2\pi T}) \tag{16}$$

where

$$\alpha(T) = \alpha_i + \alpha_H(T) \quad . \tag{17}$$

A calculation of H_{c2} in the Shiba theory has not yet been done. Presumably such a calculation would also show the property of additive pair-breaking since the result would have to reduce to Equation (16) in the limits both of weak exchange coupling and of zero impurity concentration. If so, the temperature dependence of H_{c2} in the Shiba theory should be the same as calculated by FM in the AG theory.

This concept of additive pair-breaking with a temperature-independent pair-breaking parameter, α_i, is exactly what measurements of H_{c2} can test. These tests can be made independently of some of the approximations made in the explicit calculations, as we will explain. The Kondo effect, which arises from the quantum mechanical nature of the impurity spins, or impurity spin alignment, may cause deviations from this simple result.

In principle, Equation (16) can be inverted to give $\alpha(T)$. We can then write

$$\alpha(T) = f(T) \ , \tag{18}$$

where $f(T)$ is some function. Using Equation (17), $H_{c2}(T)$ can be found:

$$H_{c2}(T) = \frac{c\ f(T)}{De} - \frac{c}{De}\ \alpha_i . \tag{19}$$

Equation (19) indicates that if one measured the upper critical magnetic field of a pure superconductor which had a diffusion constant D^p, one would expect to find

$$H^p_{c2}(T) = \frac{c\ f(T)}{D^p e} \ . \tag{20}$$

If one then measured the upper critical magnetic field of the same superconductor but with magnetic impurities and with diffusion constant D, one would expect to find

$$H_{c2}(T) = \frac{D^p}{D}\ H^p_{c2}(T) - \frac{c}{De}\ \alpha_i \ . \tag{21}$$

Equation (20) has been used to obtain Equation (21). Equation (21) is the central equation in the analysis of our $H_{c2}(T)$ data.

Figure 2 illustrates what the FM theory predicted for the temperature dependence of $H_{c2}(T)$. Because α_i was independent of temperature in this theory, it affected the $H_{c2}(T)$ curves as if it were a constant background magnetic field, whose magnitude was proportional to the concentration of magnetic impurities.

How would the Kondo effect and impurity spin alignment affect the temperature dependence of H_{c2}?

Schuh and Müller-Hartmann[26] calculated H_{c2}, including the Kondo effect. Their theory was based on an earlier theory by Maki.[32] They found that the pair-breaking parameter which represented the magnetic impurities was temperature and energy dependent. This theory reduced to the FM theory in the limit of zero Kondo temperature. A representative curve of $H_{c2}(T)$ from this theory is presented in Figure 3.

The impurity spins may be aligned. This can occur either through impurity-impurity interactions or alignment of the impurity spins in the applied magnetic field. These aligned spins would produce a net exchange field on the conduction electron spins. This interaction, acting through the difference in Pauli paramagnetic susceptibility of the conduction electrons in the normal and superconducting states, would lower the free energy of the normal state relative to the superconducting state. This would lower the value of H_{c2}. However, the applied magnetic field, interacting with the conduction electron spins as indicated in Equation (9), would have the same effect on the free energy

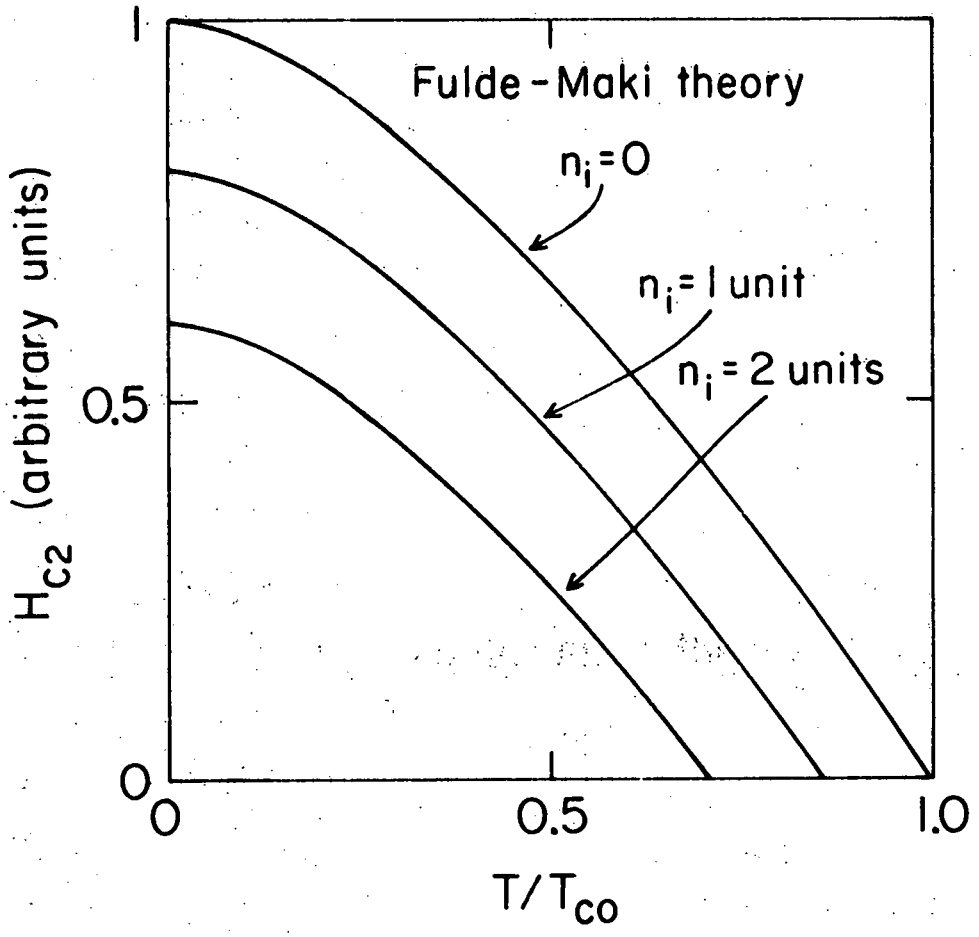

Figure 2. Plot of $H_{c2}(T)$ calculated by using the Fulde-Maki theory. Curves are shown for three values of the magnetic impurity concentration.

difference between the normal and superconducting states. The effects from the net exchange field and the external field could either add or subtract from each other. This was discussed in detail by Fischer and Peter.[30] The result was that these interactions could be represented by another pair-breaking parameter

$$\alpha_p = \frac{(g\mu_B)^2 \tau'_{so}}{2\hbar} (H_{c2} + H_s)^2 , \tag{22}$$

where

$$H_s = n_i J\langle S_z \rangle / g\mu_B \tag{23}$$

was the exchange field due to the aligned magnetic impurities, and

$$\frac{1}{\tau'_{so}} = \frac{1}{\tau_{so}} - \frac{3}{2\tau_s} \left[\frac{S(S+1) - \langle S_z^2 \rangle}{S(S+1)} \right] \tag{24}$$

was a generalized spin-orbit scattering rate. The spin-orbit scattering rate came into this because it affected the Pauli paramagnetic susceptibility of the electrons in the superconducting state. Equation (22) was expected to be valid when the mean free path between spin-orbit scatterings, ℓ_{so}, was much less than the coherence length in the pure superconductor, ξ_0.

Figure 3 illustrates what these effects could do to the temperature dependence of H_{c2}. All of the curves are normalized to have the same slope at T_c. Curve a shows $H_{c2}(T)$ for a superconductor with magnetic impurities, calculated by using the FM theory. Curve b shows $H_{c2}(T)$ for an alloy in which the Kondo temperature is about one tenth of the

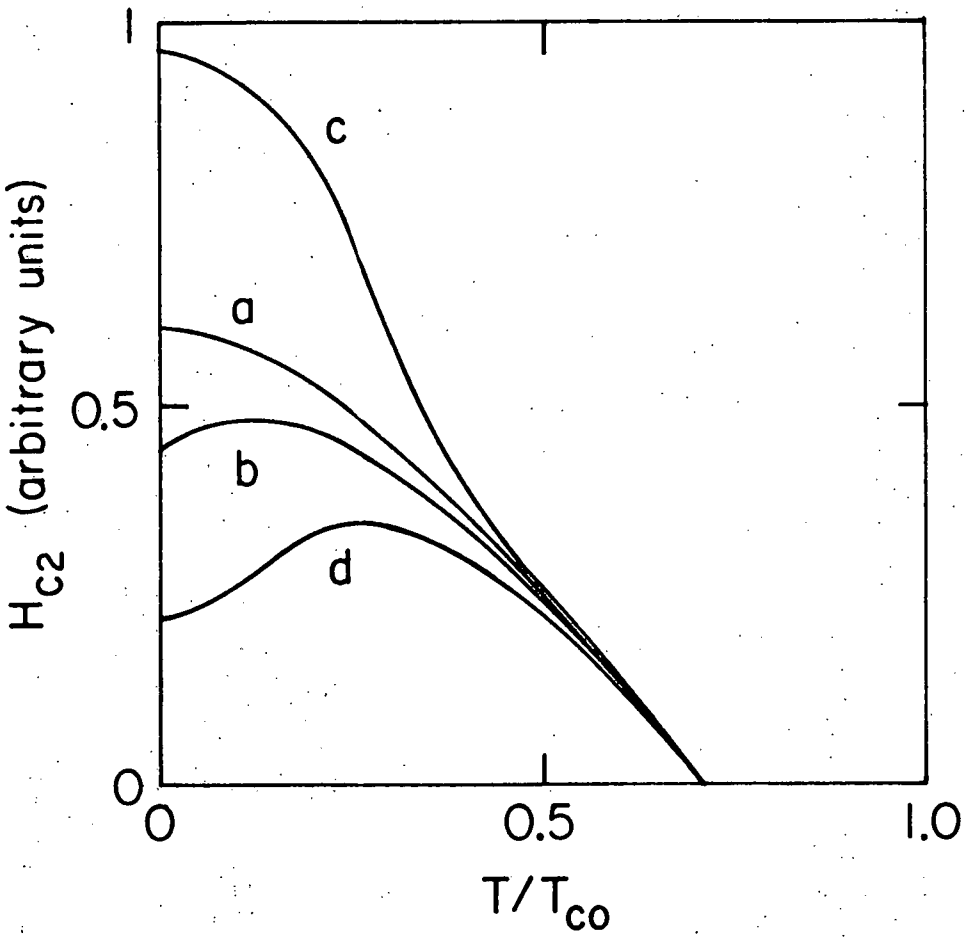

Figure 3. Plot of $H_{c2}(T)$ showing possible deviations from the Fulde-Maki theory. The curves are explained in the text.

transition temperature of the pure superconductor. Curves c and d show the effects of impurity spins aligning with the external field; in c the exchange field adds to the applied field; in d it subtracts from the applied field.

All of the theories discussed so far assumed that the electron-phonon coupling was weak. Rainer et al[33] have shown that strong electron-phonon coupling could change the shape of $H_{c2}(T)$. However, this should only affect H^{p}_{c2} (see Equation (21)), so that the concept of additive pair-breaking may still be valid, and we can test this.

D. Previous Work

Measurements of $H_{c2}(T)$ on superconductors containing rare earth impurities showed that additive pair-breaking applies to these systems. This work was well reviewed in references 20 and 34. A study of $H_{c2}(T)$ in the Mo-Re-Fe system was made by Barth et al.[35] Their data were consistent with the FM theory of additive pair-breaking. However, their data were sparse, and the scatter in their data was large enough that they were only able to test the gross features of the theory. The scatter in our data is less than 1/10 of the scatter in theirs, and we took twice as many data points on each sample.

Previous measurements of $H_{c2}(T)$ on quench-condensed films of pure indium[36] and pure lead[37] have been made. Our data are consistent with these, as will be discussed later.

E. Purpose of This Experiment

The purpose of this experiment was to see whether the destructive effects of magnetic impurities and applied magnetic fields on the

superconducting state were additive, with a temperature independent pair-breaking parameter describing the effect of the magnetic impurities, as one would expect from the FM theory. We hoped to be able to identify the cause of any deviation from the FM theory from a knowledge of the qualitative effects of interactions which were ignored in the theory.

For these purposes, very precise measurements of $H_{c2}(T)$ were needed. To narrow the width of the field region in which the transitions occurred, we scribed the edges of our samples away from the middle. This technique of eliminating edge effects, unlike the technique of coating the entire film with a layer of a paramagnetic metal like Fe,[37] does not affect the properties of the middle of the film. Unfortunately, to do this scribing, we had to use an electrode geometry which did not allow a precise measurement of the sample resistivity. Because the resistivity of the gold electrodes was about the same as the resistivity of the sample films, and because there may have been some contact resistance between the electrodes and the sample, the current flow pattern in the samples was very uncertain. Therefore, we could not determine the diffusion constant experimentally, and quantitative comparison of our $H_{c2}(T)$ data with the theoretical values could not be made.

Indium and lead were chosen as the host superconductors because they had transition temperatures which were easily accessible in a pumped liquid He^4 cryostat, because they had low evaporation temperatures,[38] and because they had smoothly varying densities of states which should not have been affected much by either quench-condensing or alloying with small amounts of manganese.

Manganese was chosen as the impurity because data on In-Mn and Pb-Mn alloys indicated that Mn supported a localized moment in these quench-condensed materials, because Mn was known to have a strong effect on the value of T_c for In[39] and Pb,[40] and because it had a low evaporation temperature.[38]

Because of the low solubility of manganese in both indium and lead, the sample films had to be quench-condensed at liquid helium temperatures, or else the manganese would precipitate out. Furthermore, the samples had to be kept cold while they were rotated and scribed, and while data were taken. The samples could not be warmed until after all of the data were taken.

II. BRIEF DESCRIPTION OF A TYPICAL RUN

This section is a general description of the procedures and equipment used during a typical run. A detailed description is presented in Appendix A.

At the beginning of each run, a quartz substrate was carefully cleaned, and gold electrodes were evaporated onto it. Then the substrate was clamped to the substrate holder. A couple of things were done before the substrate holder could be attached to the cryostat. The wires used later to make four-terminal measurements of the sample resistance were silver-painted to the gold electrodes. A mechanism used to scribe the edges of the sample away from the middle was screwed into place where it straddled the substrate. The prepared substrate holder was then attached to the substrate holder support which was already screwed to the inner liquid helium (LHe) reservoir.

The substrate was oriented parallel to the floor, and the LHe and liquid nitrogen (LN) temperature heat shields were put into place around the inner LHe reservoir and the substrate holder. Then the outer vacuum jacket and the evaporator housing were attached to the cryostat. Pellets of the desired alloy concentration (see Appendix G) were loaded onto a conveyor belt, and the conveyor belt was inserted through the wall of the evaporator housing.

At this point, the cryostat was ready to be leak tested. After any leaks were sealed, the cryostat was cooled down.

Two hours or more after the LHe was put into the inner LHe reservoir, a sample film was made. The sample was made by dropping the alloy

pellets off the conveyor belt, through a chute, and into a hot tungsten boat. Each pellet evaporated in a few seconds. Some of the evaporated metal passed through holes in the heat shields and condensed on the substrate, overlapping the gold electrodes. When preparation of the film was finished, the substrate holder was rotated 90° so that the sample film was perpendicular to the floor and parallel to the magnet's pole faces. Then the two edges of the sample which did not overlap the gold electrodes were mechanically scribed away from the central portion of the sample. Scribing the sample dramatically reduced the width of the superconducting transition, as is discussed in Appendix D. Finally, shutters were closed over the holes in the heat shields. The cryostat was allowed to thermally equilibrate for 20 minutes or more before any measurements were made because experience showed that measurements which were taken during this time were always irreproducible.

The first measurement made on every sample was the resistive transition in zero magnetic field. If the transition width was small enough, the experiment went on. A Hall probe, attached to the back of the substrate holder, was calibrated against a rotating coil gaussmeter. Then the resistance of the film as a function of field strength was measured at several temperatures. The value of the upper critical magnetic field at a given temperature was inferred from these resistance versus field curves, as we describe in Appendix D.

The sample temperature was coarsely obtained and regulated by pumping on the inner LHe reservoir through a manostat. The temperature was finely regulated by an electronic feedback circuit which used a

carbon resistor sensing element attached to one arm of the substrate holder assembly. The temperature measurement and regulation procedures are described in detail in Appendix A.

The magnetic field was generated by an electromagnet with four-inch diameter pole faces and a four-inch gap spacing. Fields from 0 to 4 kG could be obtained. The field was measured, as mentioned above, with a Hall probe. A detailed description of the magnet and the Hall probe circuit are in Appendix A.

When the desired number of resistance-versus-field curves had been taken, the Hall probe calibration was checked, and the position of the resistive transition in zero field was remeasured. Then the cryostat was allowed to warm up to room temperature slowly over the next day or two.

When the cryostat reached room temperature, the substrate was removed. A thin (~1000Å) layer of silver was evaporated onto the sample so that the sample thickness could be measured by using an interferometric method due to Tolansky.[41]

Finally, the tungsten boat was inspected for signs of wear, and the metal which had condensed onto the heat shields, the sample scribing assembly, the conveyor belt, and the chute, was cleaned off. Cleaning was usually a combination of wiping with a Kimwipe soaked with acetone and scraping with a metal tweezers or the wooden end of a Q-tip.

III. RESULTS AND DISCUSSION

A. In-Mn

Characteristics of the four In-Mn samples on which critical field measurements were made are listed in Table I. Many other samples were made on which no critical field data were taken, either because of some mechanical failure in the cryostat or because the width of the resistive transition in zero field was judged to be too large. These will not be discussed.

A discussion of the shapes of the resistive transition curves is given in Appendix D. Three points on the transition curves were chosen as the critical point so there were three different sets of data for each sample. It turns out that the main conclusions of the experiment are the same for all three data sets. Figures 23-26 show which data set corresponds to which point on the resistive transition curves.

The critical field data and a fit to the theory of Fulde and Maki are shown in Figures 4, 5, 6, and 7. As described in Appendix E, the zero-temperature value of the critical field, $H_{c2}(0)$, and the transition temperatures of the alloy and of the pure material were used as fitting parameters. Tables of the measured and calculated values of $H_{c2}(T)$ are presented in Appendix E. The error bars on the data points would be about the size of the data points (see Appendix F).

We can use the chemically measured manganese concentration, the measured transition temperature, and the value of T_{c0} obtained as is described in Appendix E, together with the AG prediction for the dependence of T_c/T_{c0} on impurity concentration, to obtain a value for

Table I. In-Mn sample film characteristics. d is the film thickness, ΔT_c is the 10 % - 90 % transition width, and I is the measuring current in the film.

Sample	a/o Mn ± 5 %	d (Å) ± 2 %	T_c (K)	ΔT_c (mK)	I (μA)
5	0	1880	4.069	3	50
7	0	1410	4.172	4	50
13	0.030	1930	2.745	10	100
19	0.039	2546	2.222	38	93

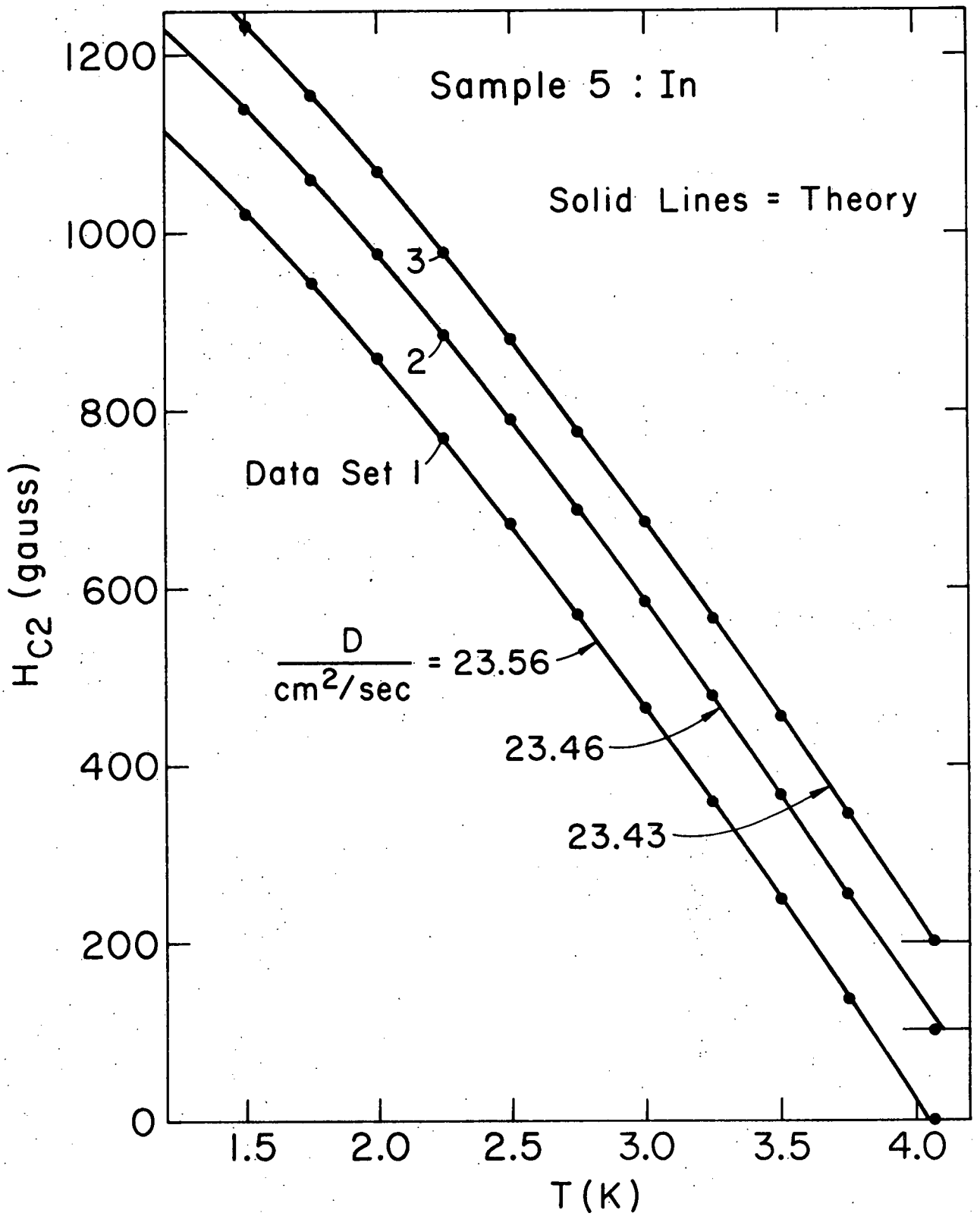

Figure 4. Plot of the experimental values of $H_{c2}(T)$ for In-Mn sample 5. Data sets 2 and 3 are displaced upward by 100 and 200 gauss respectively for clarity. The solid curve was calculated by using the Fulde-Maki theory.

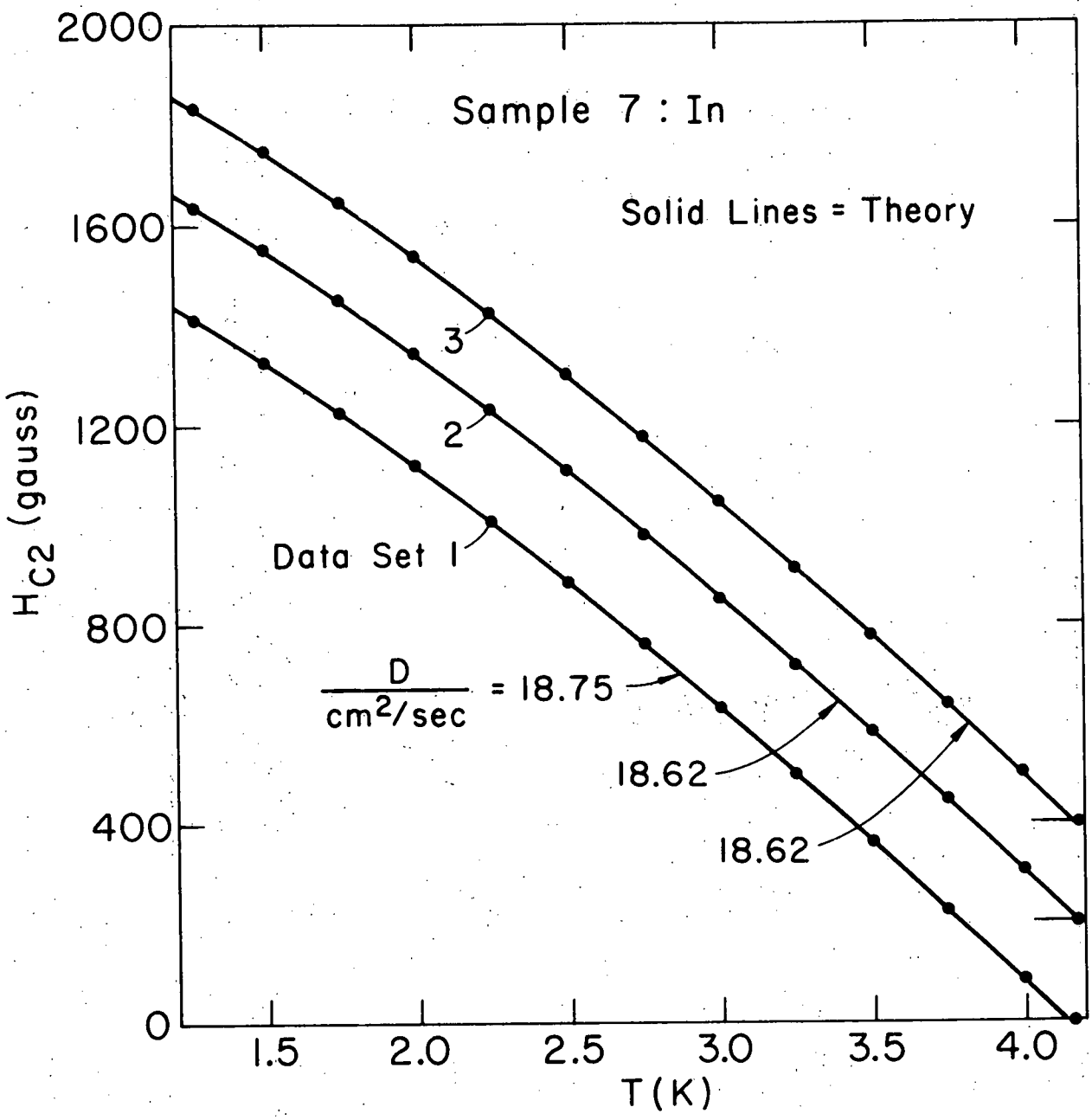

Figure 5. Plot of the experimental values of $H_{c2}(T)$ for In-Mn sample 7. Data sets 2 and 3 are displaced upward by 200 and 400 gauss respectively for clarity. The solid curve was calculated by using the Fulde-Maki theory.

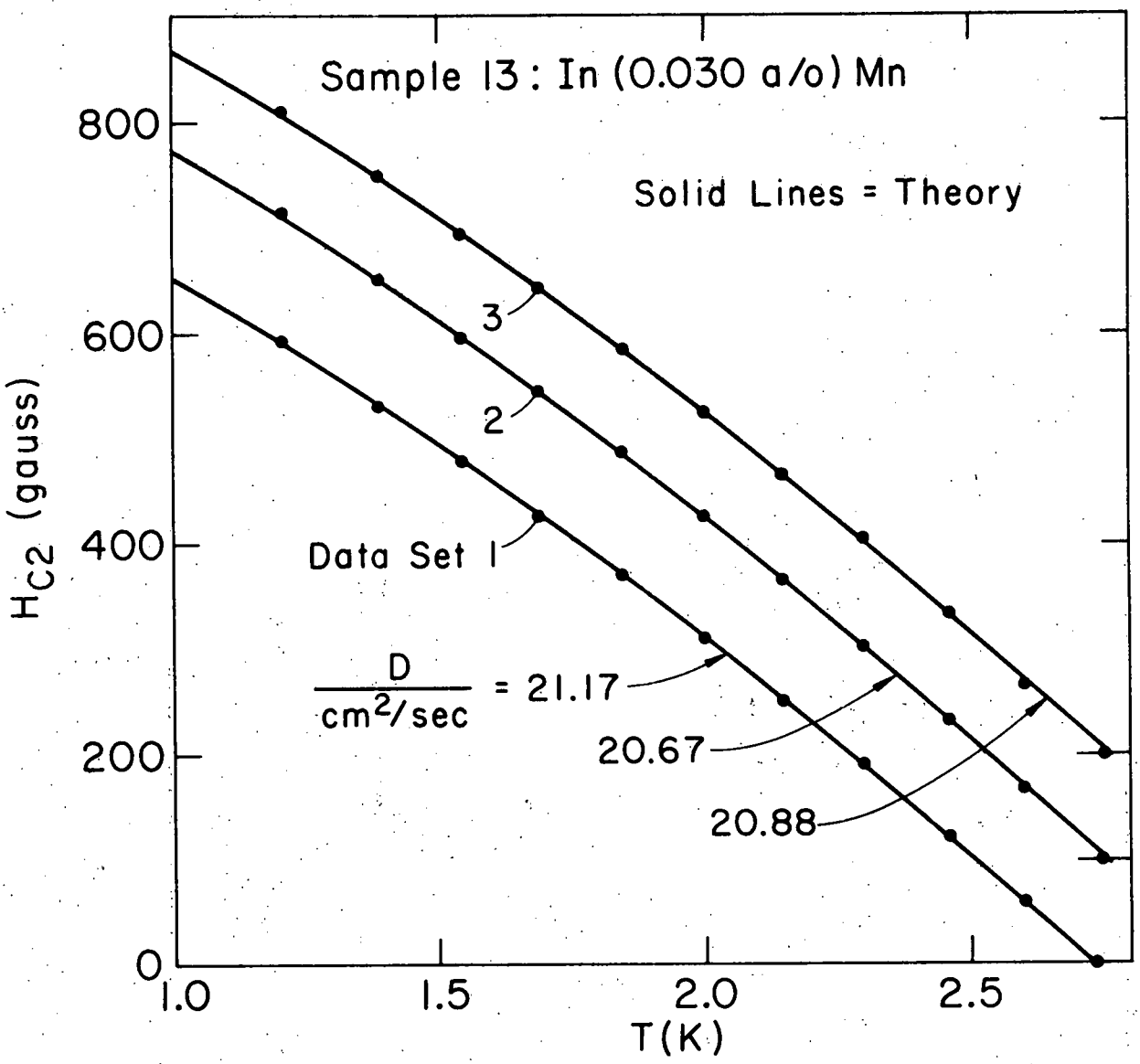

Figure 6. Plot of the experimental values of $H_{c2}(T)$ for In-Mn sample 13. Data sets 2 and 3 are displaced upward by 100 and 200 gauss respectively for clarity. The solid curve was calculated by using the Fulde-Maki theory.

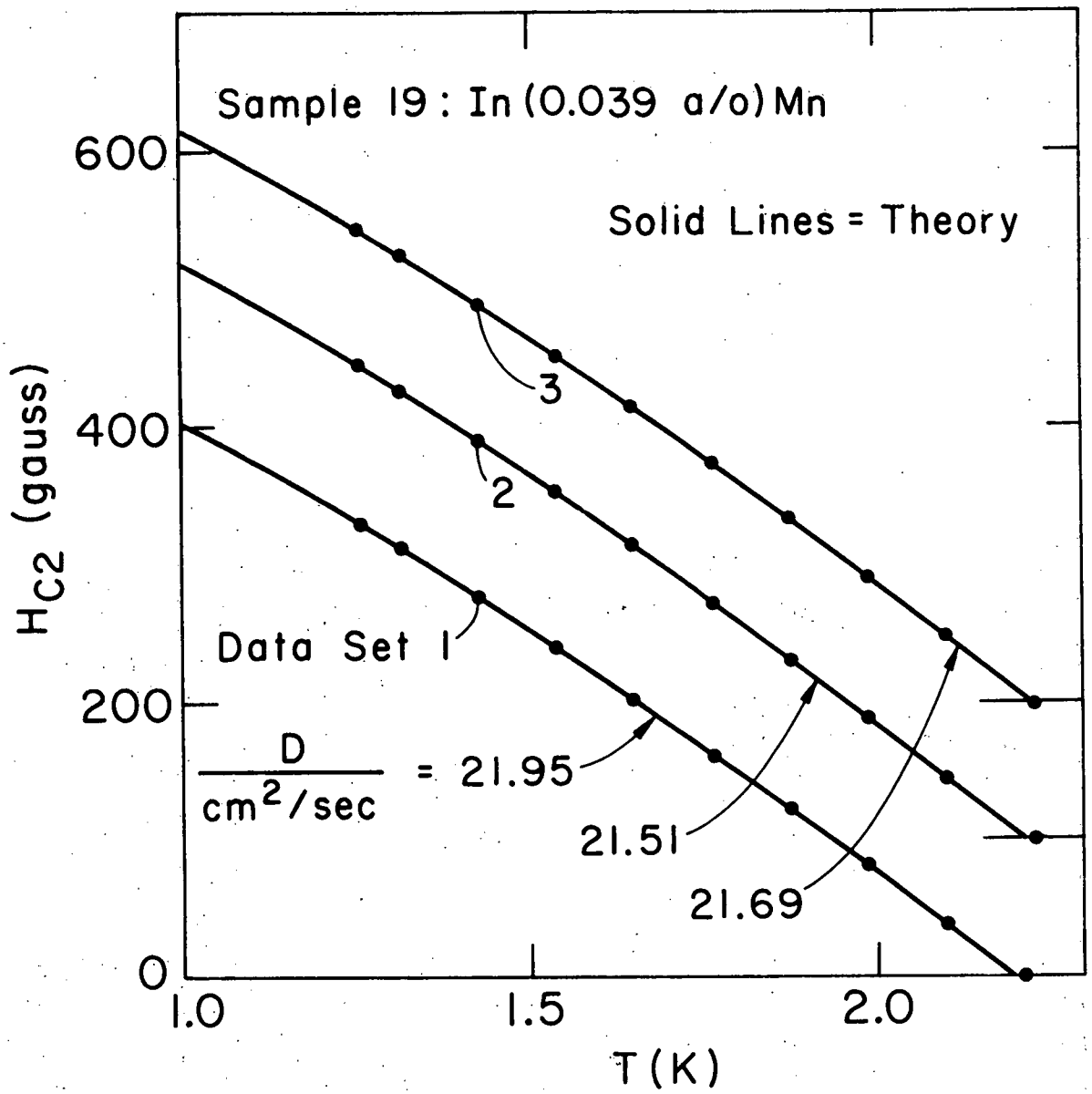

Figure 7. Plot of the experimental values of $H_{c2}(T)$ for In-Mn sample 19. Data sets 2 and 3 are displaced upward by 100 and 200 gauss respectively for clarity. The solid curve was calculated by using the Fulde-Maki theory.

n_{cr}, the critical concentration of impurities, for samples 13 and 19. Both of these samples indicate that $n_{cr} = 0.066 \pm 0.003$ a/o, which value compares well with the values 0.066 a/o from Opitz[39] and 0.070 a/o from Bjerkaas et al.[1]

Because of the peculiar electrode geometry which we had to use, we were only able to determine the resistivities of our samples to ±40 %. This estimate was based on models of our samples made with Teledeltos[42] conducting paper. To within this 40 % uncertainty, all four of the samples on which H_{c2} data was taken had the same resistivity, 10 μΩ-cm. Bergmann[36] measured the resistivity of quench condensed indium films and found a resistivity of 5 μΩ-cm.

Using the Goodman approximation[43] to the Gor'kov[44] relation between the resistivity and κ,

$$\kappa = \kappa_0 + 7.53 \times 10^3 \rho \gamma^{1/2} , \qquad (25)$$

where ρ is the resistivity in Ω-cm, and γ is the electronic heat capacity in erg/cm^{3}K^2, we can verify that the samples were type II materials. Substituting $\rho = 10^{-5}$ Ω-cm, and[45] $\gamma = 1.06 \times 10^3$ erg/cm^{3}K^2, and[46] $\kappa_0 = 0.062$, we find $\kappa = 2.5$. Since $\kappa > \sqrt{1/2}$, the samples were type II materials.

The electron mean free path in the sample films can be determined both from the resistivity and from the value of D found by fitting the data with the theoretical curves. Using a value of[47] 1110 μΩ-cm^2 for $\rho\ell$ and following Bergmann,[36] a value for v_f of 0.97×10^8 cm/s, the mean free path is either

$$\ell = \frac{3D}{v_f} \approx 65 \text{ Å} \tag{26}$$

or

$$\ell = \frac{\rho\ell}{\rho} \approx 111 \text{ Å} \tag{27}$$

Because of the large uncertainties in both ρ and $\rho\ell$, this agreement is good. Anderson and Ginsberg[48] have discussed the experimental values of $\rho\ell$ for indium.

The ideal coherence length, ξ_0, can be estimated with the formula[49]

$$\xi_0 = \frac{\hbar v_f}{\pi\Delta} \approx \frac{\hbar v_f}{\pi x 1.76\ k_B T_{c0}} \approx 3400 \text{ Å} \tag{28}$$

We can now check to see if the samples were indeed dirty, bulk films, using relations (13) and (14). We find

$$\ell/\xi_0 \approx 1/40 \quad , \tag{29}$$

$$d/\sqrt{\xi_0 \ell} \approx 4 \quad . \tag{30}$$

Therefore, the samples were dirty, reasonably bulk, films.

The temperature dependence of H_{c2} agrees with the form calculated by Fulde and Maki for weak electron-phonon coupling superconductors. This is somewhat surprising since quench-condensed indium is known to be a moderately strong-coupling superconductor.[50]

Bergmann[36] found that $(dH_{c2}/dT)\big|_{T_{c0}}$ for his quench-condensed indium films was about 240 gauss/K. In our indium films, we find $(dH_{c2}/dT)\big|_{T_{c0}}$ is about 400 gauss/K. Since our films had about twice the resistivity of Bergmann's, and $(dH_{c2}/dT)\big|_{T_{c0}}$ is proportional to the resistivity, this is good agreement.

There is no evidence from our results for either ferromagnetic alignment of the impurity spins, or of alignment of the spins with the applied field. There is also no indication of the Kondo effect.

B. Pb-Mn

Table II lists characteristics of the six Pb-Mn samples on which H_{c2} data were taken. Two other samples were made on which no H_{c2} data were taken because of mechanical failure. These will not be discussed.

A discussion of the shapes of the resistive transition curves is presented in Appendix D. Three points on the transition curves were chosen as the critical point, so there were three different sets of data for each sample. It turns out that the main results of the experiment are the same for all three data sets. Figure 8 shows which data set corresponds to which point on the transition curves.

Figure 9 shows the measured values of T_c/T_{c0} plotted versus n_i/n_{cr}, with n_{cr} = 0.310 a/o, and compared to the AG prediction. The good agreement between the data and the theory indicates that there were probably no impurity-impurity interactions in the samples.[31] The value for n_{cr} of 0.310 a/o does not agree well with Barth's[40] value of 0.236 a/o.

To within the 40 % uncertainty discussed earlier, the resistivities of all of our Pb-Mn samples were 22 μΩ-cm. Using Equation (25), and a value for γ of[51] 1640 erg/cm^{3}K^2, and a value for κ_0 of[37] 0.38, we find κ = 7.1 . Using the constancy of the product $\rho\ell$, and an average value for $\rho\ell$ of 1.4×10^{-5} μΩ-cm^2 (see Koepke and Bergmann[37] for a discussion of experimental values of $\rho\ell$), we estimate that the electron mean free path is $\ell \approx 64$ Å.

Table II. Pb-Mn sample film characteristics. d is the film thickness, ΔT_c is the 10 % - 90 % transition width, and I is the measuring current in the sample.

Sample	a/o Mn ± 5 %	d (Å) ± 2 %	T_c (K)	ΔT_c (mK)	I (μA)
C	0	1650	7.206	3	56
H	0	1815	7.205	2	56
D	0.057	1800	6.339	3	38
E	0.128	1500	4.804	6	38
F	0.160	1470	4.494	6	38
G	0.200	1210	3.711	5	56

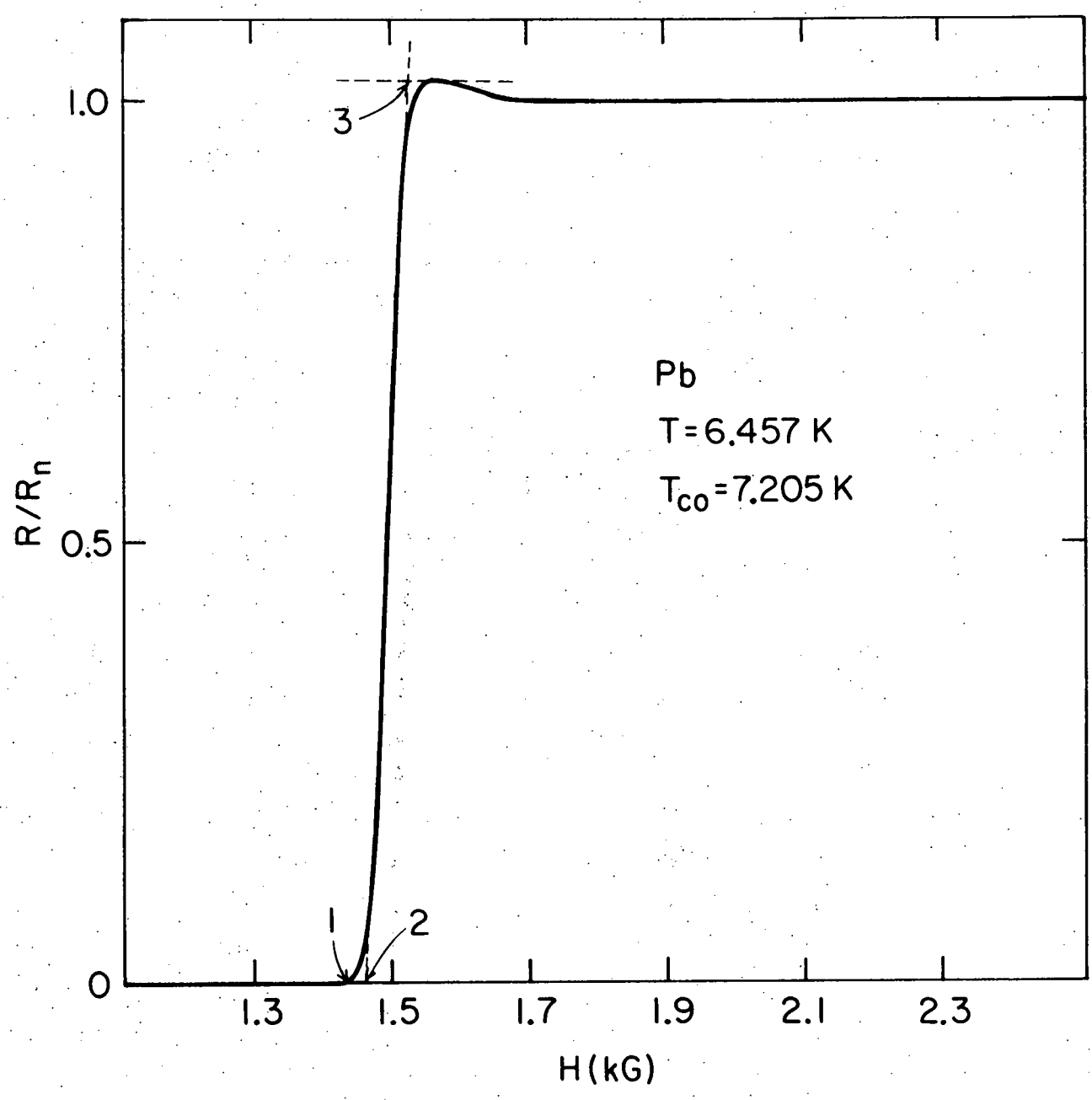

Figure 8. Resistive transition of a pure lead film, sample C, in a magnetic field. The graph shows which point on the transition corresponds to which data set.

Figure 9. Plot of T_c/T_{c0} vs. n_i/n_{cr} for the Pb-Mn samples. The critical concentration, n_{cr}, was chosen to provide a reasonable fit to the theoretical curve of Abrikosov and Gor'kov.

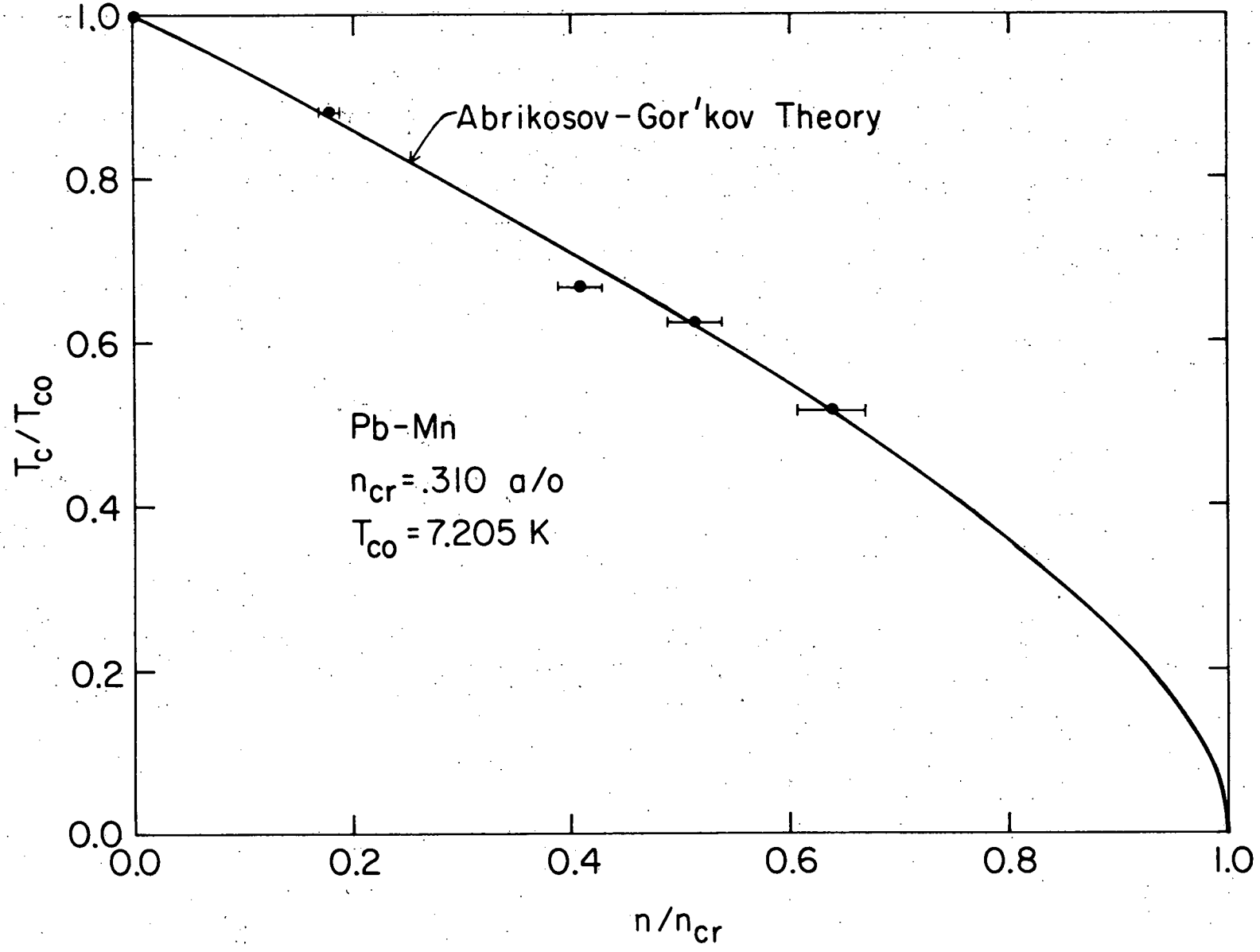
Abrikosov-Gor'kov Theory
Pb-Mn
n_{cr} = .310 a/o
T_{co} = 7.205 K
T_c/T_{co}
n/n_{cr}
0.0
0.2
0.4
0.6
0.8
1.0

The ideal coherence length, ξ_0, calculated using Equation (28), is about 960 Å.

From these numbers, we find that

$$\ell/\xi_0 \approx 1/15 \quad , \tag{31}$$

$$d/\sqrt{\xi_0 \ell} \approx 6 \quad . \tag{32}$$

Therefore the samples were dirty, reasonably bulk, type II materials.

The temperature dependence of H_{c2} for the Pb-Mn samples is qualitatively different from the prediction of Fulde and Maki (see Figure 10). This is probably due in part to the strong electron-phonon coupling present in lead. A calculation of $H_{c2}(T)$ incorporating the strong electronic-phonon coupling was done by Rainer and Bergmann[52] using values of α^2F from Knorr and Barth.[53] They concluded that the α^2F data were not good enough to use to obtain reliable values for $H_{c2}(T)$ because they did not give an accurate value for the zero-field transition temperature. This same calculation, done on other materials, e.g., $Pb_{0.75}Cu_{0.25}$,[54] accurately reproduced the zero-field transition temperature.

In order to apply the theory to our data, we differentiated Equation (21) to obtain

$$\frac{dH_{c2}}{dT} = \frac{D^P}{D} \frac{dH^P_{c2}}{dT} - \frac{c}{De} \frac{d\alpha_i}{dT} \tag{33}$$

If the pair-breaking effect of the magnetic impurities is temperature independent, then $d\alpha_i/dT = 0$. In this form, the theory could easily be compared to the data.

Figure 10. Plot of the experimental values of $H_{c2}(T)$ for the Pb-Mn samples, data set 3.

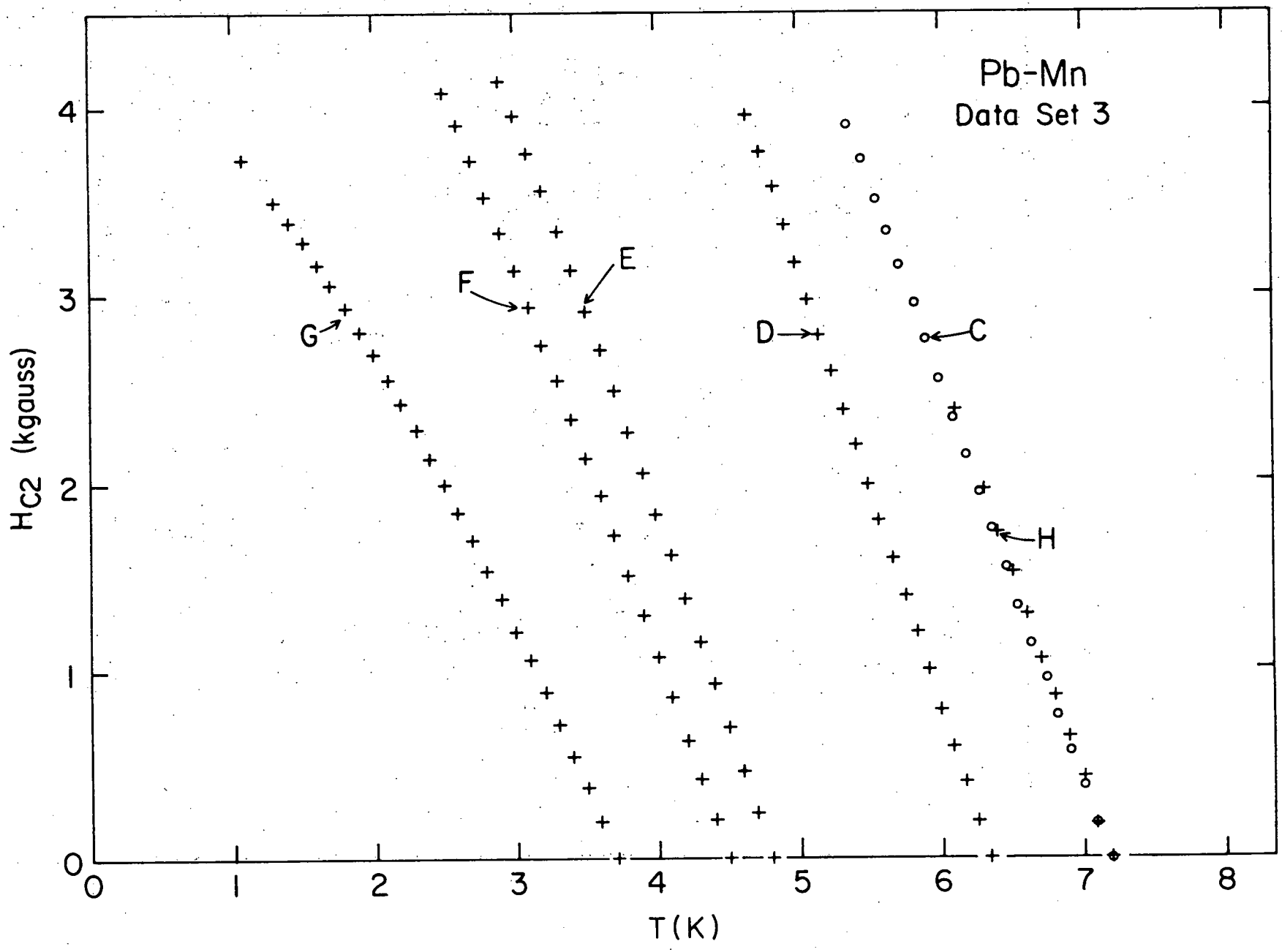
Pb-Mn
Data Set 3
H_{C2} (kgauss)
T(K)
0
1
2
3
4
5
6
7
8
E
F
G
D
C
H

To obtain dH_{c2}/dT from the data, we first fitted the data with polynomials (see Appendix E), and then differentiated the polynomials. Since D could only be determined reliably to ± 40 % experimentally, it was used as a fitting parameter. From Equation (35), one expects that $D \cdot dH_{c2}/dT$ as calculated from each sample would all fall on a smooth curve. Figure 11 shows that one can choose values of D for each sample and data set so that this happens. The actual values of D which were used to obtain Figure 11 are given in Table VII.

Note that if the pair-breaking effect of the magnetic impurities is temperature dependent, with this method of analysis, the discontinuity in the derivative of H_{c2} which would occur when the impurity concentration was changed would not be seen. This is because D has been chosen to connect the derivatives from different samples smoothly. However, there would still be a discontinuous change in the second derivative.

There is no evidence for either spin ordering or the Kondo effect. A glance at Figure 3 shows what features would be expected in the dH_{c2}/dT curves if these effects were present.

There is, however, a bump in dH_{c2}/dT which is evident in Figure 11 for the pure lead data (samples C and H), the Pb-Mn sample D data, and to a lesser extent for the Pb-Mn sample F data. This bump corresponds to a region of positive curvature in the $H_{c2}(T)$ data. This positive curvature is also evident in the data of Koepke and Bergmann.[37]

The uncertainty in the shape of the dH_{c2}/dT curves is about ± 1 % for data sets 2 and 3, and it is about ± 2 % for data set 1. The uncertainties in the data are discussed in Appendix F.

Figure 11. Plot of the experimental values of $D \cdot dH_{c2}/dT$ vs. T/T_{c0} for the Pb-Mn samples. dH_{c2}/dT was calculated from the data by fitting the data with a polynomial and then differentiating the polynomial. D was a fitting parameter chosen to give the smoothest composite curves.

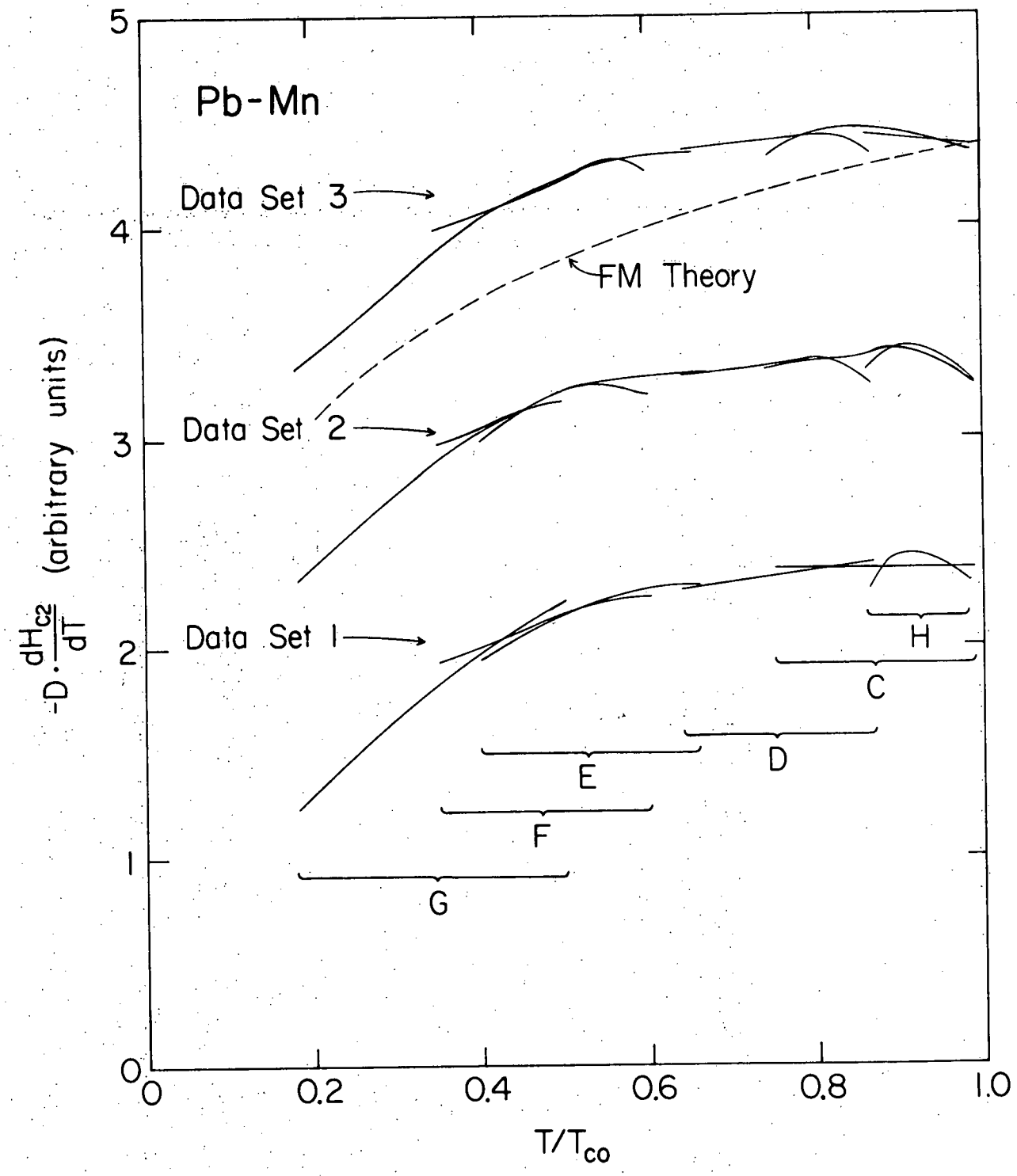
Pb-Mn
Data Set 3
FM Theory
Data Set 2
Data Set 1
H
C
D
E
F
G
$-D \cdot \frac{dH_{c2}}{dT}$ (arbitrary units)
T/T_{co}
0
1
2
3
4
5
0.2
0.4
0.6
0.8
1.0

Koepke and Bergmann found that their quench-condensed pure lead films had a resistivity of about 18 μΩ-cm, and a value of dH_{c2}/dT of about 2.9 kgauss/K. Our pure lead films had resistivities of about 22 μΩ-cm and a value of dH_{c2}/dT of about 2.2 kgauss/K. Since dH_{c2}/dT is proportional to ρ, this agreement is neither good nor unreasonable.

IV. CONCLUSION

We measured the upper critical magnetic field of quench-condensed films of In-Mn and Pb-Mn. These films were dirty type II materials. They were intermediate between being thin films and being bulk samples. The edge effects common in a resistive measurement of H_{c2} were eliminated by scribing the edges of the samples away from the middle.

The critical field data on pure indium and lead are consistent with the results of Bergmann, and Koepke and Bergmann.

The pair-breaking effects of the magnetic impurities and the applied magnetic field appear to be additive in both In-Mn and Pb-Mn. Furthermore, the pair-breaking parameter representing the magnetic impurities appears to be temperature-independent in both systems. These results support the FM theory.

The temperature dependence of H_{c2} for the In-Mn samples is the same as that expected from the FM theory. The temperature dependence of H_{c2} for the Pb-Mn samples is different from that expected from the FM theory, probably because of strong electron-phonon coupling.

There is a region of positive curvature near T_c in the $H_{c2}(T)$ data for Pb-Mn. The cause of this positive curvature is not known.

Appendix A.

Detailed Description of a Typical Run

1. Substrate preparation.

The substrates were optically polished pieces of z-cut quartz[55] which were 7/8 by 5/8 by 0.04 inches. The substrates used during the In-Mn runs were selected at random from the 5 substrates which we had. During the Pb-Mn runs, the same side of the same substrate was used for every sample. We now describe the procedure used to prepare a substrate for reuse.

The substrate was dunked into a small beaker of toluene to remove any Apiezon[56] N grease remaining from the previous run. Then it was put into a beaker of aqua regia to dissolve the previous sample and electrodes. The bare substrate was washed in tap water and dishwashing liquid, rinsed with lots of distilled water, and finally swished in beakers of reagent grade acetone, toluene, and isopropyl alcohol. Finally, it was put into a hot isopropyl alcohol vapor degreaser for several hours. The degreaser was left on for several hours, and then turned off and allowed to cool before the substrate was removed. The substrate was held with a Teflon-tipped tweezers while it was inspected for dirt. If it was still dirty, it was carefully wiped several times with a Kimwipe[57] soaked with reagent grade acetone, and the cleaning procedure was repeated, starting with washing with dishwashing liquid.

The substrates were inspected for dirt by looking at them under an optical microscope at the lowest magnification, which was 7x. The

substrate was held so that it reflected the microscope light almost into the lens. It was extremely important to look at the substrate against a dark background during this inspection. Using this technique, we found that the substrates were more highly polished on one side than on the other.

Once the substrate was clean, gold electrodes could be evaporated onto it. The substrate was placed into a recess in a block of copper, with the more highly polished side of the substrate faced away from the block. A mask for the electrodes was placed over the substrate and screwed down. The whole assembly was then placed into a small vacuum chamber, and the electrodes were evaporated onto the substrate. The pressure in the chamber stayed below 4×10^{-4} torr during the evaporation. The substrate was left in the vacuum chamber until it was used.

Three different electrode geometries were used during the course of this investigation. They are shown in Figure 12.

2. Attaching the substrate to the substrate holder

The substrate holder (described in detail in Appendix B) had been prepared to receive the substrate as follows. The recess in the substrate holder which would hold the substrate was cleaned with toluene and acetone. A small blob of N grease for a thermal link between the substrate and substrate holder was then put in the middle of the recess. The substrate holder was heated with a hot air gun until the N grease started to melt. The substrate holder was put immediately into a bell jar which was quickly evacuated with a mechanical pump. Bubbles of gas in the grease expanded

Figure 12. Electrode and sample geometries used. The symbols I and V indicate where the voltage and current leads for the four-terminal measurement of the sample resistance were attached.
A. Geometry used for In-Mn samples 5 and 7.
B. Geometry used for In-Mn sample 13.
C. Geometry used for In-Mn sample 19 and for all of the Pb-Mn samples.

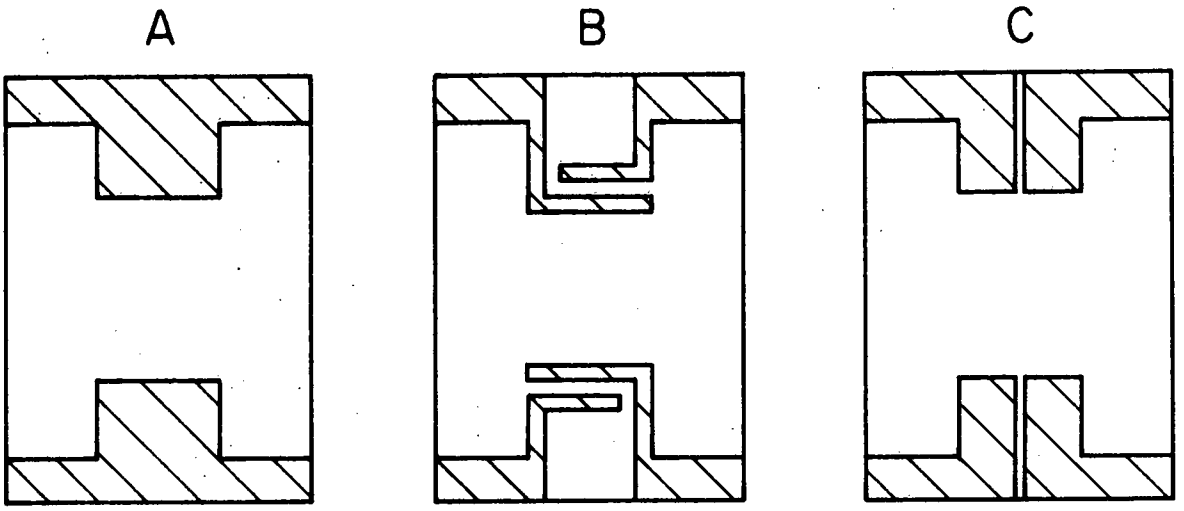

Above: Without Sample Film
Below: With Scribed Sample Film

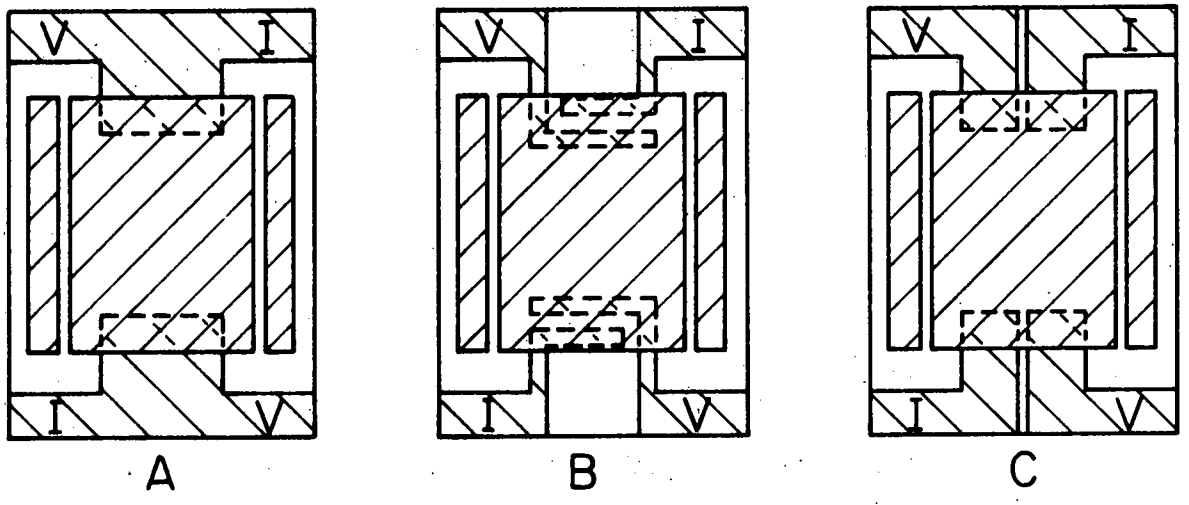

Bare Substrate | Gold Electrode | Sample Film

Substrate

in the reduced pressure and burst out of the grease. When all of the bubbles were gone, the substrate holder was removed from the bell jar and reheated to remelt the grease. It was ready for the substrate.

While the grease was still liquid, the substrate was laid on top of it and positioned in the recess. Phosphor bronze clamps at the ends of the recess were tightened down on the substrate to hold it in place and to squeeze out the excess N grease. The grease flowed easily under the substrate, filling the space between the substrate and the holder with a thin layer which provided a good thermal link. The excess grease went into the moat around the recess. After the grease had spread, the screw holding the clamp on one end of the substrate was loosened, the end of a phosphor-bronze coil spring was put under the screw head, and the screw was tightened. (The purpose of the spring will be explained later.) The four wires used to measure the sample resistance were attached to the gold electrodes with silver paint.[58]

Next, the assembly for scribing the sample edges away was screwed into place, straddling the substrate, and the set screws holding the scribing pins were loosened. The string around the brass blocks of the scriber was looped over the dangling end of the coil spring. The brass blocks were moved into the correct positions to mask the substrate during the sample film evaporation. The substrate holder was then ready to be attached to the substrate holder support.

The axle on the substrate holder was inserted into the hole in the side arm already attached to the cryostat. Then the other side arm, which was attached to the substrate holder, was screwed to the substrate

holder support. The wires from the Ge resistor, the Hall probe, and the sample electrodes were connected to the appropriate pins in the Teflon pin holding collar. The substrate holder was rotated by hand from the horizontal to vertical position to be sure that it would rotate easily during the experiment. Then it was returned to the horizontal position. At this point, all of the electrical circuits were checked.

3. Closing the cryostat

When the substrate holder was in position in the cryostat, oriented parallel to the floor, the cryostat was assembled around it. A detailed description of the cryostat is given in Appendix B. A small clamp was clamped to the end of the scriber string so that the string would pass through the holes in the heat shields when the heat shields were put into place. The heat shields were placed upside down on a desk, one inside the other, and a three-foot piece of copper wire was threaded through the holes in the shields for the rotation string. The heat shields, still one inside the other, were then held right-side-up under the inner LHe reservoir, and the upper end of the copper wire was tied to the rotation string. A small clamp was attached to the other end of the copper wire to keep some tension in the wire. This tension kept the rotation string from coming out of the pulley which was attached to the substrate holder. The LN shield was held immobile while the LHe shield was slid up the wire, over the knot and onto the string, and screwed to the bottom of the outer LHe reservoir. Three nylon 1-72

screws oriented perpendicular to the axis of the LHe shield were used to position the substrate holder over the hole in the shield. If the clamp on the scribing string did not come through the hole in the shield, it was fished out with a tweezers.

Next, the LN shield was slid up the wire, over the knot and onto the string, and screwed to the bottom of the LN reservoir. (Thin pieces of indium were put between the shields and the reservoirs to improve the thermal contact.) The clamp on the scriber string was removed and clamped to the rotation string about an inch from the end. Then the copper wire was detached from the rotation string. Loose overhand knots were tied in the ends of both strings. Finally, the vacuum jacket was screwed into place around the heat shields.

The next step was to attach the pulley tube to the vacuum jacket and connect the strings in the tube with the strings hanging from the substrate holder. As explained in Appendix B, the pulley tube contained pulleys which could be turned from outside of the cryostat. The rotating and scribing strings were attached to the appropriate strings in the pulley tube, and the strings in the pulley tube were wound around the pulleys in the tube, so that one could pull on the rotating and scribing strings by turning the pulleys in the tube.

First, the front section of the pulley tube was attached to the vacuum jacket. Then the strings hanging down from the substrate holder were tied to the pulley tube strings. Knots which had been tied in the ends of the pulley tube strings kept the other strings from slipping off. The pulley tube strings were wrapped around the back pulleys a couple

of times to put some tension in the elastic. This tension kept the strings from coming out of the pulleys. When the strings were in place, the back section of the pulley tube was attached. The axle for the sample rotation was engaged with the back pulley. The sample-scribing pulley assembly was retracted so that it would be out of the way during the sample evaporation. Finally, the scribing string was put into the notches in the edges of the holes in the heat shields, and the heat shield shutters were closed.

The last thing done before the cryostat was evacuated was to load pellets containing the desired Mn concentration onto the conveyor belt. A description of the alloy fabrication techniques is in Appendix G.

The pellets came from an ingot with the desired Mn concentration. The ingot was chemically analyzed to determine that it was homogeneous, and to determine the Mn concentration. A chunk of metal (about 200 mg), was cut from the ingot with a clean razor blade. Then the surface of the chunk was scraped with the razor blade to remove any oxide layer. The chunk was weighed and cut up into pellets. During the In-Mn runs through run 12, the chunk was cut up into about 100 pellets. In later In-Mn runs, and during all of the Pb-Mn runs, about 45 pellets were made. This was because the smaller pellets had a greater tendency to stick to the sides of the chute which guided them into the hot tungsten boat. Each of the smaller pellets added about 20 Å to the sample film's thickness, and each of the larger pellets added about 40 Å.

During all of the In-Mn runs, the pellets were cut before the cryostat was assembled. They were out in the air for the three hours

it took to assemble the cryostat. Because of the greater oxidizing rate of Pb, the Pb-Mn pellets were cut after the cryostat was assembled. They were in the air for only about 25 minutes before being inserted into the cryostat. At this point, the cryostat was supposed to be vacuum tight. It was rough pumped out with a mechanical pump pumping through a LN-cooled cold trap. When the pressure in the cryostat dropped to about 25×10^{-3} torr, the line to the roughing pump was closed, and the line to an oil diffusion pump (CVS model PMCS-2C)[59,60] was opened. Then the cryostat was checked for vacuum leaks with a mass spectrometer type leak detector. Any leaks were repaired, and the cryostat was left to pump down to a pressure of about 2×10^{-5} torr. This usually took a couple of hours, and when it was done, the cryostat was ready to be cooled.

4. Cooling the substrate

First, LN was put into the LN reservoir. Whenever this initial transfer was done, the pressure in the cryostat dropped from a little over 10^{-5} torr to a little over 10^{-6} torr in a few minutes. When the LN reservoir was full, LN was transferred into the outer LHe reservoir and then into the inner LHe reservoir. The resistance of the carbon resistor in the temperature regulating circuit was monitored during the transfer into the inner LHe reservoir; its resistance rose sharply from about 160 Ω to about 190 Ω as soon as the LN began to condense on the floor of the reservoir. The LN was left in the LHe reservoirs for about an hour. Then, with the LN transfer tubes pushed to the bottom of the reservoirs, about 5 psi of nitrogen gas was put into the LHe reservoirs.

This pressure forced the LN back up through the transfer tubes and out of the LHe reservoirs. To boil away the residual LN, the LHe reservoirs were sealed and pumped out with a mechanical pump for about 15 minutes. Then one atm of helium gas was put into the LHe reservoirs.

Then LHe was transferred into the outer and inner LHe reservoirs. Before the transfer, the transfer tube was cooled by transferring a small amount of LHe into the room. An electrical resistor probe attached to the end of a thin stainless steel tube was connected as one arm of a Wheatstone bridge to enable one to determine when the surface of the LHe reached the top of the reservoirs. After this and all other LHe transfers, no data were taken for at least one hour because data which were taken too soon after a LHe transfer were always found to be irreproducible. It usually took an hour or two after the first transfer for the Ge resistor to reach thermal equilibrium; the carbon resistor took about 15 minutes.

During all runs, the LN reservoir was filled twice a day. During the In-Mn runs, the LHe reservoirs were filled once a day; during the Pb-Mn runs, the outer reservoir was filled once a day, and the inner reservoir was filled as needed.

5. Making, rotating, and scribing the sample film

After the first LHe transfer of the run, and after the cryostat had attained thermal equilibrium, the sample film was made. The inner LHe reservoir was pumped on to cool the LHe to about 1.5 K. While this was happening, the valves controlling the water flow to the water-cooled

posts holding the tungsten boat, and to the water-cooled chute, were opened. A current was put through the boat and it was slowly increased from 0 to about 50 amps by using a Variac[61] variable transformer. In this way the temperature of the boat was raised slowly to about 1400 C, so that the outgassing boat never caused the pressure in the cryostat to rise above 5×10^{-6} torr. After the boat had outgassed for several minutes, the current through the boat was lowered to about 40 amps so the temperature of the boat was about 1100 C. The same boat temperature was used for all runs, both In-Mn and Pb-Mn. The boat glowed bright orange, and its temperature was measured with a Leeds and Northrup[62] optical pyrometer.

The shutter on the evaporator and the shutters on the heat shields were opened. The alloy pellets on the conveyor were dropped, one by one if possible, into the hot tungsten boat. Each pellet took from 1 to 3 seconds to evaporate. The temperature of the germanium resistor was monitored during the evaporation by watching the voltage across it on a digital voltmeter. The temperature was typically about 5.5 K before the first few pellets were evaporated. After the first few pellets were evaporated, the sample film apparently became quite reflective because the temperature dropped to about 4.75 K. As each pellet hit the boat, the temperature of the substrate holder increased by a few tenths of a degree. When the pellet had completely evaporated, the temperature suddenly dropped back nearly to the original temperature.

After all of the pellets had been evaporated, the current to the boat was cut off, and the power supply was disconnected. The movable scriber pulley rod was pushed into the cryostat as far as it would go.

The sample holder was then rotated until it clicked into place, or, after a switch was installed, until the switch indicated that the sample holder was fully rotated. The scriber pulley was engaged, and the scriber was pulled across the sample film. During the In-Mn runs, the knob which moved the scriber was turned until the opposing tension in the string indicated that the scriber was at the end of the track. During the Pb-Mn runs, the position of the scriber was determined by measuring the electrical resistance between the sample and ground with a Simpson meter. When the scribing pins first touched the sample, the resistance between the sample and ground went from infinity almost to zero. The scriber knob was turned until the resistance went back to infinity. The scriber knob was then turned back one turn to put some slack in the string. This slack allowed the coil spring on the substrate holder to pull the knot in the scriber string up to the brass block and out of the way of the shutter on the LHe heat shield. The slack also allowed the shutter to close over the string and not be pried back open by tension in the string. After the sample had been quench-condensed rotated to a position perpendicular to the floor, and scribed, the heat-shield shutters were both closed. Helium gas was bled into the inner LHe reservoir to raise the helium temperature to 4.2 K, and the temperature was maintained by pumping on the LHe through a manostat. If everything went successfully up to this point, there was a sample film in the cryostat ready to be studied.

6. Temperature regulation and measurement

The temperature of the sample was determined by the four-terminal d.c. resistance of a Cryocal[63] germanium resistor, serial number 3659. The resistor had been calibrated against another Cryocal germanium resistor which had been purchased from Cryocal with a calibration table. The calibration of the resistor used in this experiment against the resistor calibrated by Cryocal is described in Appendix H. When all of the In-Mn and Pb-Mn data had been taken, the calibration of the Ge resistor was checked against the 1958 He^4 vapor pressure temperature scale, and was found to be unchanged.

The Ge resistor had been covered with N grease and inserted into a hole in a small copper block. One centimeter of the plastic insulation on the leads had been cut away and varnished to the copper block through a layer of cigarette paper. The resistance of the Ge resistor was independent of the current in the resistor at all operating temperatures as long as the voltage across it was less than 7 millivolts. The temperature of the sample was measured with this resistor to an accuracy of about $\pm 0.1\,\%$, and to a precision of about $\pm$ 0.5 mK.

Temperatures below 4.2 K were obtained and coarsely regulated by pumping on the inner LHe reservoir through a manostat. The manostat held the LHe bath temperature constant to several millikelvin per hour. Fine temperature regulation was achieved with an electronic feedback circuit.

Briefly, the feedback circuit worked like this. An Allen-Bradley carbon resistor with a room temperature resistance of 150 Ω was attached to the substrate holder support. It was the fourth arm of a transformer

bridge. The arm opposite to it was a decade resistance box. There was also a 1000 Ω heater attached to the substrate holder support. While the electronic temperature regulator was operating, there was always a current in the heater. When the temperature of the sample holder drifted away from the desired value, this induced a change in the resistance of the carbon resistor away from the resistance value set on the decade resistor. This, in turn, induced an error signal from the bridge. This error signal was amplified, synchronously rectified by a lock-in amplifier, and added to the current in the heater so that the temperature of the substrate holder would change, causing the resistance of the carbon resistor to return to the value set on the decade resistance box. The bridge was operated at 490 Hz. It could regulate the temperature from 1.2 to 7.2 K to about 2 parts in 10^5.

The magnetic field dependence of the carbon resistor was checked at 2 and 3.6 K. This check was done by using the manostat to hold the temperature of the carbon resistor constant and then measuring the change in the resistance of the carbon resistor when the applied field was increased from 2 to 4 kgauss. We assumed that the resistance of the carbon resistor was quadratic in the field,[64] so we multiplied the measured resistance change by 4/3 to get the change in resistance corresponding to a change in the field of 0 to 4 kgauss. Using this number and the derivative of the carbon resistor's resistance with respect to temperature, we obtained the change in the resistance corresponding to a change in field from 0 to 4 kgauss in units of millikelvin. The resulting values were 0.7 and 0.4 mK at 2 and 3.6 K respectively. Because the effect was so small, no corrections to the data were made.

A different procedure was used to obtain and regulate temperatures above 4.2 K. The manostat was used to hold the inner LHe reservoir at atmospheric pressure. The heater was used to boil away the LHe from the inner reservoir. This was done by putting a constant amount of power, usually about 1/4 watt, into the heater, waiting for the substrate holder to come to steady state, usually at about 5 K, and then balancing the temperature-regulation bridge and waiting some more. The bridge stayed balanced until all of the LHe was gone. When the bridge became unbalanced, the decade resistance box was set to the desired resistance value. The heater warmed up the substrate holder to the appropriate temperature, and then regulated the temperature there.

Data were taken for 8 to 12 hours while there was no LHe in the inner reservoir before a small amount of LHe was transferred into the inner reservoir to cool it down again. Note that when this small amount of LHe was put into the inner reservoir, the tip of the transfer tube was not inserted through the constriction above the reservoir. Rather, the LHe was put in above the constriction and allowed to run down into the reservoir. This way, the higher temperature helium gas that preceded the liquid helium did not go into the reservoir and heat it up.

7. Magnetic field generation and measurement

The magnetic field for this experiment was generated by a Varian[65] V4004 electromagnet. The magnet was water-cooled, and had its own power supply and current regulator. The whole system generated a field which was rated to be stable to 0.1 % against line voltage changes or load resistance changes

of 10 %. The maximum ripple in the field was supposed to be less than 0.01 % of the field. The magnet was used with four-inch diameter pole faces and a four-inch pole gap spacing. The maximum current output of the power supply was four amps; this produced a field of four kgauss. The field was supposed to be homogeneous to 1 % in a one-inch diameter sphere centered between the pole faces.

The magnet was mounted on an aluminum cart which moved on tracks. It was mounted sideways so that the long vertical cryostat would fit between the pole faces without hitting the magnet's base. Stops at the end of the track allowed the magnet to be accurately repositioned.

The magnetic field was measured with a bismuth-film Hall probe manufactured by American Aerospace Controls.[66] The reference output of a Princeton Applied Research[67] model 120 lock-in amplifier in series with a standard resistor and an adjustable resistor was used to provide the current in the Hall probe. The lock-in was operated at 1 kHz. The same lock-in was used to measure the amplitudes of the voltage across the standard resistor and the transverse voltage across the probe. The lock-in output was read from a digital voltmeter. To reduce noise, the input signals to the lock-in were amplified by a PAR 113 preamplifier in the differential mode. The phase of the lock-in was adjusted so that there was no detected signal across the standard resistor at a phase 90° away. The best value for the lock-in time constant was 1 second.

Up through In-Mn run 13, the current in the probe was 200 μA; thereafter the current was 400 μA. The sensitivity of the probe was approximately 0.02 μV/G or 0.04 μV/G respectively.

The Hall probe was calibrated twice during each run, before and after taking all of the sample resistance versus magnetic field curves. The probe was calibrated against a Rawson-Lush 929-M2[68] rotating-coil gaussmeter which had been calibrated against an NMR probe. For fields less than 1 kgauss, and for temperatures less than 4.2 K, the calibration of the Hall probe was independent of temperature to better than 1 gauss. Hence, for the In-Mn runs, the probe was calibrated at only one temperature, 4.2 K. For the Pb-Mn runs, where fields up to 4 kG were used, and temperatures of up to 7.2 K were reached, the probe had to be calibrated at three or four temperatures. The calibration changed by about 1 % per degree Kelvin at a field of 3 kgauss and a temperature of about 7 K. The temperature dependence decreased with decreasing fields and temperatures. The field value assigned to a value of Hall voltage, V_H, measured at temperature T, was determined by interpolating between the values indicated by the calibration data at temperatures immediately above and below T. The calibration data were fit with polynomials, and the polynomials were used to determine H from V_H from a particular set of calibration data.

The Hall probe was calibrated by measuring the field at the center of the volume between the magnet pole faces with the gaussmeter, and then rolling the magnet up to the cryostat and measuring the field with the Hall probe. A styrofoam block with a cylindrical hole bored through it was used to position the gaussmeter between the pole faces. The gaussmeter was moved and rotated in the hole to achieve the maximum field reading.

The same Hall probe was used in all runs, and it apparently deteriorated with time and use. During run H, it was quite erratic in fields greater than 2 kgauss. Therefore, the high-field data from run H was discarded.

After all of the In-Mn and Pb-Mn data had been taken, the rotating coil gaussmeter calibration was checked against an NMR probe, and found to still be accurate.

Appendix B.

Detailed Description of the Apparatus

1. The cryostat

The cryostat (see Figure 13) was a pumped He^4 cryostat. It was constructed almost completely of brass and copper to avoid distortion of the magnetic field which would result from using magnetic materials like stainless steel. The region of the cryostat within six inches of the sample was made completely from non-magnetic materials. Hard solder was used in the construction of the LHe reservoirs and heat shields because soft solder would become superconducting and distort the magnetic field.

The inner LHe reservoir was surrounded by a heat shield which was screwed to the bottom of the outer LHe reservoir. Both of them were surrounded by a heat shield which was screwed to the bottom of the LN reservoir. Thin pieces of indium were used between the heat shields and the reservoirs for better thermal contact. There were one-inch diameter holes in the bottoms of the heat shields through which the sample film could be evaporated onto the substrate. Movable shutters covered these holes.

Tiny holes in the heat shields allowed the string for the sample rotation to pass through. Slots cut perpendicular to the edges of the one-inch diameter holes in the heat shields held the string for the sample scribing mechanism so that the shutters could be closed and opened before the sample evaporation without binding on the string.

(After the sample was evaporated, the scribing string hung straight down through the center of the hole, but since there was no tension in the string, the shutters could be simply closed over it.) The inside of the LHe heat shield from the bottom to a point above the Teflon collar on the inner LHe reservoir was lined loosely with 10 mil Mylar to both thermally and electrically isolate the leads between the sample holder and the Teflon collar from the heat shield.

The cryostat was evacuated with a diffusion pump backed by a Welch 1402[69] mechanical pump. A Bendix GPH-320[70] Penning Gauge in the line between the diffusion pump and the cryostat indicated an ultimate pressure of about 2×10^{-7} torr. In the sample chamber, which was at about 4 K, the pressure was probably an order of magnitude or more lower.

The electrical leads connecting the pins in the hermetic seal in the cryostat vacuum sheath to the pins in the Teflon pin holder were made of eight feet of #36 insulated constantan wire. There were 40 wires all together. Bundles of 10, 10, 8, 8, and 4 wires were separately covered with woven fiberglass sleeving to keep them apart and so to minimize cross talk. The wires were wrapped around the LN shield once and then were varnished to it with Ge 7031 varnish[71] through cigarette paper. They were wrapped around the outer LHe reservoir twice and then also varnished to it through cigarette paper. Finally, they were wrapped around the inner LHe reservoir three times and then varnished to it through cigarette paper. Electrical connection pins were Cd-Bi soldered to the ends of the wires and placed into holes in the Teflon pin holding collar. The collar kept the pins from touching each other and the surrounding heat shield.

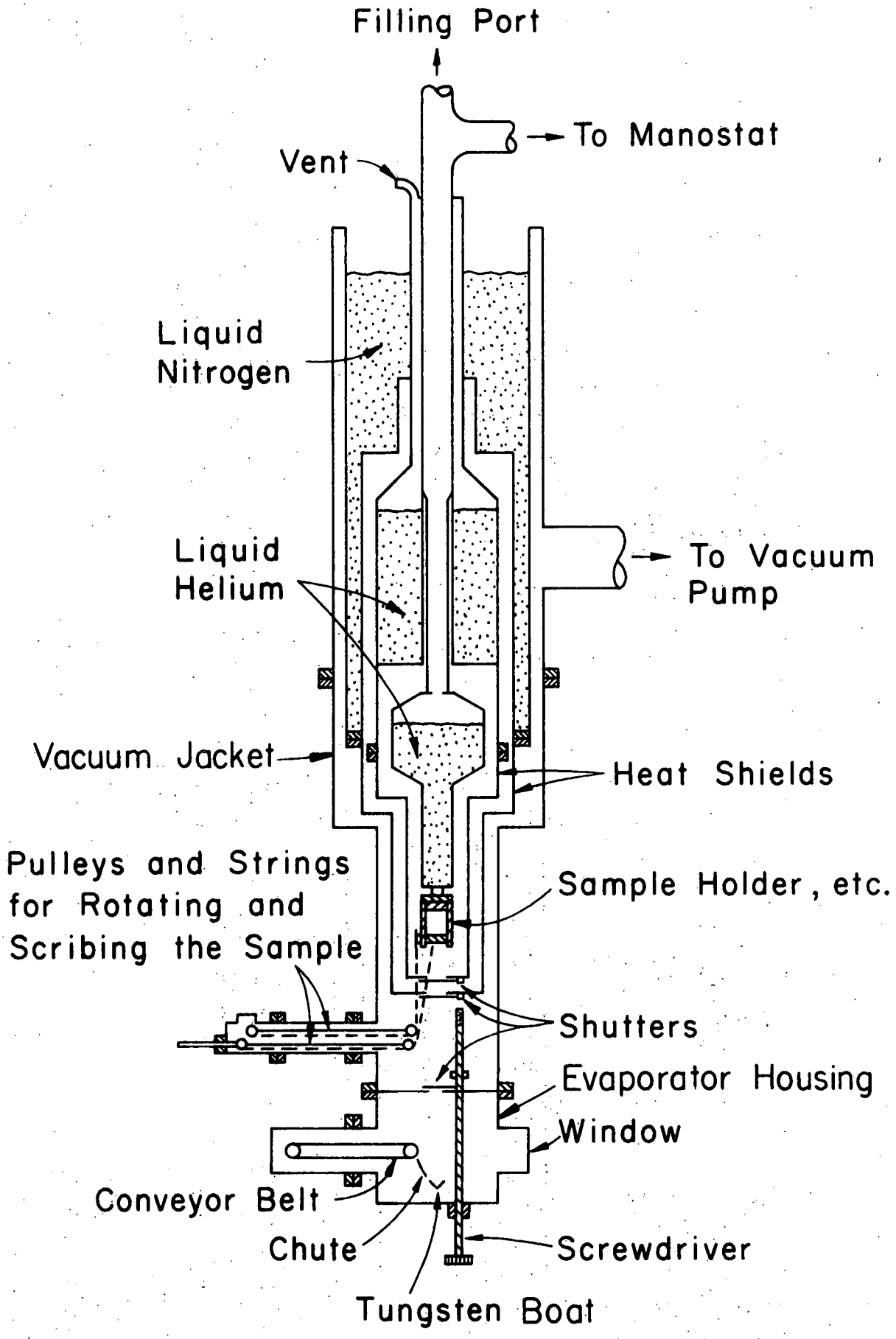

Figure 13. The cryostat.

2. The evaporator housing

The evaporator housing (see Figure 13) was attached to the bottom of the cryostat vacuum jacket. Two water-cooled copper posts, which were electrically insulated from the housing, passed through the bottom of the housing. A boat made from 1 mil tungsten sheet was clamped to these posts. There was a conveyor belt and a water-cooled chute just above and to the side of the boat. The belt itself was made from 1 mil Mylar. It was used to drop pellets of metal through the chute into the boat. There was a Pyrex window opposite the conveyor belt. A screwdriver which could be raised, lowered, and rotated from outside the cryostat was built into the bottom of the evaporator housing. This screwdriver opened and closed shutters on the top of the evaporator housing and on the bottoms of the LN and LHe heat shields.

3. The substrate holder and support assembly

The substrate holder was made from a solid piece of copper which was subsequently gold plated to increase thermal contact between itself and other pieces screwed to it and to reduce light absorption (see Figure 14). The substrate rested in a recessed area on the front of the substrate holder. This area, composed of a flat area surrounded by a moat, was slightly larger than the substrate, and the flat area was recessed by an amount which was slightly less than the thickness of the substrate. Axles (B) on which the substrate holder could rotate were silver-soldered to the copper block.

Figure 14. Front view of the substrate holder.
A. Gold-plated, solid copper block.
B. Round axles silver-soldered to A.
C. Recessed area for holding the substrate.
D. Moat for excess N grease.
E. Screw holes for the thermal links to the brass blocks in the sample-scribing assembly.
F. Notches in which the sample resistance wires were varnished to part A.
G. Four screw holes for the scribing assembly.
H. Substrate.
I. Gold electrode.
J. Silver paint.
K. Voltage leads.
L. Current leads.
M. Nylon 1-72 screw.
N. Phosphor-bronze clamp varnished on the side against the substrate.
O. The scribing pins rested here after scribing the sample.
P. The scribing pins rested here before scribing the sample.
Q. Phosphor-bronze coil spring.

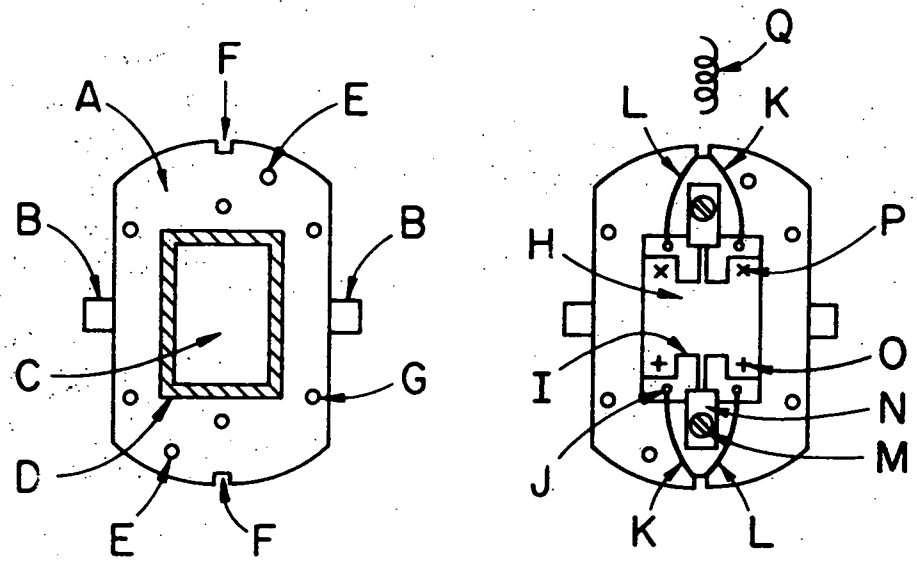

Without Substrate

With Substrate

Front View of the Substrate Holder

Two-phosphor bronze clamps (N) pressed the substrate against the holder. The side of the clamps which was against the substrate was covered with varnish (Ge 7031) and cigarette paper to insulate it. The clamps were held down with nylon 1-72 screws (M). The electrical leads to the sample (K and L) were bent so that they maintained electrical contact with the electrodes without help, and then they were silver-painted to the electrodes. The leads were thermally grounded to the substrate holder with varnish and cigarette paper in the canals (F).

The two holes (E) and the four holes (G) and the coil spring (Q) were parts of the sample scribing assembly. See Section 4 in this appendix, for a description of the sample-scribing assembly.

Figure 15 shows the substrate holder and the substrate holder support. The substrate holder axles fitted into hubs (A) in the two support arms. The left support arm had a slot (B) for the electrical leads to pass through. This arm was thermally connected to the substrate holder positioning piece (E) with a bundle of 16 #30 copper wires, about 3 centimeters long, Cd-Bi soldered at each end. This arm was always left connected to the substrate holder. To remove the substrate holder from the cryostat, only the screws holding the arm to the rest of the support, and the screw holding the rotation pulley (I) on to the axle, were loosened. The right support arm contained an Allen-Bradley carbon resistor which was used in the temperature control circuit. This arm was silver-soldered to the piece to which the heater (O) was attached.

The support assembly was screwed to the LHe reservoir (C) with a brass washer coated with N grease in between them to act as a thermal

Figure 15. Substrate holder with support assembly. For clarity, some parts are shown in the side view which are not shown in the back view, and vice versa.

A. Hub.
B. Slot for electrical leads.
C. Inner liquid helium reservoir.
D. Brass washer used as a weak thermal link.
E. Substrate holder positioning track.
F. Thermal link from substrate holder to side support arm: Sixteen #30 copper wires, each 3 cm long, were Cd-Bi soldered at both ends.
G. Substrate holder.
H. Copper sheet holding the Hall probe.
I. Pulley for rotating the substrate holder.
J. Copper block holding the Ge resistor.
K. 50 Ω Allen-Bradley carbon resistor used to regulate the sample temperature.
L. Heat sink made of cigarette paper and varnish.
M. Electrical connection pins.
N. Teflon pin holder.
O. 1000 Ω heater.
P. Phosphor-bronze leaf spring.
Q. Roller to position the substrate holder.
R. Tunnel for electrical leads.
S. Axle.
T. Set screw to hold the Teflon pin holder in place.

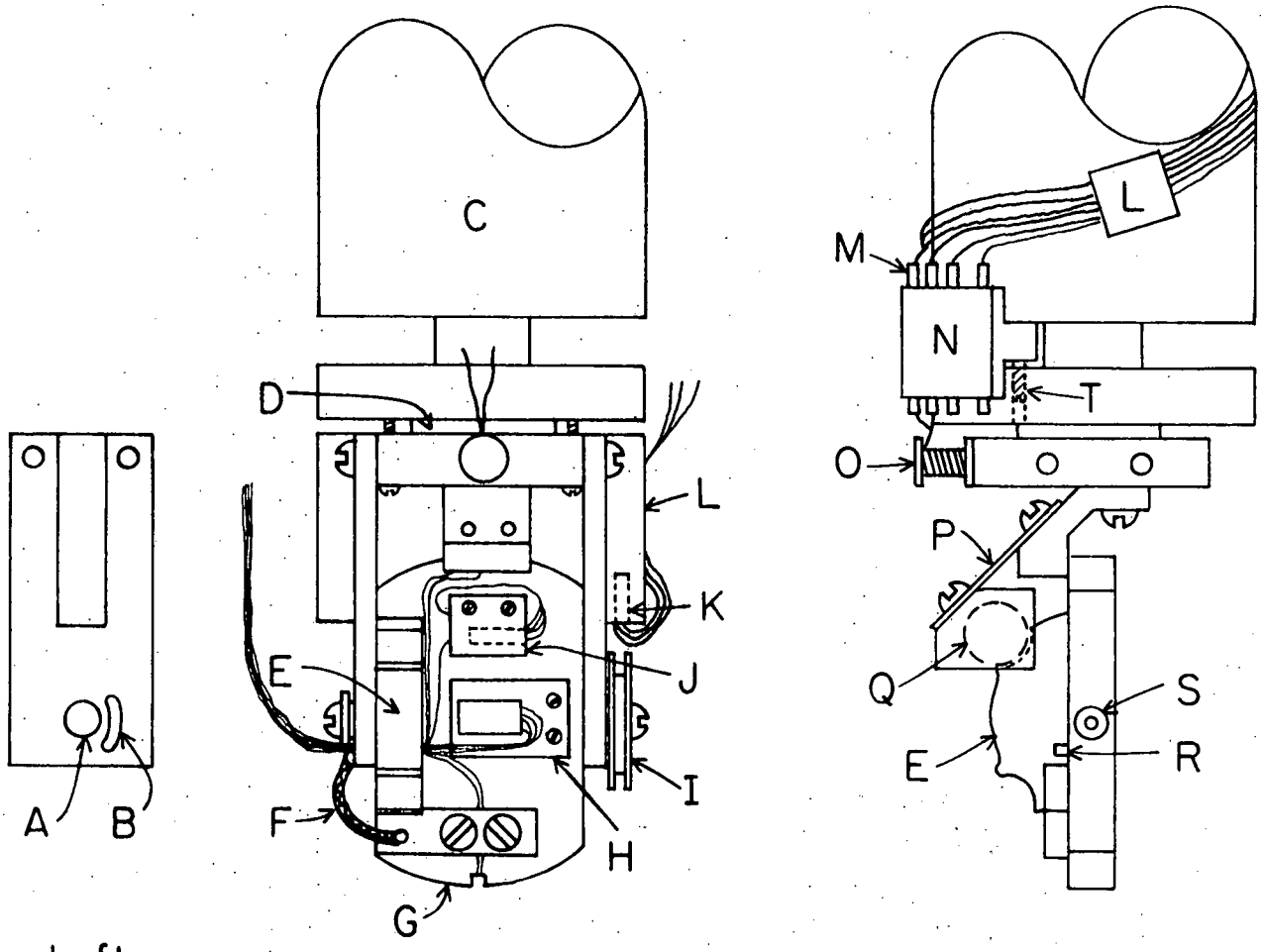

Left Support Arm

Back View

Side View

Substrate Holder with Support Assembly

weak link. This weak link allowed the temperature of the assembly to be controlled with a minimum of heat dissipation and LHe boil off. A heater (O) made of 1000 ohms of 0.005 mil diameter manganin wire, bifilarly wound on and varnished to a copper form, was screwed to the support assembly with N grease in between. The heater was used for temperature regulation.

A small copper block (J) containing a Ge resistor was screwed to the back of the substrate holder. The leads from the resistor were thermally grounded to the small block with varnish and cigarette paper. A 1/32-inch thick piece of copper (H) with a Hall probe varnished to it was attached to the back of the substrate holder also. The electrical leads from the sample, the Ge thermometer, and the Hall probe all passed through a tunnel (R) in part (E), the slot (B), and then went up to the Teflon pin holder (N).

The side view in Figure 15 shows how the roller (Q) was spring loaded with a phosphor-bronze leaf spring (P). It shows the roller in the notch holding the substrate holder in the position which it had after the rotation. The roller was actually attached to the side of a block of copper, which was attached to the leaf spring.

The side view also shows the Teflon pin holding collar (N). N grease was put between the collar and the LHe reservoir (C), and a set screw (T) held the collar in place.

4. The sample film-scribing assembly

The sample film-scribing assembly is shown in Figure 16. Two brass blocks (B and E) moved in a channel cut into two pieces of Teflon (H).

Figure 16. The sample film-scribing assembly
A. Scribing pins.
B. Brass block.
C. Phosphor-bronze leaf spring.
D. A single #36 copper wire, 3 cm long, for thermal grounding, Cd-Bi soldered to the brass block and to a small washer.
E. Brass block.
F. Canal for the stopping peg.
G. Fifteen lb. test braided Nylon fishing line.
H. Teflon tracks.
I. Stopping pegs.
J. Phosphor-bronze leaf spring to hold the Teflon track down.
K. Knot.

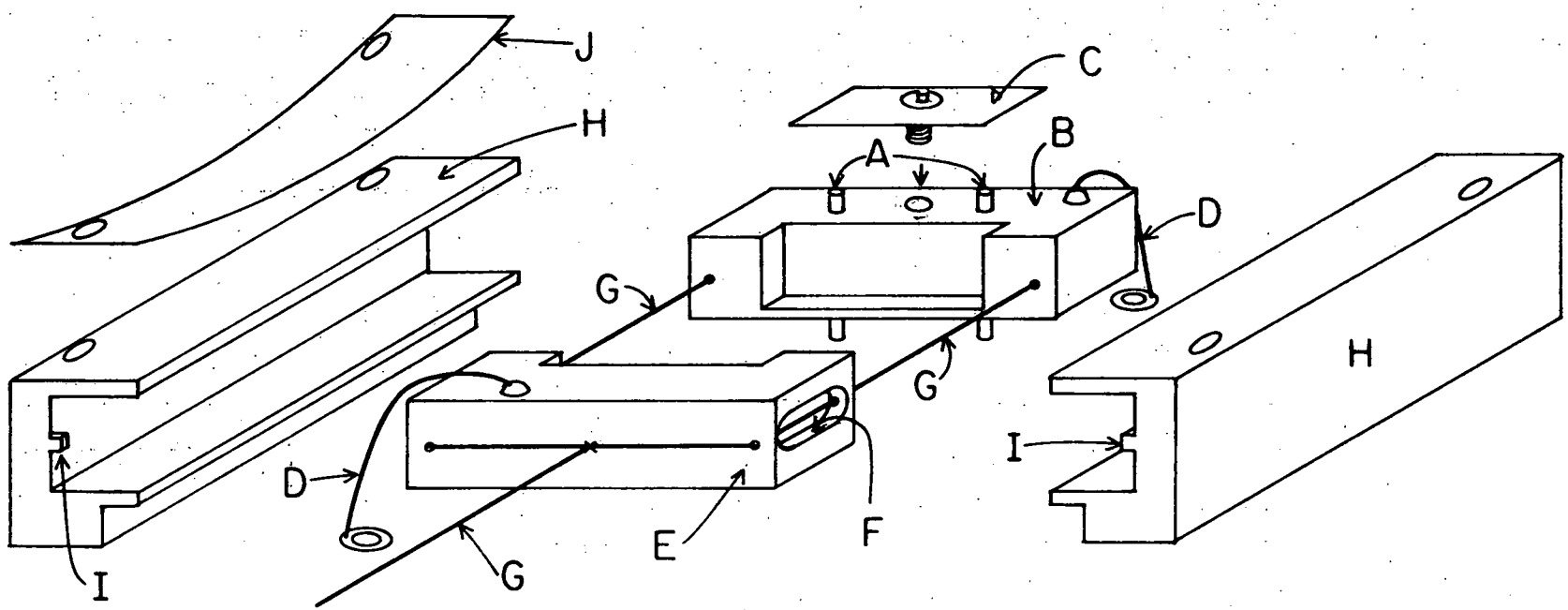

Sample Film-Scribing Assembly

The Teflon pieces were screwed to the front of the substrate holder (Figure 14). Because the Teflon contracted much more than the brass screws which were used to hold it down, it was necessary to have phosphor-bronze leaf springs between the screw heads and the Teflon blocks to keep the Teflon pressed against the substrate holder at low temperatures. The stopper (I) moved in the channel (F).

The brass blocks (B and E) were thermally and electrically grounded with wires (D) Cd-Bi soldered to washers which were screwed down to the substrate holder. Two beryllium-copper pins (A) were inserted into holes in part (B). When the scriber was not attached to the substrate holder, the pins were held in place with set screws. The set screws are not visible in the Figure. When the scriber was put into position over the substrate, the set screws were loosened, and the phosphor-bronze leaf spring (C) was screwed down onto the pins to hold them against the substrate. The friction of the pins against the substrate kept the scriber from moving when tension was put into the string (G). The brass blocks also masked the substrate during the sample film evaporation.

The string (G) was actually a piece of braided Nylon fishing line. It ran around both brass blocks. On the back side of part (B), the string looped over a coil spring (part Q in Figure 14). After the film was scribed, some slack was put into the string, and the coil spring pulled the knot (K) up against piece (E). This was necessary to keep the knot (K) from blocking the shutter on the LHe heat shield.

5. The pulley system for rotating and scribing the sample

Figure 13 shows how the pulley tube was attached to the cryostat vacuum jacket. It also shows how the strings in the systems for rotating and scribing the sample passed through the heat shields. A detailed sketch of the pulley tube is shown in Figure 17.

The upper set of pulleys was used to rotate the sample. It was rigidly attached to the pulley tube at the flange which was attached to the vacuum jacket. The lower pulley system was used to scribe the sample. It was moved by sliding the movable rod through a quick connect. It is shown in position just before scribing the sample; the stop is up against the flange.

Both strings were wrapped around the pulleys and fastened down the same way. The string from the substrate holder came down around the first pulley, and was tied to the string from the pulley tube. The string from the pulley tube had a knot in its end to keep the other string from slipping off under tension. The pulley tube string was wrapped once around the back pulley, then it came out through a notch in the pulley and went under a screw which clamped the string to the pulley. From there it went back through the notch, and was wrapped around the pulley enough times to stretch the elastic. The elastic kept tension in the strings so that they did not come out of the pulleys.

The back pulley in the sample-rotating system was engaged as soon as the pulley tube was completely attached to the cryostat vacuum jacket. The back pulley in the sample-scribing system could not be engaged until after the sample film had been evaporated and rotated. The window facilitated engaging the pulleys.

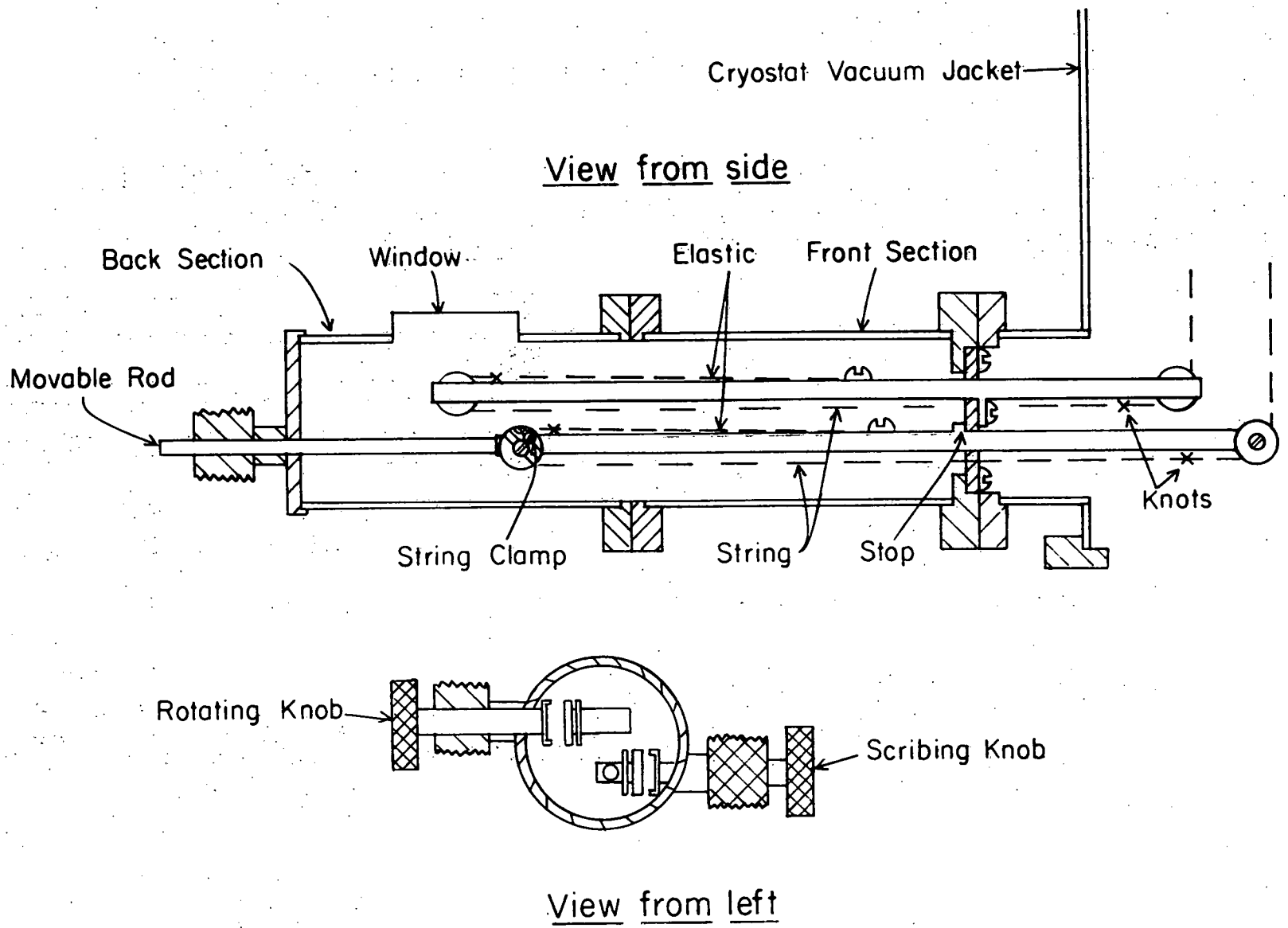

Figure 17. The pulley tube.

Appendix C.

Data Taking Procedures

In this Appendix we discuss the procedures used to measure the resistance of the sample as a function of temperature in zero magnetic field and as a function of magnetic field at a constant temperature. Since the procedures used during the Pb-Mn runs differed somewhat from those used during the In-Mn runs, they are described separately. The resistive transition curves obtained by using these procedures are discussed in Appendix D.

1. In-Mn data

The first measurement made on every sample was of the resistive transition in zero magnetic field. The manostat was adjusted to hold the inner LHe bath temperature just below the transition temperature. The temperature regulator was used to step the sample temperature through the transition. At appropriate temperature intervals, the sample was allowed to come to thermal equilibrium, and then its resistance was measured. The sample temperature was obtained from the resistance of the Ge resistor.

The sample resistance was measured by using a four-terminal d.c. method. The current was provided by two parallel 1.3 volt mercury cells which were in series with an adjustable resistor and a 1 Ω standard resistor. Fifty to one hundred μA were used. The voltage across the sample was measured with a digital voltmeter to a precision of ± 0.5 μV. The current in the sample was determined by measuring the voltage across the standard resistor with a digital voltmeter.

After the zero-field transition had been observed, if the sample seemed good, measurements of the resistive transition in a magnetic field were made. Each of these measurements was made at a constant temperature.

The temperature was measured before the magnetic field was turned on. The temperature regulator was used to keep the temperature constant. Then the magnetic field was slowly stepped through the transition. At appropriate field intervals, the sample resistance and the voltage across the Hall probe were measured. When the field was above the transition field, the sample was heated to about 1 K above its transition temperature in zero field to be sure that it was completely normal. Then the sample was allowed to cool back to the original temperature, and the field was stepped back down through the transition. This was an attempt to find out whether there was any hysteresis in the transition. None was ever found.

2. Pb-Mn data

The zero field resistive transition in the Pb-Mn runs was measured just as in the In-Mn runs.

The procedure used to obtain the resistance-versus-field curves differed from the method used in the In-Mn runs. At each temperature, about 12 data points were taken using the method described in the In-Mn section above. These data points were concentrated in the region where the sample resistance was increasing rapidly with the increasing magnetic field. A continuous resistance-versus-field curve was obtained

by amplifying the voltage across the sample with a Keithley Nanovoltmeter,[72] and putting the amplified signal into the Y-axis of a Moseley X-Y chart recorder.[73] The amplified Hall voltage was put into the X-axis of the chart recorder. As the magnetic field was increased slowly (about 1 gauss/sec to avoid joule heating caused by the changing field), through the transition, the chart recorder plotted the sample resistance as a function of Hall voltage. The discrete data points were used to quantitatively determine the Hall voltage at the transition.

Appendix D.

Discussion of the Shape of the Resistive Transition

There were two primary factors which determined the shape of the resistive transition. These were the geometry of the sample and electrodes and (probably) microscopic inhomogeneities. Since the In-Mn transition curves differed from the Pb-Mn curves, they are discussed separately.

1. In-Mn data

A common problem in resistive measurements of the superconducting transition in thin films is that the edges of the film have different properties from the middle of the film. Therefore, the edges of the samples which did not overlap the electrodes were scribed away. The resistive transitions of a pure indium film before and after scribing are shown in Figure 18. Scribing caused the transition temperature to move down by several tenths of a degree, and sharpened the width of the transition by a factor of about 60. This indicated that the edges had a higher transition temperature than the rest of the film. The zero-field resistive transitions of samples 5, 7, 13 and 19 are shown in Figures 18, 19, 20, and 21.

It is important to remember that the edges of the film overlapping the electrodes were not scribed. These edges should have had a much greater critical field at every temperature than the middle of the film because they apparently had a higher transition temperature and because H_{c2} increases with decreasing mean free path. No evidence of the edges

Figure 18. Zero-field resistive transition of In-Mn sample 5. The transition is shown both before and after the sample was scribed.

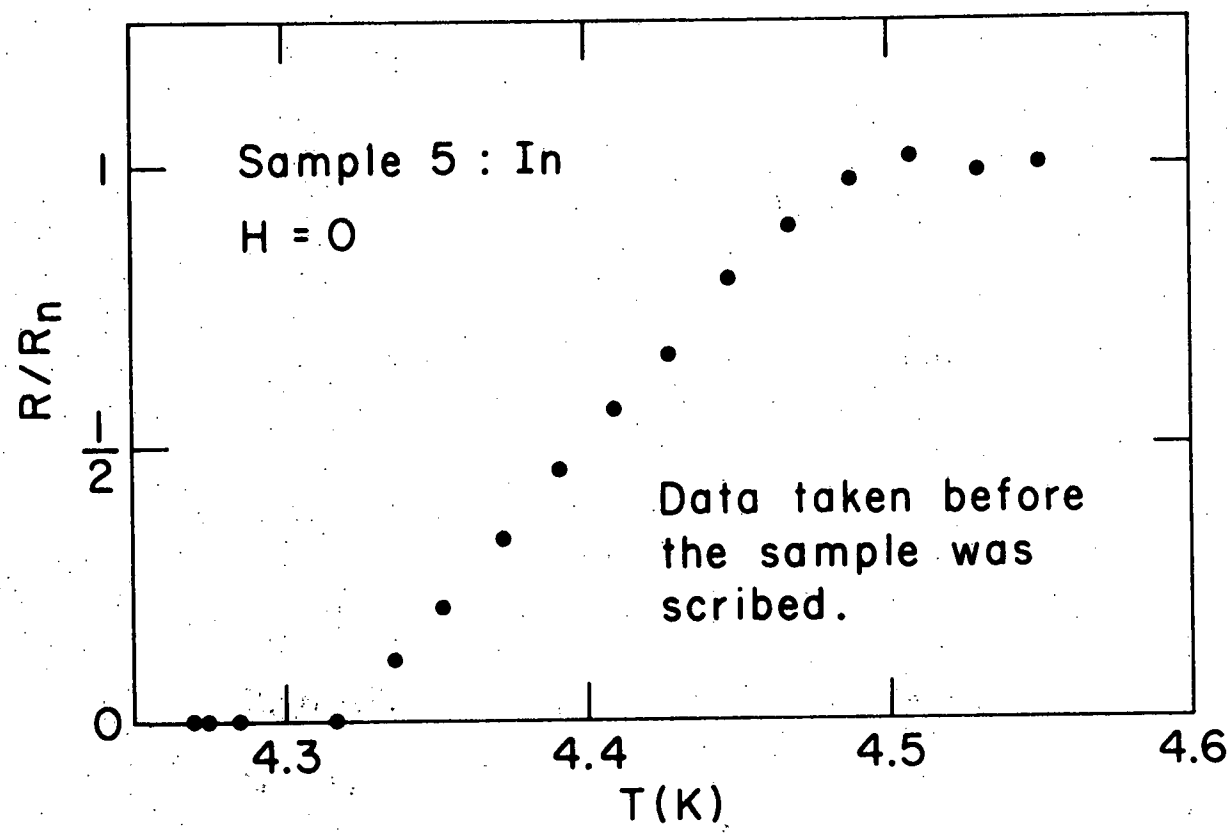
Sample 5 : In
H = 0
Data taken before the sample was scribed.
R/Rn
1
1/2
0
4.3
4.4
4.5
4.6
T(K)

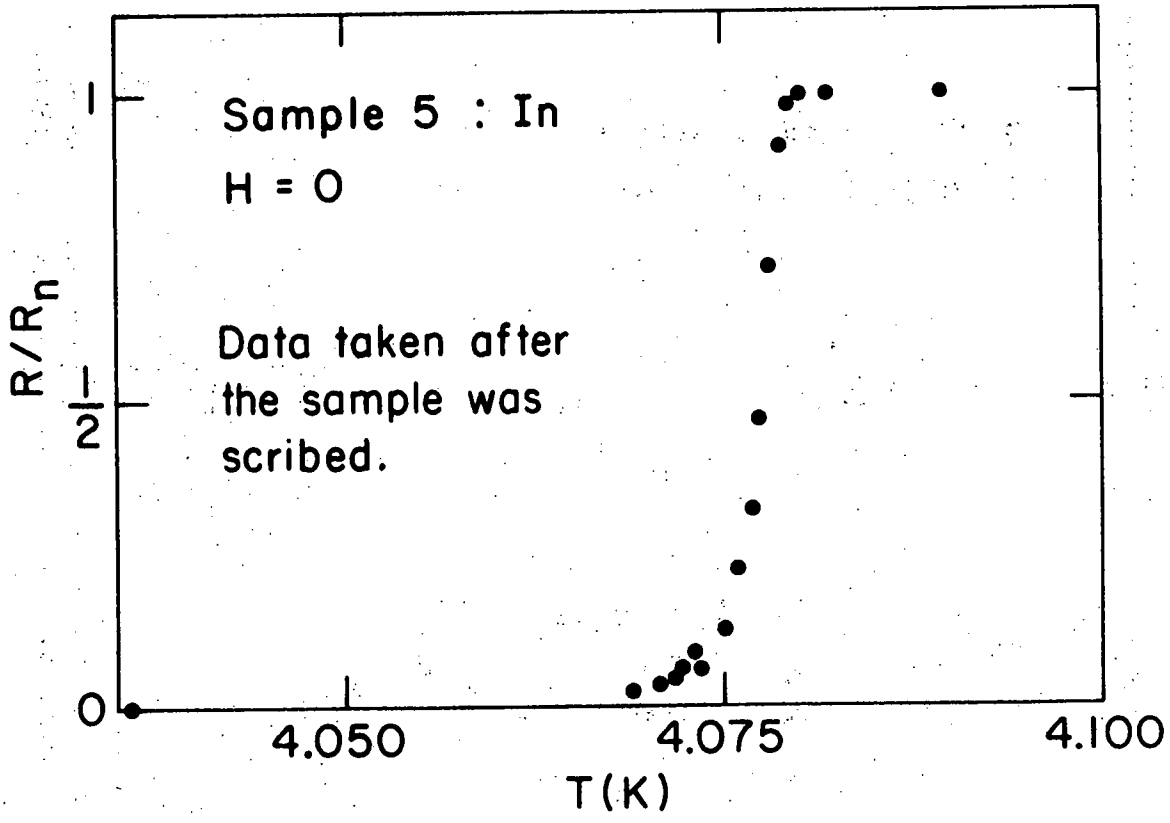
Sample 5 : In
H = 0
Data taken after the sample was scribed.
R/Rn
1
1/2
0
4.050
4.075
4.100
T(K)

Figure 19. Zero-field resistive transition of In-Mn sample 7.

Figure 20. Zero-field resistive transition of In-Mn sample 13.

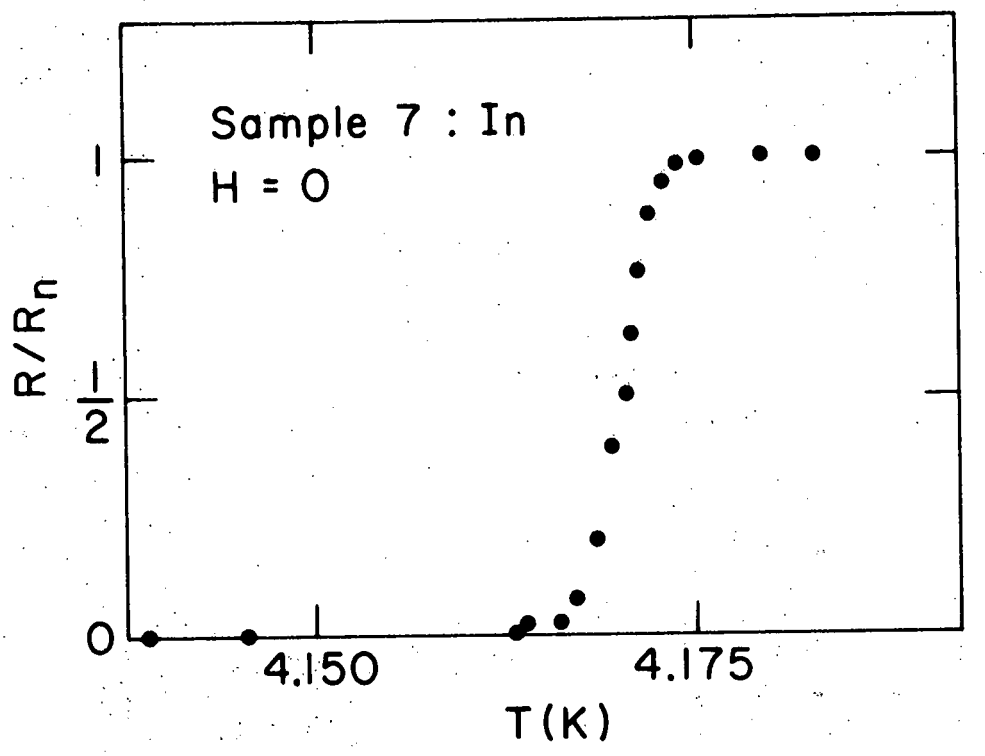
Sample 7 : In
H = 0
R/Rn
1
1/2
0
4.150
4.175
T(K)

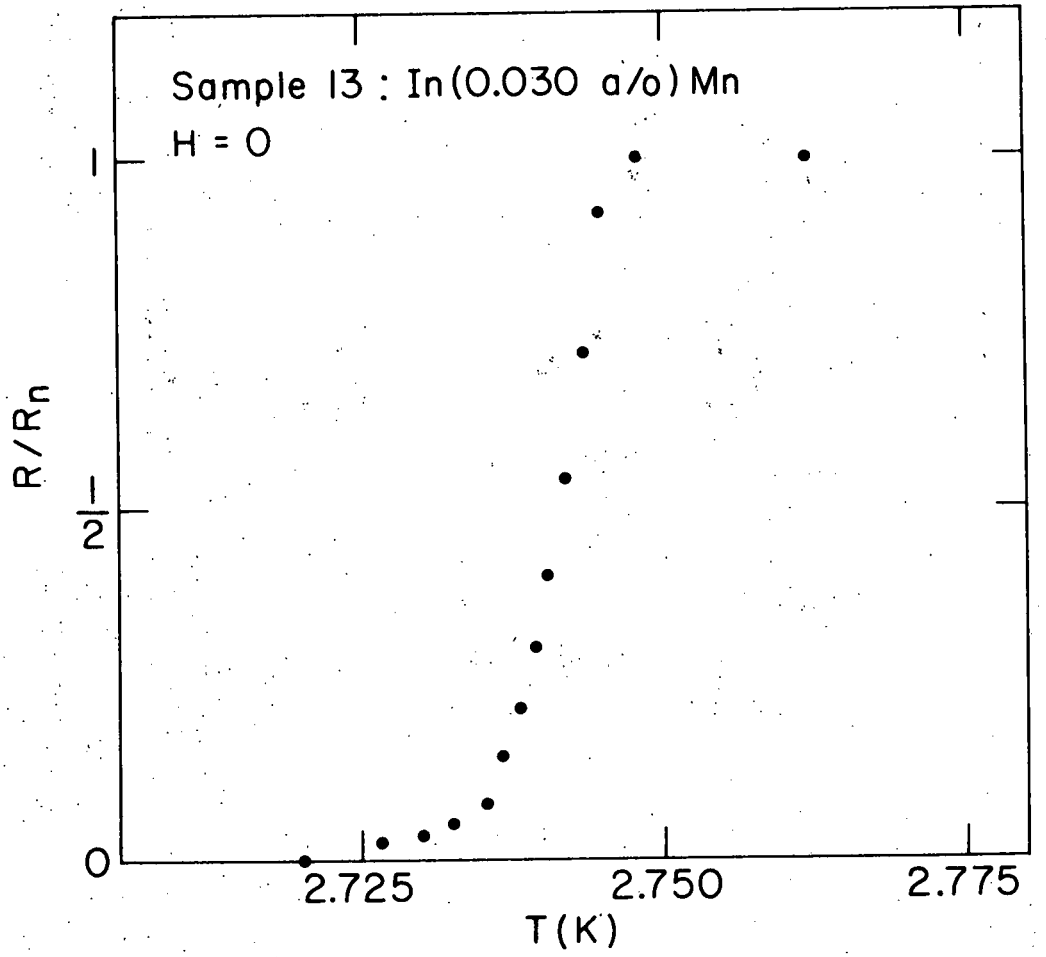
Sample 13 : In(0.030 a/o) Mn
H = 0
R/Rn
1
1/2
0
2.725
2.750
2.775
T(K)

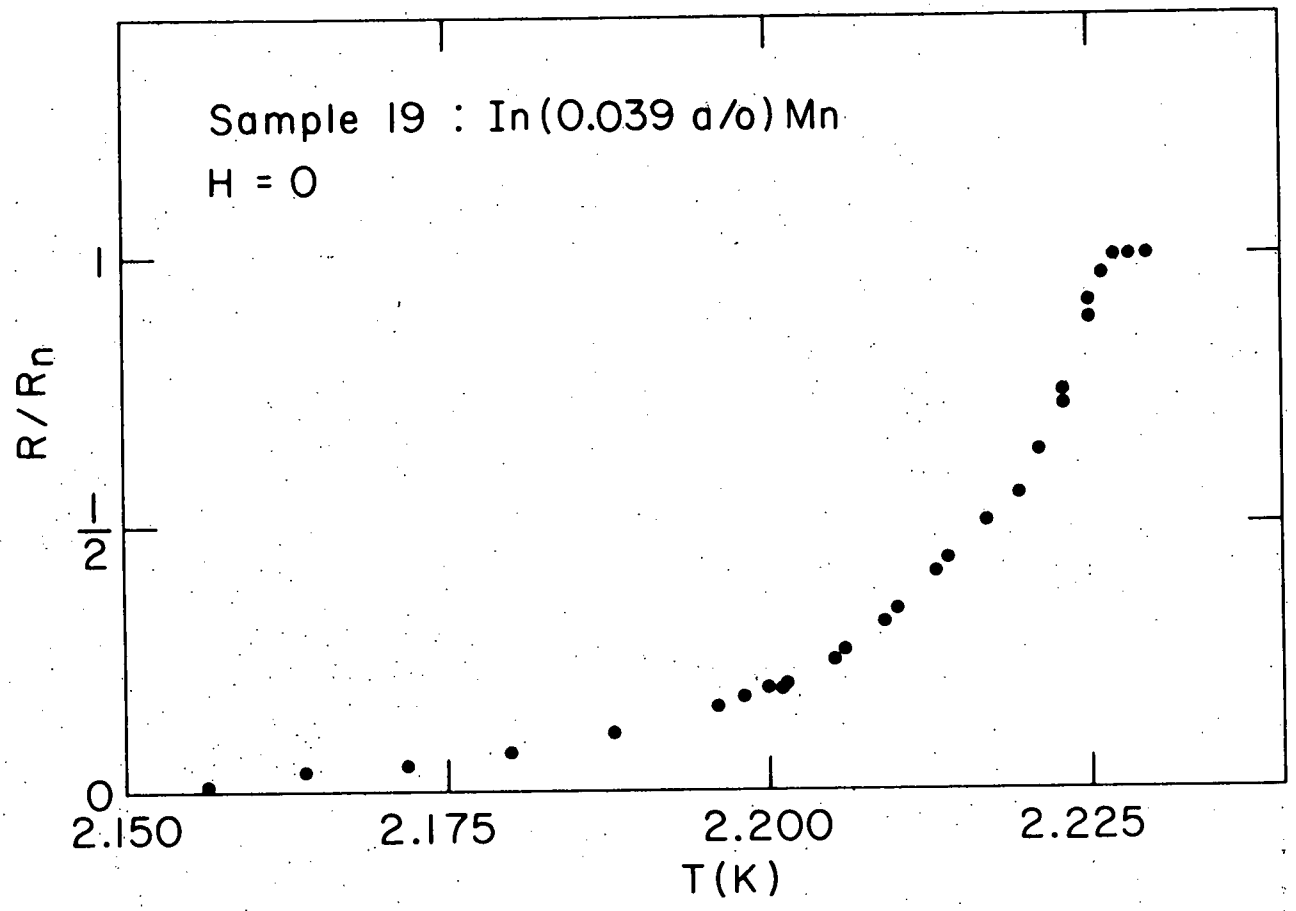

Figure 21. Zero-field resistive transition of In-Mn sample 19.

becoming normal during measurement of a resistive transition in a magnetic field was observed during the In-Mn runs. However, a measurement of both the four-terminal and two-terminal resistance of sample 13 as a function of temperature in zero field was made. The results are shown in Figure 22. When the edges of the film became superconducting, the current pattern in the film changed. This change lowered the two-terminal resistance but raised the four-terminal resistance. That this should happen has been verified using Teledeltos[42] conducting paper to model the sample.

The width of the transitions in zero field was probably due to inhomogeneities in the sample. These inhomogeneities were regions of different disorder and/or different Mn concentration. Since the transition temperature of indium depends strongly on both the amount of disorder and the amount of Mn, such regions would have had different transition temperatures and hence broadened the transition.

Sample 19 seemed to have an extraordinarily broad transition (see Figure 21). However, two other samples were made with the same Mn concentration, and they also had broad transitions.

In a magnetic field, the resistive transition of all four samples (see Figures 23, 24, 25, and 26), showed three distinct regions: a foot, a linear region, and a slow rise to the normal state resistance. The resistance in the foot was independent of the measuring current, but the resistance in the other two regions was not (see Figure 26). The current dependence was probably due to both joule heating and to filaments with a higher critical field than the rest of the film carrying most of the current.

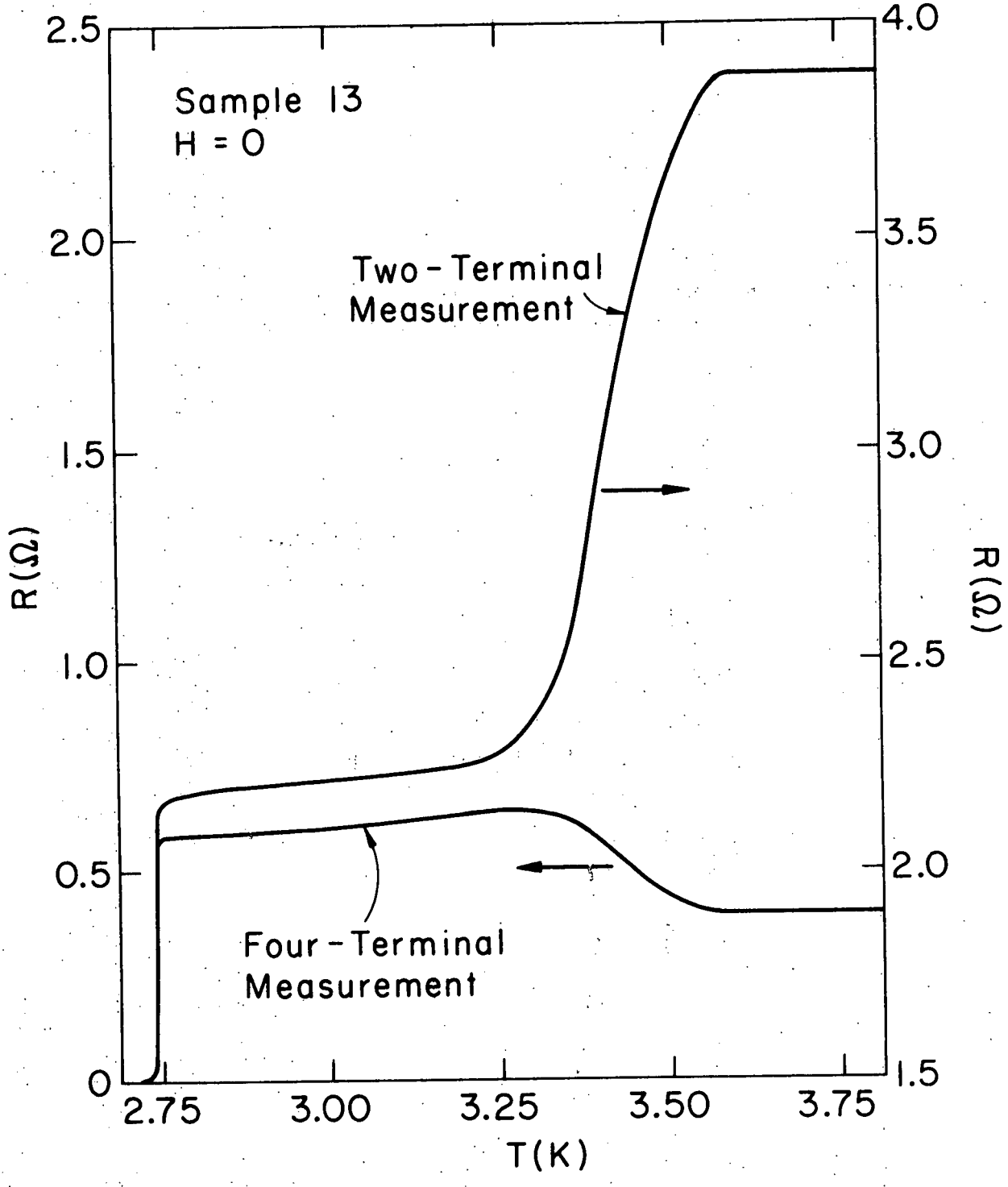

Figure 22. Zero-field resistance of In-Mn sample 13 measured by using two-terminal and four-terminal techniques. The curves are discussed in the text

THIS PAGE
WAS INTENTIONALLY
LEFT BLANK

Figure 23. Typical finite-field resistive transition of In-Mn sample 5. The points on the curve which correspond to data sets 1, 2, and 3 are indicated.

Figure 24. Typical finite-field resistive transition of In-Mn sample 7. The points on the curve which correspond to data sets 1, 2, and 3 are indicated.

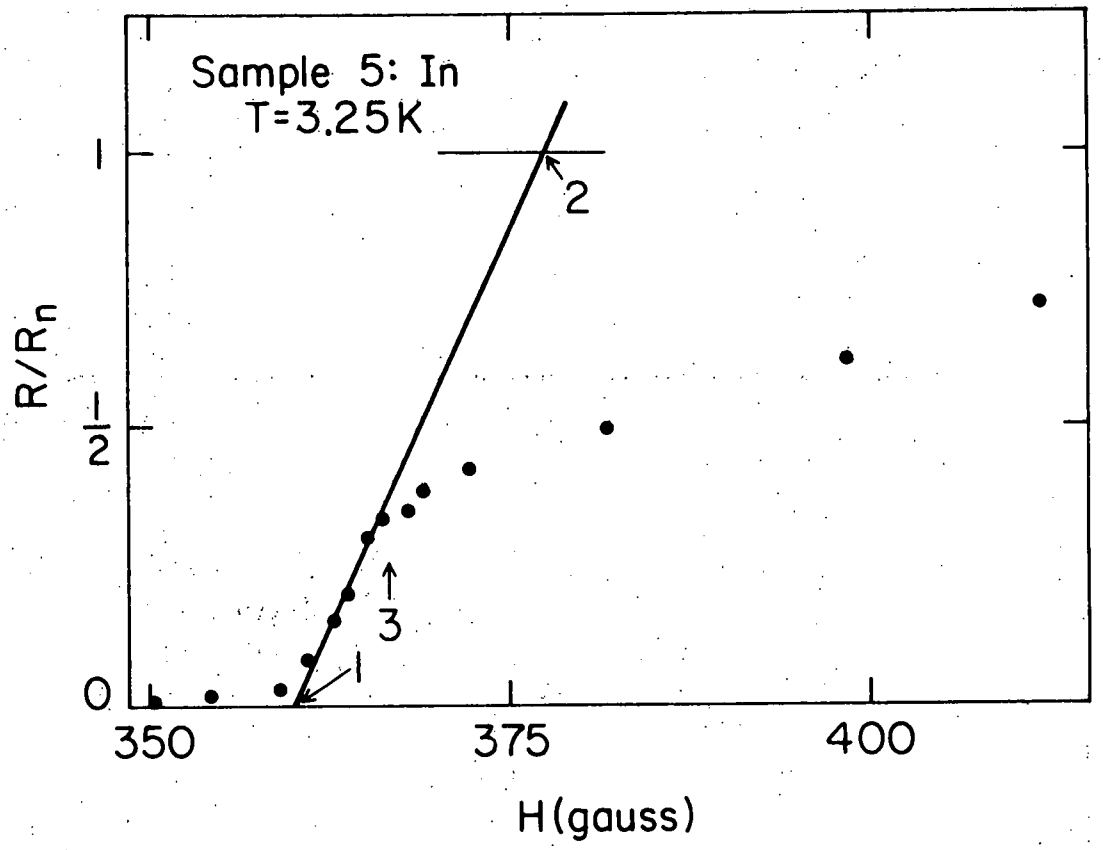
Sample 5: In
T=3.25K
R/Rn
1
1/2
0
350
375
400
H(gauss)
1
2
3

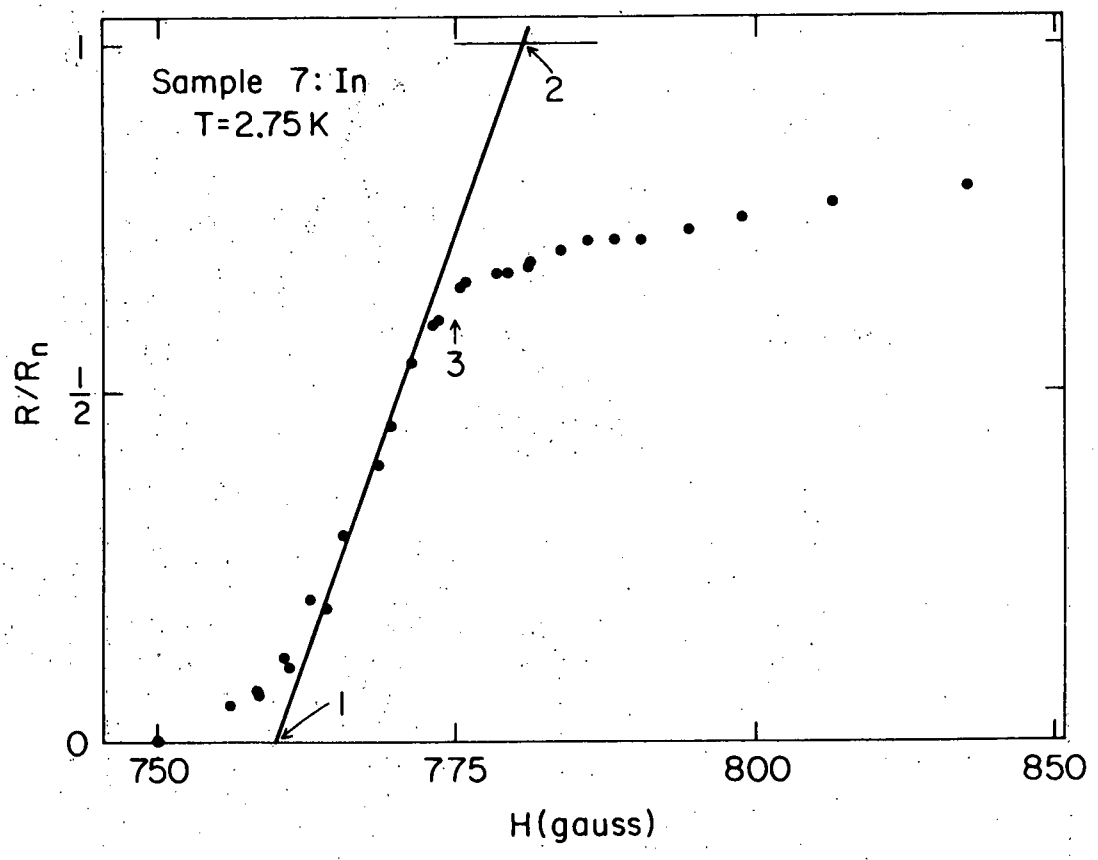
Sample 7: In
T=2.75K
R/Rn
1
1/2
0
750
775
800
850
H(gauss)
1
2
3

THIS PAGE
WAS INTENTIONALLY
LEFT BLANK

Figure 25. Typical finite-field resistive transition of In-Mn sample 13. The points on the curve which correspond to data sets 1, 2, and 3 are indicated.

Figure 26. Typical finite-field resistive transition of In-Mn sample 19. The points on the curve which correspond to data sets 1, 2, and 3 are indicated. Curves are shown for three different values of the measuring current in the sample.

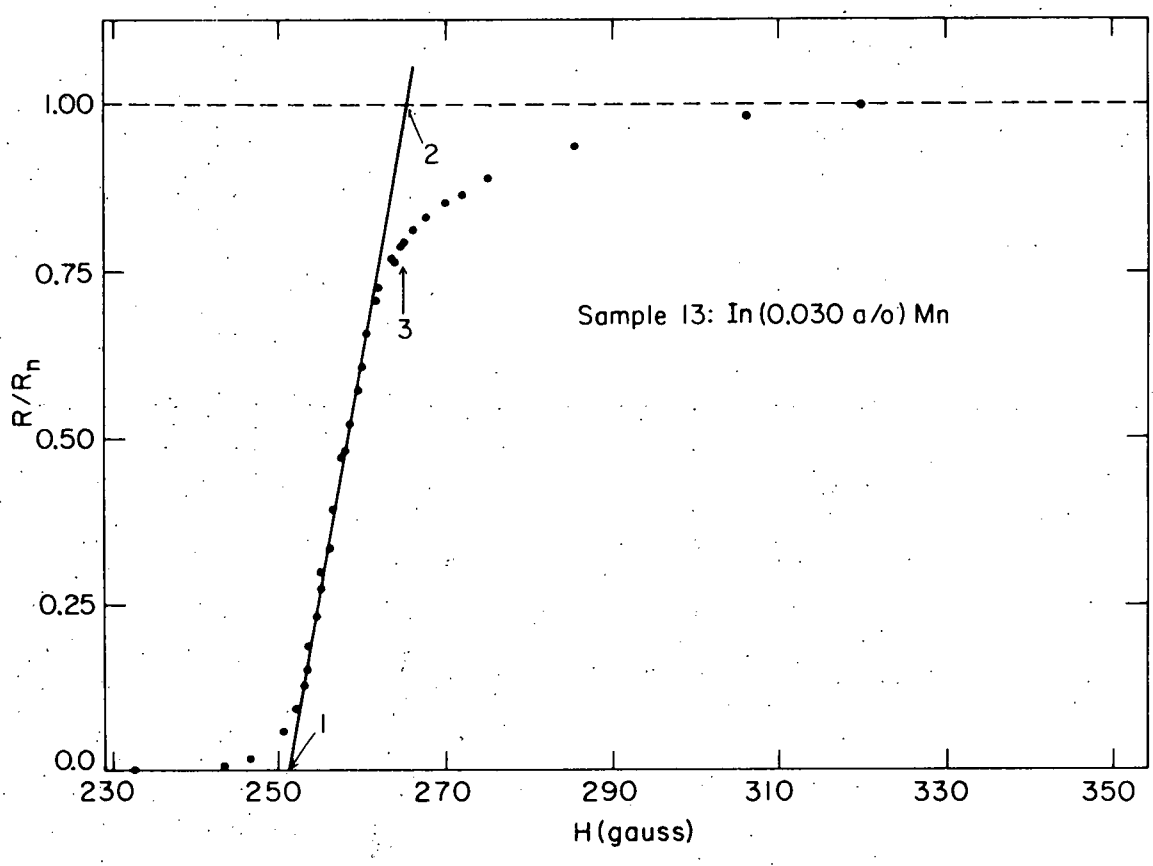
1.00
0.75
0.50
0.25
0.0
R/Rn
230
250
270
290
310
330
350
H(gauss)
Sample 13: In (0.030 a/o) Mn
1
2
3

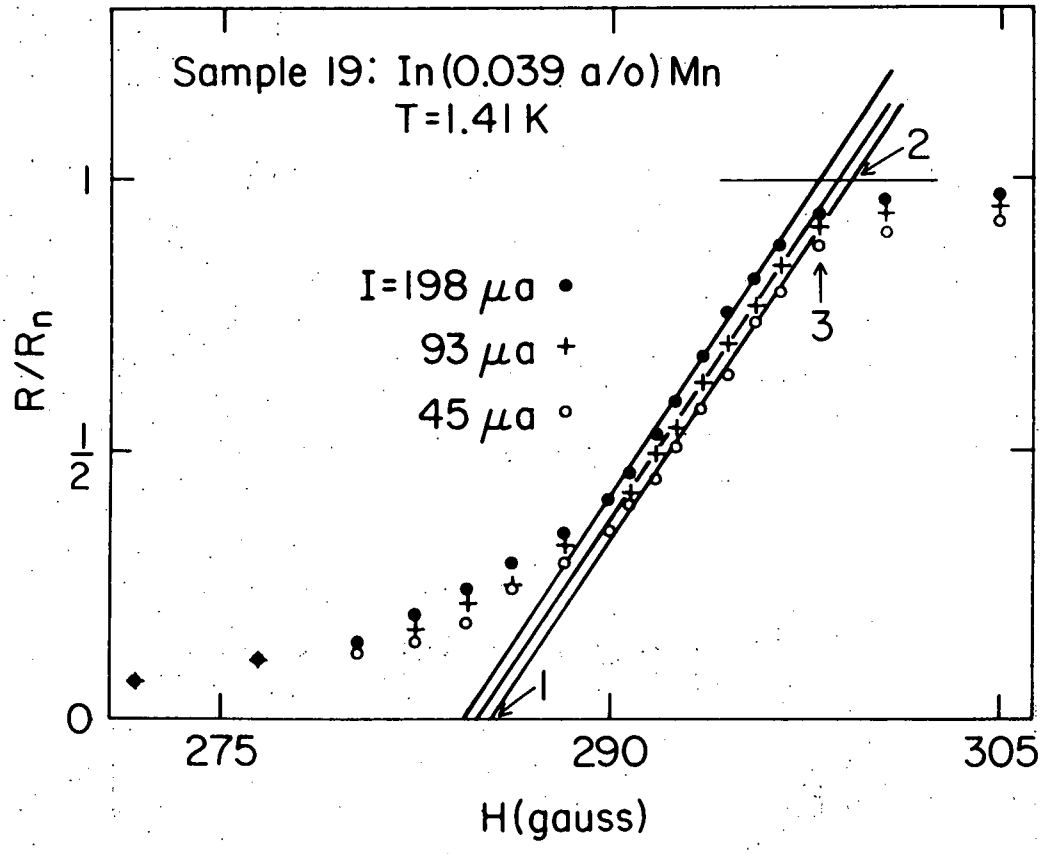
Sample 19: In (0.039 a/o) Mn
T=1.41 K
I=198 μa •
93 μa +
45 μa ∘
1
1/2
0
R/Rn
275
290
305
H(gauss)
1
2
3

Since the extrapolations of the linear part of the curve to R=0 and $R=R_n$ and the position of the knee were almost independent of the measuring current, they were selected as being representative of the position of H_{c2}. (The point where the sample resistance became non-zero was not used because it was too poorly defined.) These three points correspond to data sets 1, 2, and 3.

Previous work on this problem has been done by Cape[74] and by Miller and Cody.[75] Cape worked with chromium-plated foils and found that H_{c2} corresponded to the knee in the transition curve. Miller and Cody worked with scribed films and found that H_{c2} corresponded to the point where the sample resistance first became non-zero.

2. Pb-Mn data

Figure 27 shows the effect of scribing a pure lead film. It is evident that the edges of the film had very nearly the same transition temperature as the rest of it.

The shapes of the zero-field transitions in Pb-Mn were probably determined by broadening due to inhomogeneities, just as in the In-Mn samples. However, because the transition temperature did not depend so strongly on the degree of disorder in the film, the transitions in Pb-Mn were sharper than those in In-Mn. Figures 27 - 32 show the zero-field transitions of the Pb-Mn samples.

The edges of the film which overlapped the electrodes were not scribed. They had the same zero-field transition temperature as the rest of the film, but they presumably had a critical field which was about 8 %

Figure 27. Zero-field resistive transition of Pb-Mn sample C. Data which were taken both before and after the sample film was scribed are shown.

Figure 28. Zero-field resistive transition of Pb-Mn sample H.

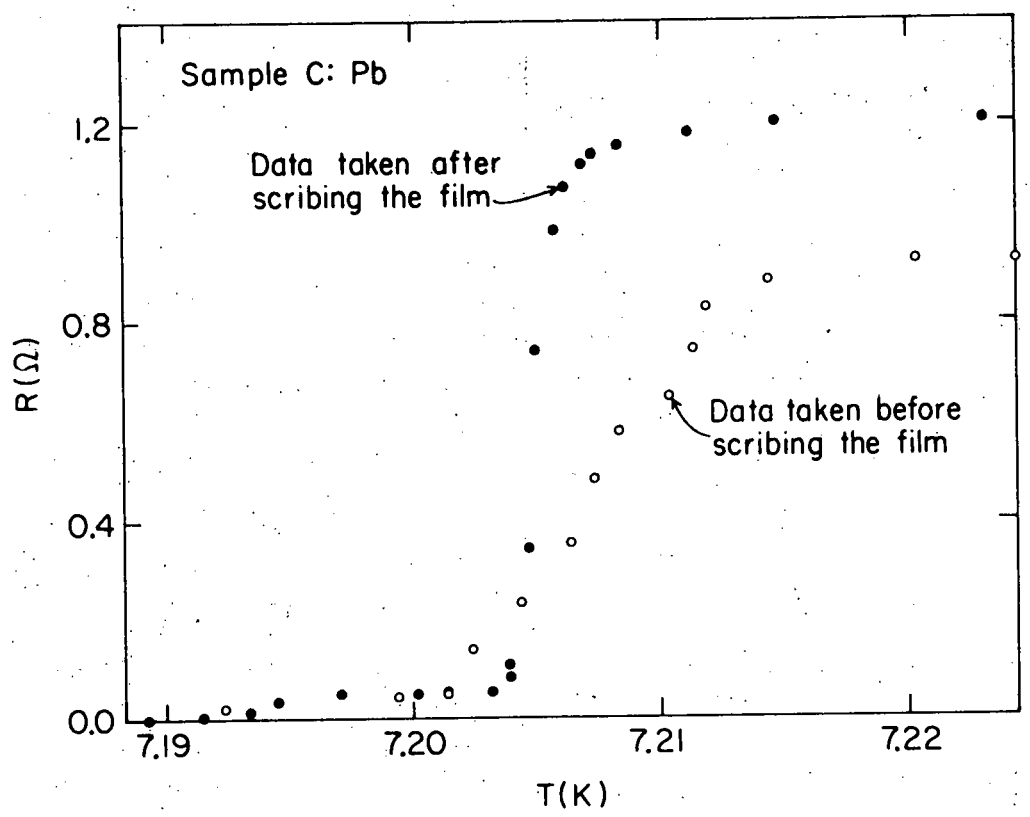
Sample C: Pb
Data taken after scribing the film
Data taken before scribing the film
R(Ω)
1.2
0.8
0.4
0.0
7.19
7.20
7.21
7.22
T(K)

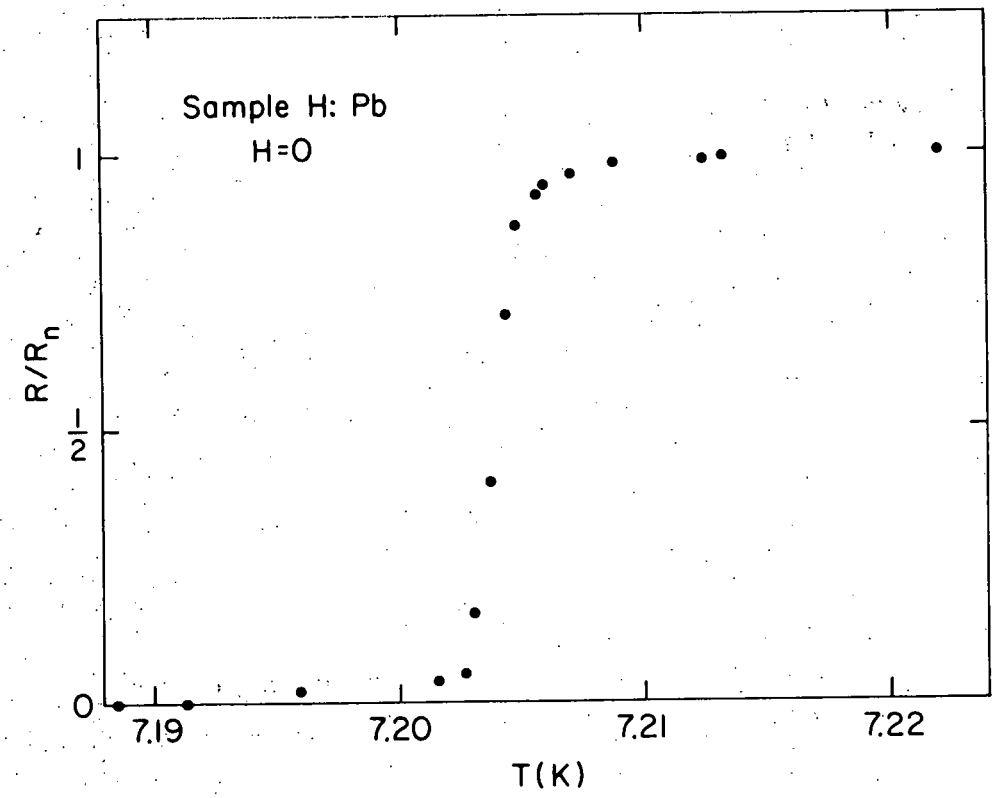
Sample H: Pb
H=0
R/Rn
1
1/2
0
7.19
7.20
7.21
7.22
T(K)

THIS PAGE
WAS INTENTIONALLY
LEFT BLANK

Figure 29. Zero-field resistive transition of Pb-Mn sample D.

Figure 30. Zero-field resistive transition of Pb-Mn sample E.

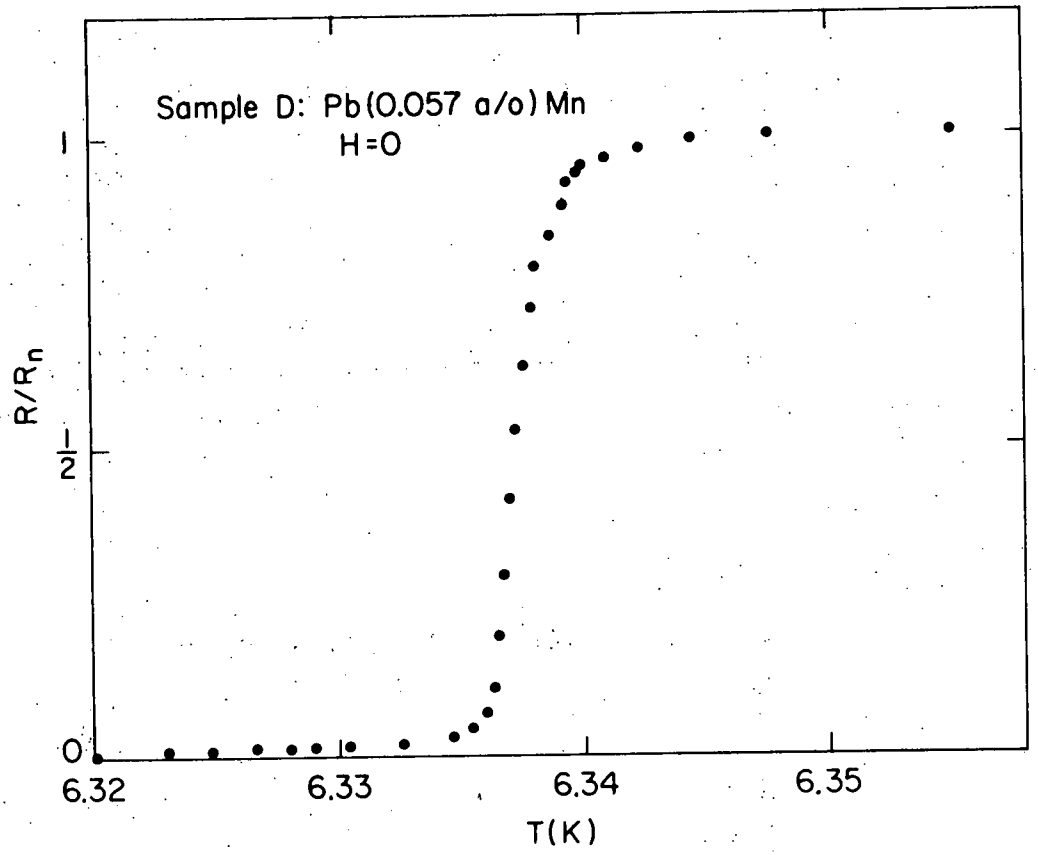
Sample D: Pb(0.057 a/o) Mn
H=0
R/Rn
1
1/2
0
6.32
6.33
6.34
6.35
T(K)

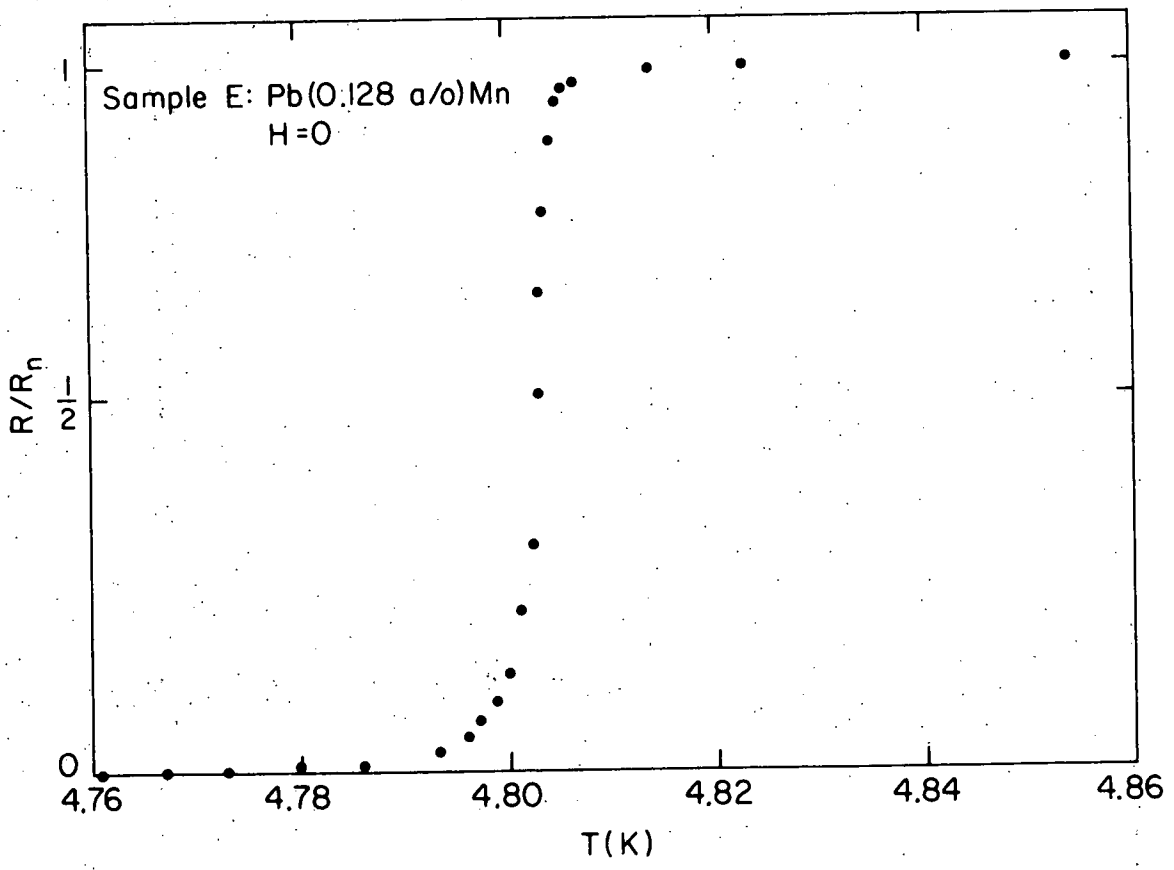
Sample E: Pb(0.128 a/o)Mn
H=0
R/Rn
1
1/2
0
4.76
4.78
4.80
4.82
4.84
4.86
T(K)

THIS PAGE
WAS INTENTIONALLY
LEFT BLANK

Figure 31. Zero-field resistive transition of Pb-Mn sample F.

Figure 32. Zero-field resistive transition of Pb-Mn sample G.

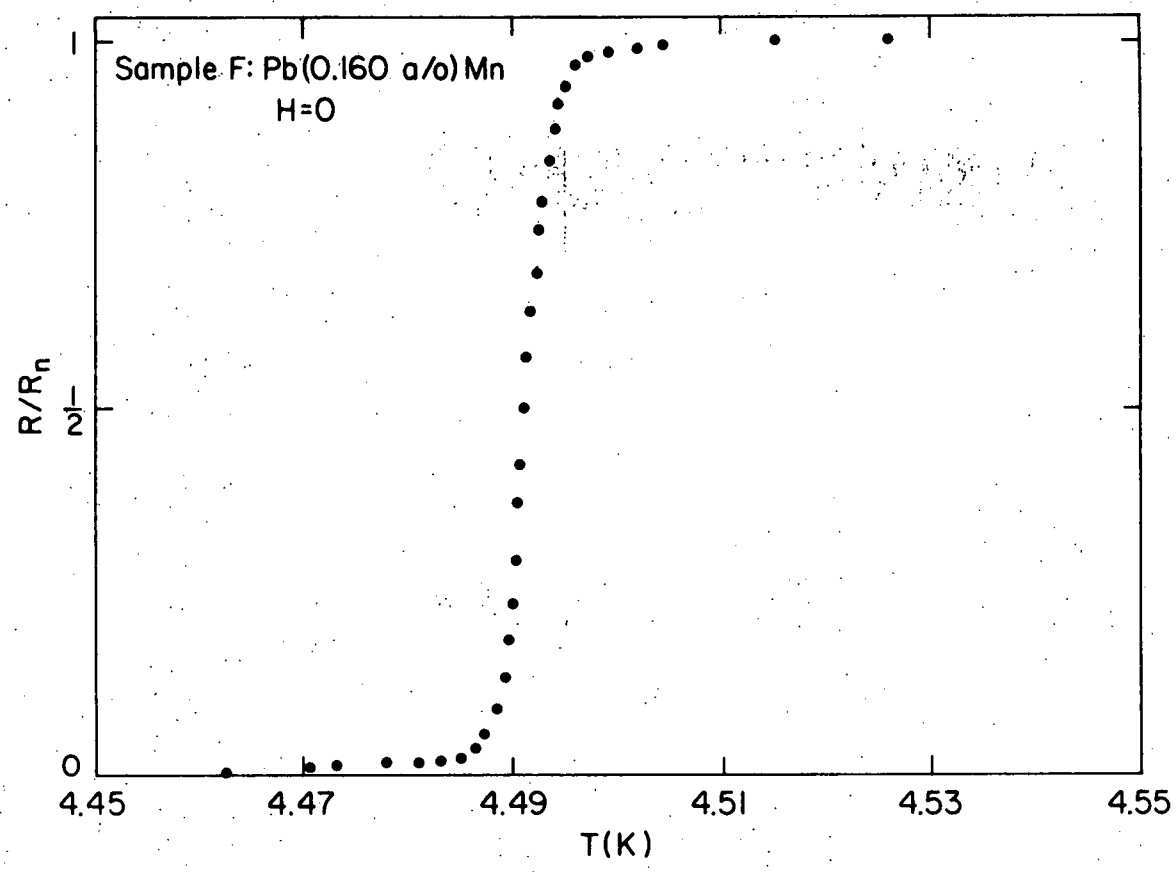
Sample F: Pb(0.160 a/o) Mn
H=0
R/Rn
1
1/2
0
4.45
4.47
4.49
4.51
4.53
4.55
T(K)

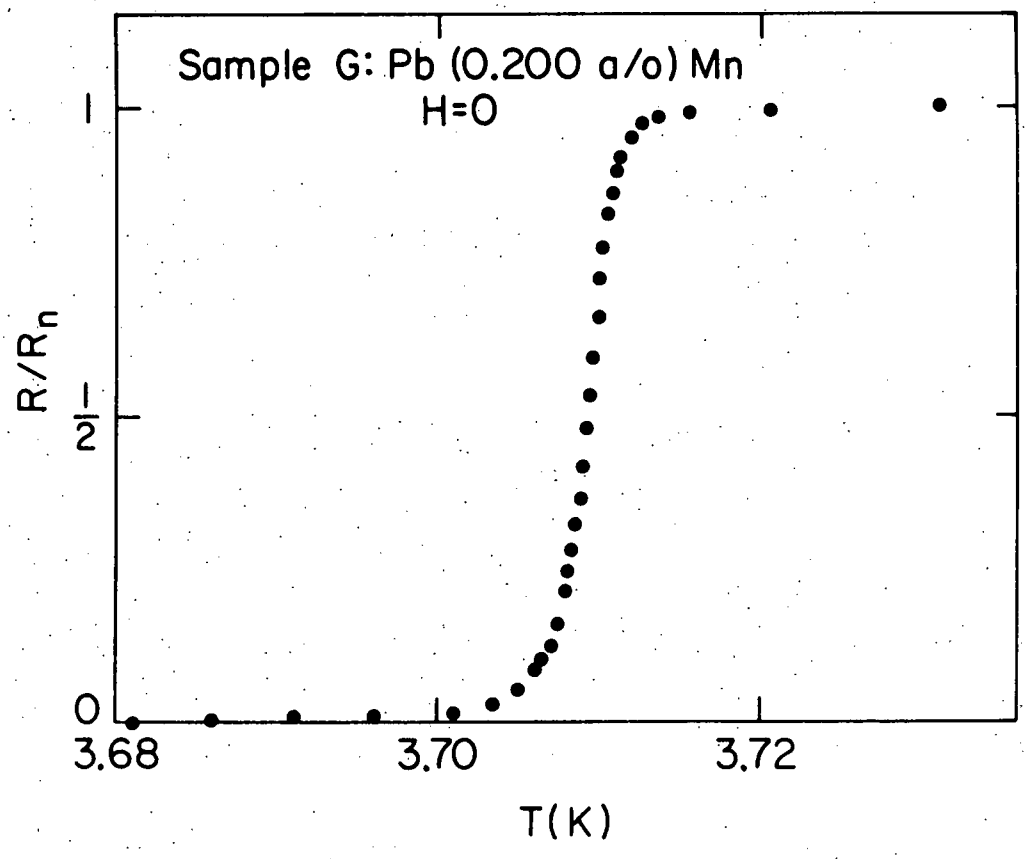
Sample G: Pb (0.200 a/o) Mn
H=0
R/Rn
1
1/2
0
3.68
3.70
3.72
T(K)

higher. Therefore, the edges went normal at a field value which was only slightly larger than the critical field value for the rest of the film. This is the cause of the bump in the R(H) curves shown in Figures 33 - 37. Note that this bump is qualitatively the same as the bump in the four-terminal resistance in Figure 22. Except for sample F, the size of the bump decreases with increasing manganese concentration. This is not understood.

Doubling and halving the measuring current had no effect on the transition curves.

Three points were selected as being appropriate places to assign the critical field. These points were where the sample resistance became non-zero, where the linear part of the curve extrapolated to 0 and where it extrapolated to the maximum resistance (see Figure 8). These three points correspond to data sets 1, 2, and 3 respectively.

THIS PAGE
WAS INTENTIONALLY
LEFT BLANK

Figure 33. Typical finite-field resistive transitions of Pb-Mn sample H. The curves for Pb-Mn sample C were quite similar to these, and they are not shown in a figure.

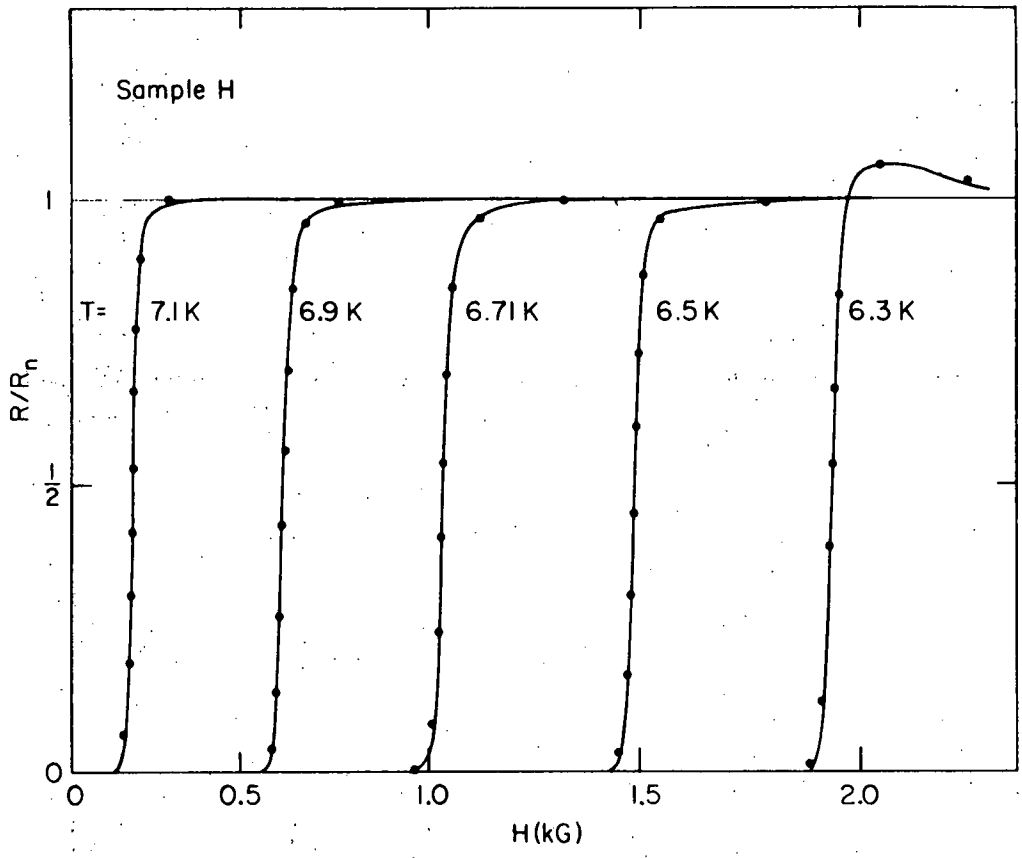
Sample H
T=
7.1 K
6.9 K
6.71 K
6.5 K
6.3 K
R/Rn
1
1/2
0
0
0.5
1.0
1.5
2.0
H(kG)

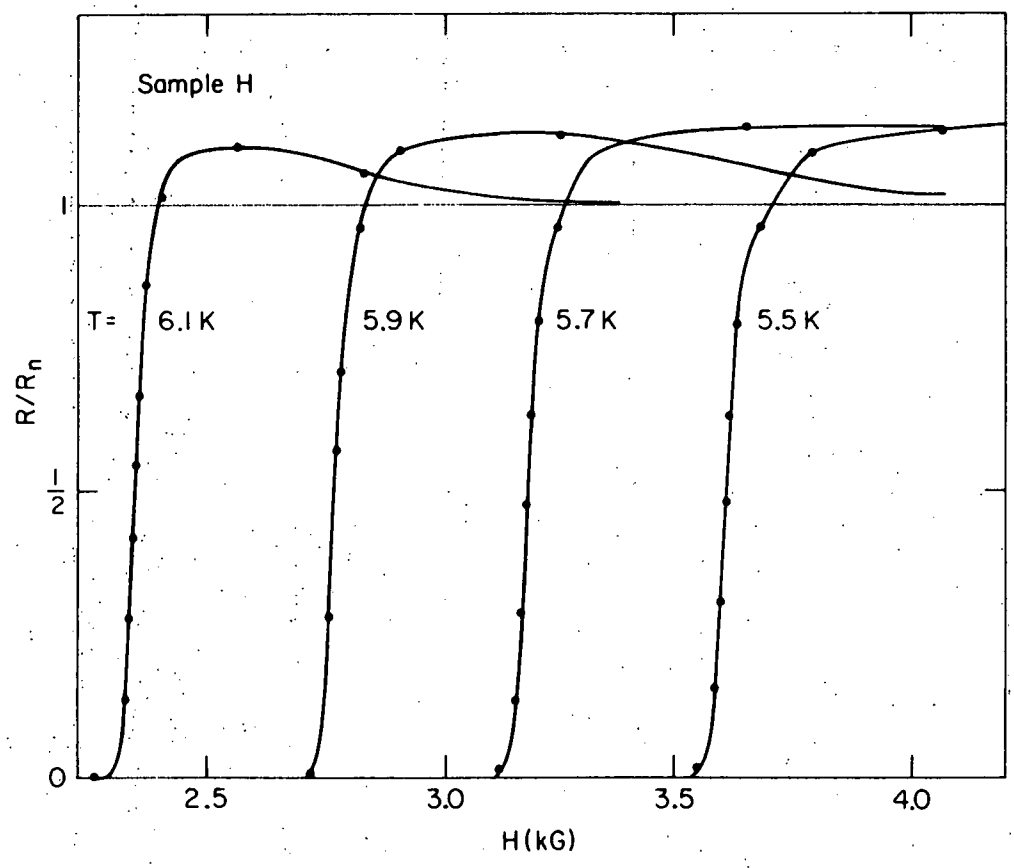
Sample H
T=
6.1 K
5.9 K
5.7 K
5.5 K
R/Rn
1
1/2
0
2.5
3.0
3.5
4.0
H(kG)

THIS PAGE
WAS INTENTIONALLY
LEFT BLANK

Figure 34. Typical finite-field resistive transitions of Pb-Mn sample D.

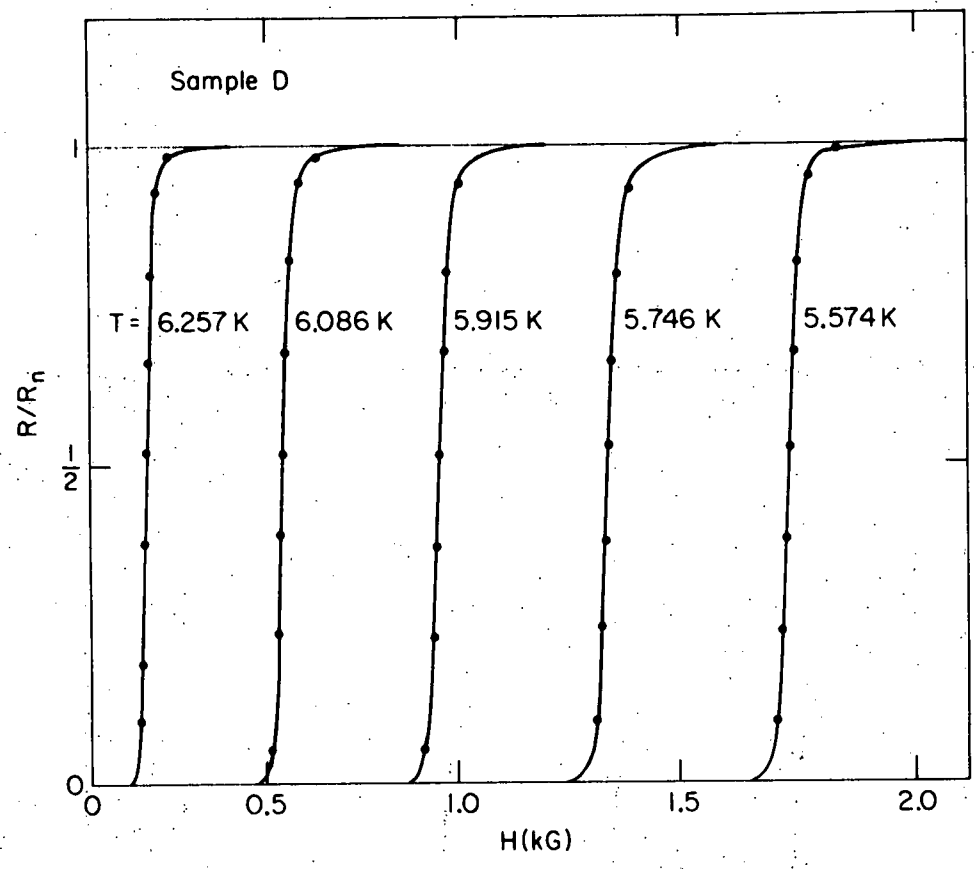
Sample D
T= 6.257 K
6.086 K
5.915 K
5.746 K
5.574 K
R/Rn
1
1/2
0
0
0.5
1.0
1.5
2.0
H(kG)

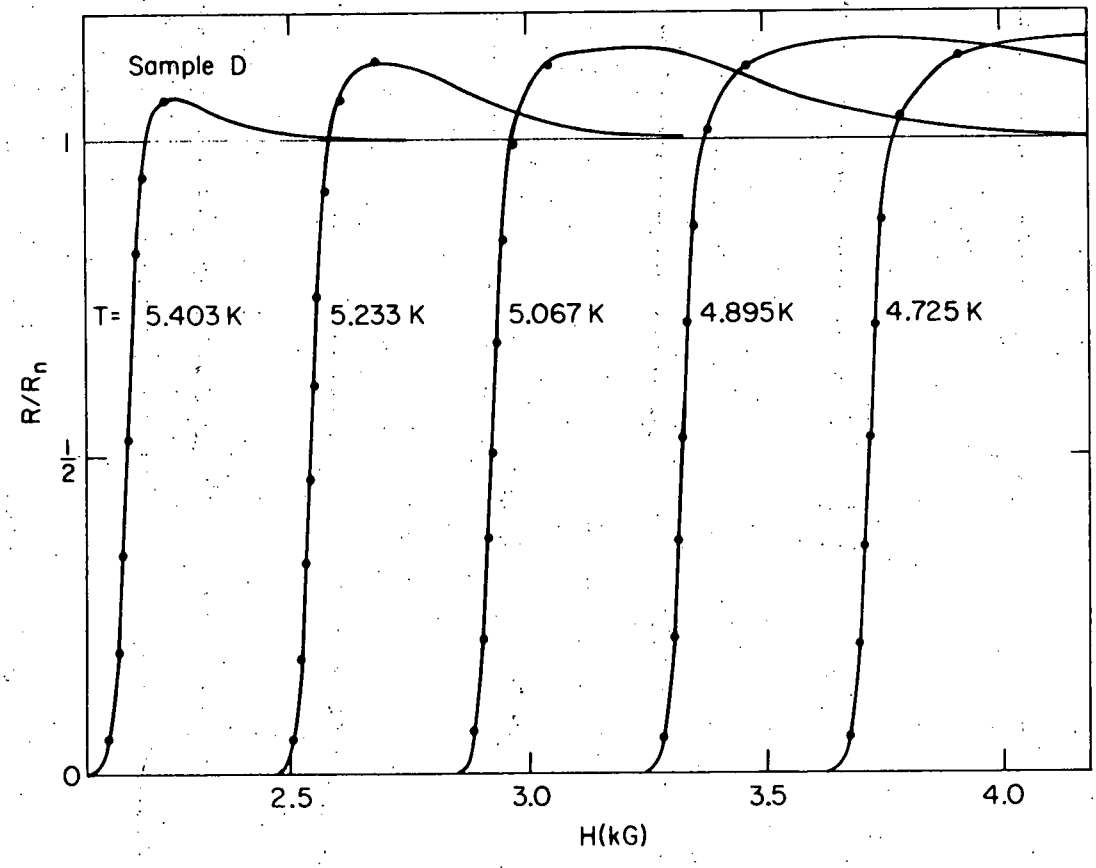
Sample D
T= 5.403 K
5.233 K
5.067 K
4.895 K
4.725 K
R/Rn
1
1/2
0
2.5
3.0
3.5
4.0
H(kG)

THIS PAGE
WAS INTENTIONALLY
LEFT BLANK

Figure 35. Typical finite-field resistive transitions of Pb-Mn sample E.

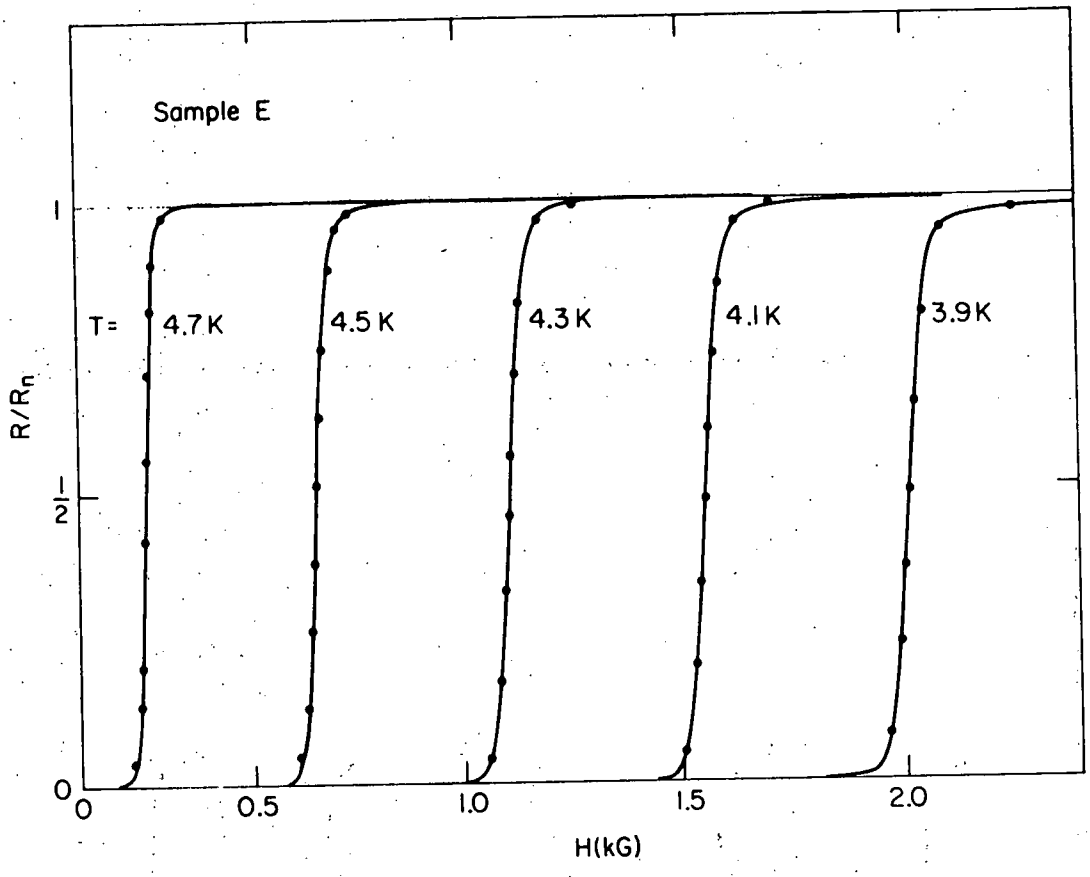
Sample E
T=
4.7 K
4.5 K
4.3 K
4.1 K
3.9 K
R/Rn
1
1/2
0
0
0.5
1.0
1.5
2.0
H(kG)

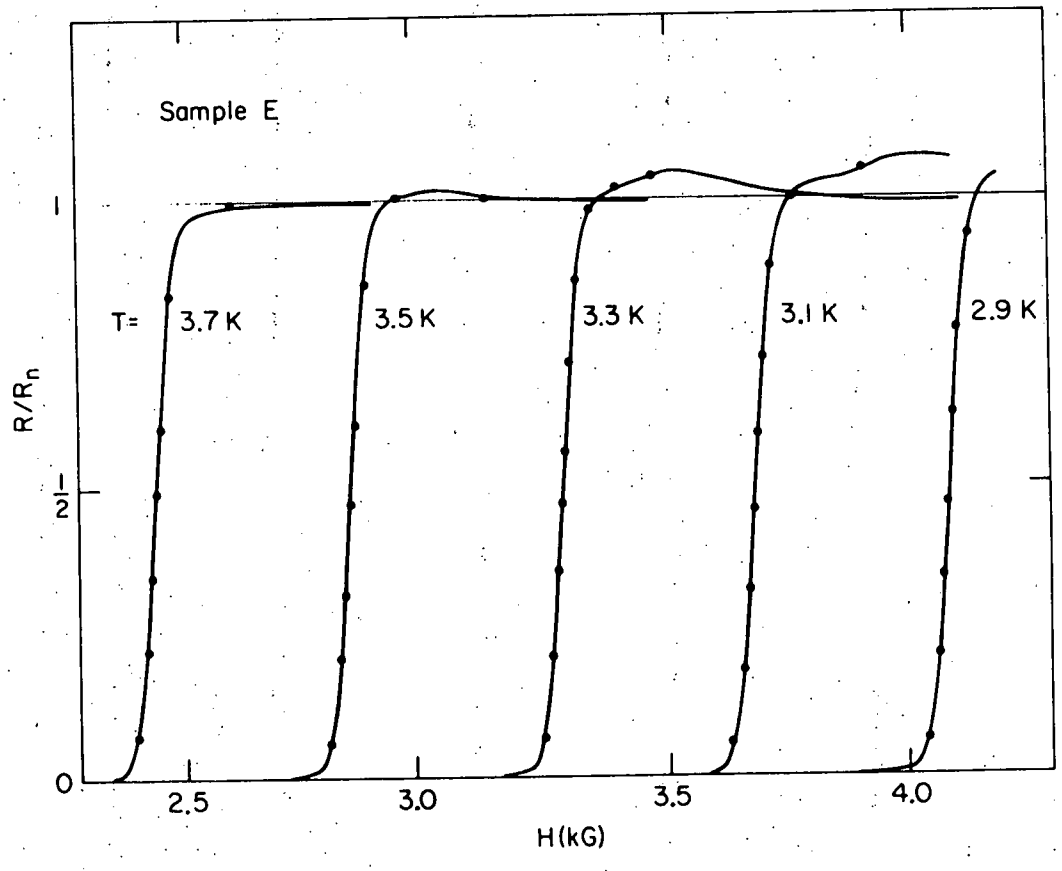
Sample E
T=
3.7 K
3.5 K
3.3 K
3.1 K
2.9 K
R/Rn
1
1/2
0
2.5
3.0
3.5
4.0
H(kG)

THIS PAGE
WAS INTENTIONALLY
LEFT BLANK

Figure 36. Typical finite-field resistive transitions of Pb-Mn sample F.

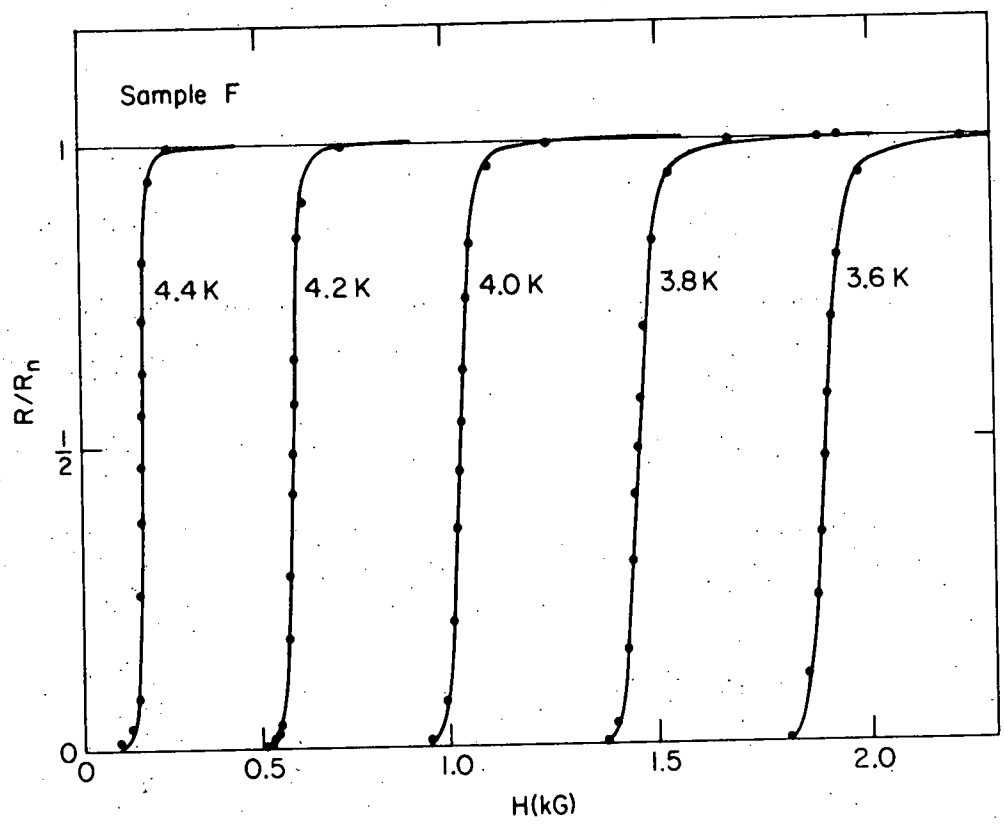
Sample F
4.4 K
4.2 K
4.0 K
3.8 K
3.6 K
R/Rn
1
1/2
0
0
0.5
1.0
1.5
2.0
H(kG)

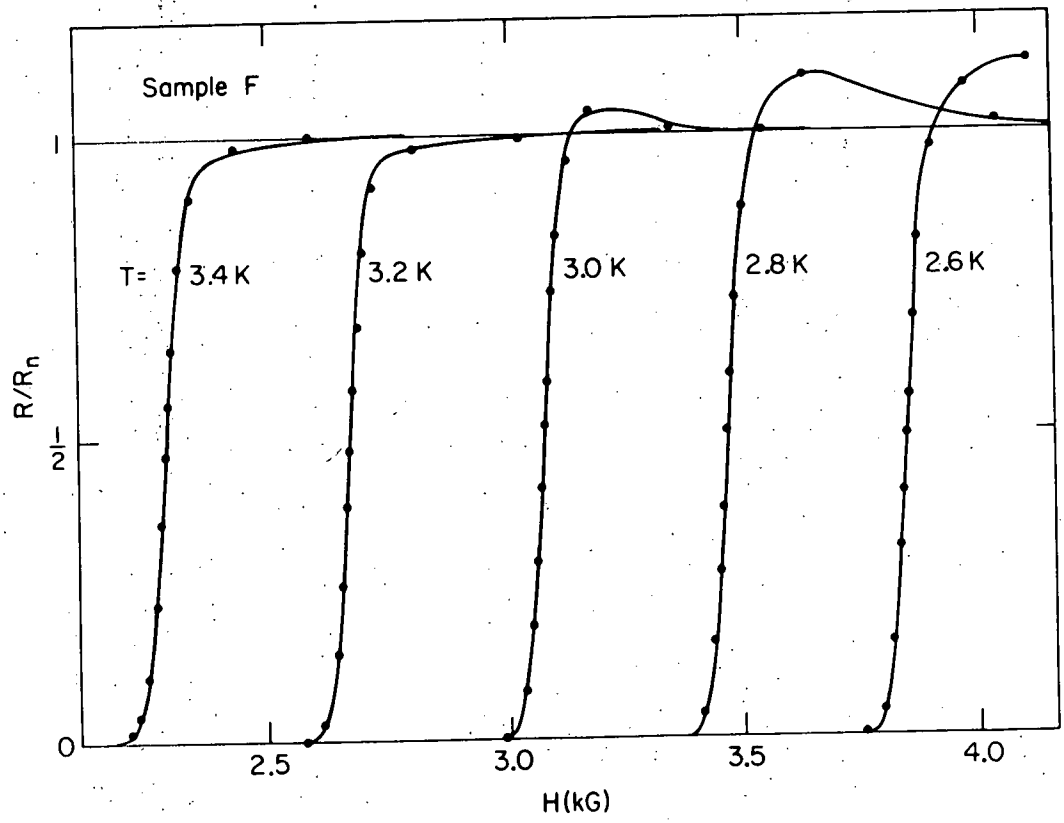
Sample F
T=
3.4 K
3.2 K
3.0 K
2.8 K
2.6 K
R/Rn
1
1/2
0
2.5
3.0
3.5
4.0
H(kG)

THIS PAGE
WAS INTENTIONALLY
LEFT BLANK

Figure 37. Typical finite-field resistive transitions of Pb-Mn sample G.

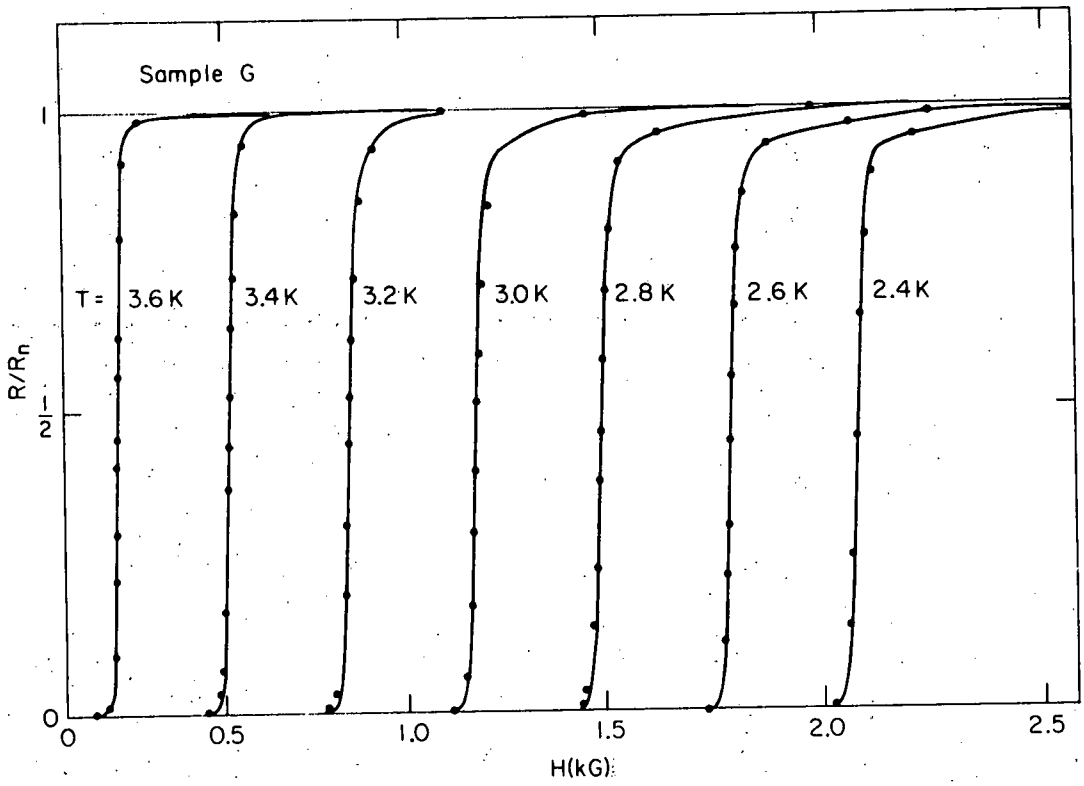
Sample G
T= 3.6 K
3.4 K
3.2 K
3.0 K
2.8 K
2.6 K
2.4 K
R/Rn
1
1/2
0
0
0.5
1.0
1.5
2.0
2.5
H(kG)

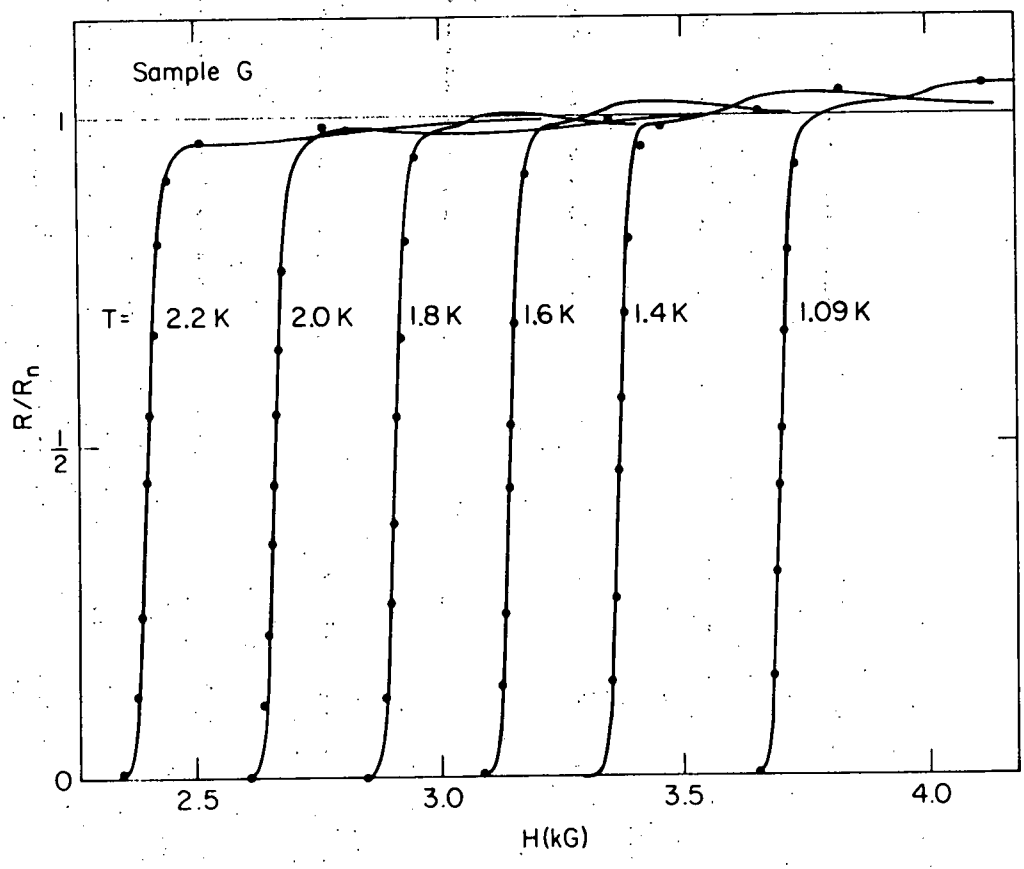
Sample G
T= 2.2 K
2.0 K
1.8 K
1.6 K
1.4 K
1.09 K
R/Rn
1
1/2
0
2.5
3.0
3.5
4.0
H(kG)

Appendix E.

Tables of Data

1. In-Mn data

To fit the Fulde-Maki theory to the In-Mn data, T_c, T_{c0}, and $H_{c2}(0)$ were used as fitting parameters. (Note that this is equivalent to using T_c, T_{c0}, and D as fitting parameters.) To fit the data on pure indium, T_{c0} was set equal to T_c, and then T_c and $H_{c2}(0)$ were varied until a reasonable fit was obtained. The theory fitted the sample 5 data quite well; the rms deviation of the finite-field data from the fit agreed with an estimate of the expected scatter in the data, 2 gauss (see Appendix F). The only discrepancy between the theory and the data was that the curve which fitted the finite-field data did not extrapolate very well to the zero-field data point in data sets 1 and 2.

The FM theory did not fit the sample 7 data as well as the sample 5 data, but the fit was still reasonable. The theory fitted the high-field data, but had difficulty with the low-field points. However, the rms deviation of the data from the theory, excluding the lowest field data point, was comparable to the estimated scatter in the data, 2 gauss. Sample 7 was the only sample for which the fit to one data set was significantly better than the fit to the other two.

The data for samples 13 and 19 were fit in a slightly different way, because in these samples T_c was not equal to T_{c0}. To determine T_{c0} self-consistently for each data set for each sample, we assumed that T_{c0} was inversely proportional to D, as the values of D and T_{c0} from the fits to the data on pure indium indicated. Then, for example, in

Table III. $H_{c2}(T)$ data on In-Mn sample 5 compared with the Fulde-Maki theory.

Sample 5: In

Data Set 1.

TEMP	HC2EXP	HC2THE	DEV	% DEV
1.500	1022.3	1025.9	3.6	0.35
1.750	945.2	944.9	-0.3	-0.03
2.000	859.4	858.2	-1.2	-0.14
2.250	768.7	766.5	-2.2	-0.29
2.500	673.3	670.3	-3.0	-0.45
2.750	570.2	570.2	-0.0	-0.01
3.000	466.0	466.5	0.5	0.11
3.250	360.2	359.7	-0.5	-0.14
3.500	249.6	250.0	0.4	0.15
3.750	137.3	137.6	0.3	0.21
4.066	0.0	-7.9	-7.9	******

RMS DEVIATION = 1.7 GAUSS.
FIT PARAMETERS: TC = 4.049 K, TC0 = 4.049 K, HC2(0) = 1306. GAUSS.
DIFFUSION CONSTANT D = 23.56 CM*CM/SEC.

Data Set 2.

TEMP	HC2EXP	HC2THE	DEV	% DEV
1.500	1041.0	1044.4	3.4	0.32
1.750	960.3	963.5	3.2	0.33
2.000	877.8	876.8	-1.0	-0.12
2.250	787.9	785.0	-2.9	-0.37
2.500	691.4	688.8	-2.6	-0.38
2.750	586.6	588.6	2.0	0.34
3.000	484.4	484.8	0.4	0.09
3.250	377.8	377.9	0.1	0.03
3.500	267.4	268.1	0.7	0.25
3.750	156.2	155.5	-0.7	-0.43
4.069	0.0	8.4	8.4	******

RMS DEVIATION = 2.1 GAUSS.
FIT PARAMETERS: TC = 4.087 K, TC0 = 4.087 K, HC2(0) = 1324. GAUSS.
DIFFUSION CONSTANT D = 23.46 CM*CM/SEC.

Data Set 3.

TEMP	HC2EXP	HC2THE	DEV	% DEV
1.500	1035.2	1036.9	1.7	0.16
1.750	953.5	955.7	2.2	0.23
2.000	870.1	868.6	-1.5	-0.17
2.250	778.3	776.4	-1.9	-0.24
2.500	682.3	679.9	-2.4	-0.36
2.750	577.3	579.3	2.0	0.35
3.000	473.9	475.2	1.3	0.28
3.250	366.9	367.9	1.0	0.27
3.500	255.6	257.7	2.1	0.81
3.750	146.0	144.8	-1.2	-0.83
4.069	0.0	-2.8	-2.8	******

RMS DEVIATION = 1.8 GAUSS.
FIT PARAMETERS: TC = 4.063 K, TC0 = 4.063 K, HC2(0) = 1318. GAUSS.
DIFFUSION CONSTANT D = 23.43 CM*CM/SEC.

Table IV. $H_{c2}(T)$ data on In-Mn sample 7 compared with the Fulde-Maki theory.

Sample 7: In

Data Set 1.

TEMP	HC2EXP	HC2THE	DEV	% DEV
1.271	1414.2	1413.5	-0.7	-0.05
1.500	1327.7	1328.7	1.0	0.08
1.750	1227.5	1228.1	0.6	0.05
2.000	1121.5	1120.1	-1.4	-0.12
2.250	1007.3	1005.8	-1.5	-0.15
2.500	886.6	886.0	-0.6	-0.07
2.750	761.0	761.2	0.2	0.02
3.000	629.8	631.9	2.1	0.34
3.249	498.0	499.2	1.2	0.24
3.500	361.7	361.7	-0.0	-0.00
3.750	222.6	221.4	-1.2	-0.54
4.000	85.5	78.0	-7.5	-8.73
4.167	0.0	-19.3	-19.3	******

RMS DEVIATION = 1.1 GAUSS.
FIT PARAMETERS: TC = 4.134 K, TCO = 4.134 K, HC2(0) = 1676. GAUSS.
DIFFUSION CONSTANT D = 18.75 CM*CM/SEC.

Data Set 2.

TEMP	HC2EXP	HC2THE	DEV	% DEV
1.271	1439.7	1437.2	-2.5	-0.17
1.500	1354.6	1352.3	-2.3	-0.17
1.750	1252.9	1251.3	-1.6	-0.12
2.000	1144.9	1143.1	-1.8	-0.16
2.250	1032.9	1028.4	-4.5	-0.43
2.500	900.8	908.2	-0.6	-0.07
2.750	780.9	783.0	2.1	0.26
3.000	650.0	653.2	3.2	0.50
3.249	515.0	520.0	5.0	0.97
3.500	378.9	382.0	3.1	0.81
3.750	244.6	241.1	-3.5	-1.42
4.000	100.7	97.2	-3.5	-3.49
4.173	0.0	-4.1	-4.1	******

RMS DEVIATION = 3.0 GAUSS.
FIT PARAMETERS: TC = 4.166 K, TCO = 4.166 K, HC2(0) = 1700. GAUSS.
DIFFUSION CONSTANT D = 18.62 CM*CM/SEC.

Data Set 3.

TEMP	HC2EXP	HC2THE	DEV	% DEV
1.271	1435.6	1432.6	-3.0	-0.21
1.500	1348.1	1347.5	-0.6	-0.04
1.750	1249.4	1246.5	-2.9	-0.23
2.000	1138.7	1138.0	-0.7	-0.06
2.250	1025.7	1023.2	-2.5	-0.24
2.500	902.2	902.8	0.6	0.07
2.750	775.4	777.4	2.0	0.26
3.000	643.4	647.5	4.1	0.64
3.249	509.0	514.1	5.1	1.00
3.500	376.1	375.9	-0.2	-0.05
3.750	237.6	234.9	-2.7	-1.13
4.000	101.3	90.8	-10.5	-10.36
4.173	0.0	-10.6	-10.6	******

RMS DEVIATION = 2.7 GAUSS.
FIT PARAMETERS: TC = 4.155 K, TCO = 4.155 K, HC2(0) = 1696. GAUSS.
DIFFUSION CONSTANT D = 18.62 CM*CM/SEC.

Table V. $H_{c2}(T)$ data on In-Mn sample 13 compared with the Fulde-Maki theory.

Sample 13: In(0.030 a/o)Mn

Data Set 1.

TEMP	HC2EXP	HC2THE	DEV	% DEV
1.211	592.2	589.2	-3.0	-0.51
1.390	531.1	532.4	1.3	0.24
1.546	476.9	479.5	2.6	0.55
1.690	426.5	428.2	1.7	0.40
1.845	369.2	370.5	1.3	0.35
2.001	310.3	310.1	-0.2	-0.08
2.151	250.3	249.9	-0.4	-0.17
2.300	190.3	188.3	-2.0	-1.07
2.460	121.3	120.2	-1.1	-0.88
2.603	57.1	57.9	0.8	1.35
2.737	0.0	-1.8	-1.8	******

RMS DEVIATION = 1.7 GAUSS.
FIT PARAMETERS: TC = 2.733 K, TC0 = 4.090 K, HC2(0) = 804. GAUSS.
DIFFUSION CONSTANT D = 21.25 CM*CM/SEC.

Data Set 2.

TEMP	HC2EXP	HC2THE	DEV	% DEV
1.211	614.3	611.5	-2.8	-0.46
1.390	551.0	553.3	2.3	0.42
1.546	496.1	499.2	3.1	0.63
1.690	445.4	446.7	1.3	0.28
1.845	386.5	387.6	1.1	0.27
2.001	325.8	325.6	-0.2	-0.05
2.151	264.6	264.0	-0.6	-0.24
2.300	201.9	200.8	-1.1	-0.53
2.460	131.1	131.1	-0.0	-0.00
2.603	66.1	67.2	1.1	1.62
2.746	0.0	1.8	1.8	******

RMS DEVIATION = 1.7 GAUSS.
FIT PARAMETERS: TC = 2.750 K, TC0 = 4.130 K, HC2(0) = 831. GAUSS.
DIFFUSION CONSTANT D = 20.65 CM*CM/SEC.

Data Set 3.

TEMP	HC2EXP	HC2THE	DEV	% DEV
1.211	611.5	607.4	-4.1	-0.66
1.390	547.8	549.9	2.1	0.38
1.546	493.8	496.3	2.5	0.51
1.690	443.0	444.3	1.3	0.29
1.845	384.6	385.8	1.2	0.31
2.001	325.3	324.5	-0.8	-0.25
2.151	264.6	263.5	-1.1	-0.43
2.300	203.4	201.0	-2.4	-1.18
2.460	133.7	132.0	-1.7	-1.28
2.603	66.1	68.7	2.6	4.00
2.746	0.0	4.1	4.1	******

RMS DEVIATION = 2.2 GAUSS.
FIT PARAMETERS: TC = 2.755 K, TC0 = 4.110 K, HC2(0) = 825. GAUSS.
DIFFUSION CONSTANT D = 20.91 CM*CM/SEC.

Table VI. $H_{c2}(T)$ data on In-Mn sample 19 compared with the Fulde-Maki theory

Sample 19: In(0.039 a/o)Mn

Data Set 1.

TEMP	HC2EXP	HC2THE	DEV	% DEV
1.258	332.1	330.8	-1.3	-0.38
1.316	314.4	313.2	-1.2	-0.38
1.428	278.4	277.9	-0.5	-0.17
1.540	239.6	241.1	1.5	0.64
1.649	202.8	203.9	1.1	0.56
1.764	163.5	163.4	-0.1	-0.08
1.874	123.0	123.3	0.3	0.28
1.987	81.8	81.1	-0.7	-0.89
2.100	38.0	37.7	-0.3	-0.86
2.212	0.0	-6.3	-6.3	******

RMS DEVIATION = 0.9 GAUSS.
FIT PARAMETERS: TC = 2.196 K, TCO = 4.080 K, HC2(0) = 552. GAUSS.
DIFFUSION CONSTANT D = 22.07 CM*CM/SEC.

Data Set 2.

TEMP	HC2EXP	HC2THE	DEV	% DEV
1.258	346.0	344.7	-1.3	-0.38
1.316	326.1	326.7	0.6	0.18
1.428	290.7	290.7	-0.0	-0.00
1.540	252.5	253.1	0.6	0.25
1.649	214.0	215.2	1.2	0.55
1.764	173.2	173.7	0.5	0.32
1.874	133.3	132.9	-0.4	-0.32
1.987	90.6	89.7	-0.9	-0.99
2.100	47.0	45.4	-1.6	-3.45
2.227	0.0	-5.7	-5.7	******

RMS DEVIATION = 0.9 GAUSS.
FIT PARAMETERS: TC = 2.213 K, TCO = 4.120 K, HC2(0) = 570. GAUSS.
DIFFUSION CONSTANT D = 21.51 CM*CM/SEC.

Data Set 3.

TEMP	HC2EXP	HC2THE	DEV	% DEV
1.258	345.0	343.4	-1.6	-0.47
1.316	325.6	325.5	-0.1	-0.03
1.428	289.2	289.8	0.6	0.21
1.540	251.7	252.6	0.9	0.34
1.649	213.7	214.9	1.2	0.57
1.764	173.2	173.9	0.7	0.38
1.874	133.5	133.3	-0.2	-0.13
1.987	91.1	90.5	-0.6	-0.63
2.100	47.5	46.6	-0.9	-1.92
2.227	0.0	-4.0	-4.0	******

RMS DEVIATION = 0.9 GAUSS.
FIT PARAMETERS: TC = 2.217 K, TCO = 4.100 K, HC2(0) = 567. GAUSS.
DIFFUSION CONSTANT D = 21.75 CM*CM/SEC.

data set 1, sample 13, the value of T_{c0} was determined with the formula

$$T_{c0}^{1,13} = T_{c0}^{1,7} - \frac{D^{1,13} - D^{1,7}}{D^{1,5} - D^{1,7}} \times \left[T_{c0}^{1,7} - T_{c0}^{1,5}\right] \qquad (34)$$

$$= 4.134\ \text{K} - \frac{21.25 - 18.75}{23.56 - 18.75} \times [4.134 - 4.049]\ \text{K}$$

$$= 4.090\ \text{K} .$$

Although this rather elaborate procedure was used to determine T_{c0}, the fit was quite insensitive to the actual value of T_{c0}. For instance, holding T_c and $H_{c2}(0)$ constant and varying T_{c0} by $\pm$ 40 mK did not appreciably change the goodness of the fit. Furthermore, for any value of T_{c0} from T_c up to about 4.4 K, values of T_c and $H_{c2}(0)$ could be found which resulted in fits as good as the ones shown in Tables V and VI.

In Tables III through VI, TEMP and HC2EXP are the experimentally measured values of T and $H_{c2}(T)$. HC2THE is a theoretical value of $H_{c2}(T)$ calculated by using the FM theory and the fit parameters indicated.

2. Pb-Mn data

The Pb-Mn data were not well described by the FM theory. In order to analyze the data, we needed the derivative dH_{c2}/dT. To obtain dH_{c2}/dT from the data, we fitted the data with polynomials, and then differentiated the polynomials. Table VII shows characteristics of the polynomial fits. The Table gives the number of coefficients in the polynomial, the rms deviation of the data from the polynomial, and the values of D used to obtain Figure 11.

Table VII. Characteristics of the polynomial fits to the Pb-Mn data.

Sample	Data Set	# of coef's	rms dev. (gauss)	D
C	1	1	4.4	1.114
	2	2	1.7	1.116
	2	3	2.3	1.116
	3	3	2.8	1.140
H	1	3	2.9	1.105
	2	3	1.5	1.101
	3	2	2.1	1.107
D	1	2	6.3	1.005
	2	2	1.6	1.005
	2	3	2.4	1.005
	3	2	1.6	1.029
	3	3	2.3	1.029
E	1	2	6.3	1.005
	2	2	2.2	1.027
	3	2	3.6	1.033
F	1	2	6.0	1.041
	1	2	5.0	1.041
	2	2	3.4	1.063
	2	3	1.6	1.063
	3	2	3.4	1.062
	3	4	2.0	1.062
G	1	3	4.4	1.224
	2	3	1.9	1.279
	3	3	2.2	1.271

Tables VIII through XIII show the experimental values of $H_{c2}(T)$ compared with polynomial fits to the data. The polynomials were fitted to the data by using a least-squares criterion; the quantity defined in Equation (35) was minimized. The computer program which did the fitting was a modified version of a program written by Brian Charles Gibson of our research group. In these tables, TEXP and HC2EXP are the experimentally measured values of T and $H_{c2}(T)$. HC2CAL is the value of $H_{c2}(T)$ calculated from the polynomial fit. Note that TC was chosen to give the best fit.

RMS DEV (CORRECTED FOR DEGREES OF FREEDOM) is equal to[76]

$$\text{RMS DEV} \times \frac{\sqrt{p}}{\sqrt{p-c}} , \qquad (35)$$

where p is the number of data points in the fit, and c is the number of coefficients in the fitting polynomial.

The data on samples C, D, and F were not well fit by a single polynomial. These data were therefore broken into two overlapping groups, and each group was fitted with a different polynomial.

An asterisk in the column next to the %DEV column means that the data point in that row was not included in the set of data points which the program fitted. Two types of data points were excluded from the fits: data points which were several standard deviations away from the polynomial which fitted the other data points, and the zero-field data points. These latter points were excluded because they deviated so far from the fits to the finite-field data in data sets 1 and 2 for all of the samples. Hence, even though the fits to the finite-field data in data set 3 extrapolated well to the zero-field data points, it did not seem consistent to include the zero-field points in the fit.

Table VIII. $H_{c2}(T)$ data on Pb-Mn sample C compared with a polynomial fit.

SAMPLE C, DATA SET 1.

HC2CAL = 0.21200E+04 G (TC-T/K)**1

TC= 7.140 K.

TEXP	TC-T	HC2EXP	HC2CAL	HC2CAL-HC2EXP	%DEV	
5.3580	1.7900	3769.3	3794.9	25.6	0.68	*
5.4510	1.6970	3592.2	3597.7	5.5	0.15	
5.5520	1.5960	3307.1	3303.6	-3.5	-0.10	
5.6340	1.5140	3207.2	3209.7	2.5	0.08	
5.7160	1.4320	3026.4	3035.9	9.5	0.31	
5.8200	1.3280	2821.1	2815.4	-5.7	-0.20	
5.9070	1.2410	2635.1	2631.0	-4.1	-0.16	
6.0010	1.1470	2432.7	2431.7	-1.0	-0.04	
6.0930	1.0550	2244.0	2236.6	-7.4	-0.33	
6.1870	0.9610	2036.1	2037.4	1.3	0.06	
6.2790	0.8690	1841.2	1842.3	1.1	0.06	
6.3690	0.7790	1658.4	1651.5	-6.9	-0.42	
6.4650	0.6830	1449.9	1448.0	-1.9	-0.13	
6.5550	0.5930	1254.3	1257.2	2.9	0.23	
6.6500	0.4980	1053.2	1055.8	2.6	0.25	
6.7410	0.4070	863.4	862.9	-0.5	-0.06	
6.8310	0.3170	670.1	672.1	2.0	0.29	
6.9220	0.2260	473.3	479.1	5.8	1.23	
7.0150	0.1330	281.3	282.0	0.7	0.24	
7.1040	0.0440	127.9	93.3	-34.6	*****	*
7.1770	-0.0290	0.0	-61.5	-61.5	*****	*

RMS DEVIATION IN HC2CAL= 4.4 GAUSS.
RMS DEV(CORRECTED FOR DEGREES OF FREEDOM)= 4.5 GAUSS.

SAMPLE C, DATA SET 3.

HC2CAL = 0.20517E+04 G (TC-T/K)**1
+ 0.63018E+02 G (TC-T/K)**2
+ -0.45725E+01 G (TC-T/K)**5

TC= 7.205 K.

TEXP	TC-T	HC2EXP	HC2CAL	HC2CAL-HC2EXP	%DEV	
5.3580	1.8470	3908.3	3908.9	0.6	0.02	
5.4510	1.7540	3720.7	3719.1	-1.6	-0.04	
5.5520	1.6530	3507.7	3509.4	1.7	0.05	
5.6340	1.5710	3339.5	3337.0	-2.5	-0.08	
5.7160	1.4890	3158.3	3163.0	4.7	0.15	
5.8200	1.3850	2944.1	2940.7	-3.4	-0.12	
5.9070	1.2980	2756.9	2753.8	-3.1	-0.11	
6.0010	1.2040	2546.6	2551.2	4.6	0.18	
6.0930	1.1120	2350.1	2352.6	2.5	0.11	
6.1870	1.0180	2152.8	2149.8	-3.0	-0.14	
6.2790	0.9260	1953.4	1951.5	-1.9	-0.10	
6.3690	0.8360	1760.2	1758.0	-2.2	-0.13	
6.4650	0.7400	1550.7	1552.2	1.5	0.10	
6.5550	0.6500	1355.5	1360.0	4.5	0.33	
6.6500	0.5550	1158.6	1158.1	-0.5	-0.04	
6.7410	0.4640	965.8	965.6	-0.2	-0.02	
6.8310	0.3740	774.5	776.2	1.7	0.22	
6.9220	0.2830	590.0	585.7	-4.3	-0.72	
7.0150	0.1900	393.9	392.1	-1.8	-0.45	
7.1040	0.1010	205.6	207.9	2.3	1.11	
7.2080	-0.0030	0.0	-6.2	-6.2	*****	*

RMS DEVIATION IN HC2CAL= 2.8 GAUSS.
RMS DEV(CORRECTED FOR DEGREES OF FREEDOM)= 3.0 GAUSS.

Table VIII. (cont.)

SAMPLE C, DATA SET 2.

HC2CAL = 0.21215E+04 G (TC-T/K)**1
+ -0.83057E+00 G (TC-T/K)**5

TC= 7.174 K.

TEXP	TC-T	HC2EXP	HC2CAL	HC2CAL-HC2EXP	%DEV	
5.3580	1.8160	3834.2	3836.3	2.1	0.05	
5.4510	1.7230	3646.2	3642.8	-3.4	-0.09	
5.5520	1.6220	3431.1	3431.8	0.7	0.02	
5.6340	1.5400	3260.7	3259.9	-0.8	-0.02	
5.7160	1.4580	3086.8	3087.7	0.9	0.03	
5.8200	1.3540	2868.5	2868.8	0.3	0.01	
5.9070	1.2670	2682.7	2685.2	2.5	0.09	
6.0010	1.1730	2488.3	2486.7	-1.6	-0.06	
6.0930	1.0810	2293.3	2292.1	-1.2	-0.05	
6.1870	0.9870	2092.6	2093.2	0.6	0.03	
7.2030	-0.0290	0.0	-61.5	-61.5	*****	*

RMS DEVIATION IN HC2CAL= 1.7 GAUSS.
RMS DEV(CORRECTED FOR DEGREES OF FREEDOM)= 1.9 GAUSS.

SAMPLE C, DATA SET 2.

HC2CAL = 0.19707E+04 G (TC-T/K)**1
+ 0.23556E+03 G (TC-T/K)**2
+ -0.10377E+03 G (TC-T/K)**3

TC= 7.183 K.

TEXP	TC-T	HC2EXP	HC2CAL	HC2CAL-HC2EXP	%DEV	
5.9070	1.2760	2682.7	2682.6	-0.1	-0.00	
6.0010	1.1820	2488.3	2487.1	-1.2	-0.05	
6.0930	1.0900	2293.3	2293.6	0.3	0.01	
6.1870	0.9960	2092.6	2094.0	1.4	0.07	
6.2790	0.9040	1894.4	1897.4	3.0	0.16	
6.3690	0.8140	1705.4	1704.3	-1.1	-0.07	
6.4650	0.7190	1500.9	1498.0	-2.9	-0.19	
6.5650	0.6280	1306.6	1304.8	-1.8	-0.14	
6.6500	0.5330	1098.6	1101.6	3.0	0.27	
6.7410	0.4420	912.6	908.1	-4.5	-0.49	
6.8310	0.3520	714.5	718.4	3.9	0.54	
6.9220	0.2610	527.2	528.6	1.4	0.26	
7.0150	0.1680	338.0	337.2	-0.8	-0.22	
7.1040	0.0790	157.6	157.1	-0.5	-0.31	
7.2030	-0.0200	0.0	-39.3	-39.3	*****	*

RMS DEVIATION IN HC2CAL= 2.3 GAUSS.
RMS DEV(CORRECTED FOR DEGREES OF FREEDOM)= 2.6 GAUSS.

Table IX. $H_{c2}(T)$ data on Pb-Mn sample H compared with a polynomial fit.

SAMPLE H, DATA SET 1.

HC2CAL = 0.20338E+04 G (TC-T/K)**1
+ 0.17909E+03 G (TC-T/K)**2
+ -0.66035E+02 G (TC-T/K)**5

TC= 7.169 K.

TEXP	TC-T	HC2EXP	HC2CAL	HC2CAL-HC2EXP	%DEV	
6.1040	1.0650	2278.5	2278.6	0.1	0.01	
6.2980	0.8710	1874.4	1874.2	-0.2	-0.01	
6.4000	0.7690	1652.7	1652.1	-0.6	-0.03	
6.5000	0.6690	1433.5	1431.9	-1.6	-0.11	
6.6020	0.5670	1200.6	1206.9	6.3	0.52	
6.7090	0.4600	977.3	972.1	-5.2	-0.53	
6.7980	0.3710	760.3	778.7	18.4	2.42	*
6.8990	0.2700	560.2	562.1	1.9	0.34	
6.9980	0.1710	354.4	353.0	-1.4	-0.39	
7.1020	0.0670	136.2	137.1	0.9	0.64	
7.1910	-0.0220	0.0	-44.7	-44.7	*****	*

RMS DEVIATION IN HC2CAL= 7.9 GAUSS.
RMS DEV(CORRECTED FOR DEGREES OF FREEDOM)= 3.6 GAUSS.

SAMPLE H, DATA SET 2.

HC2CAL = 0.20026E+04 G (TC-T/K)**1
+ 0.22686E+03 G (TC-T/K)**2
+ -0.88507E+02 G (TC-T/K)**4

TC= 7.189 K.

TEXP	TC-T	HC2EXP	HC2CAL	HC2CAL-HC2EXP	%DEV	
6.1040	1.0850	2317.5	2317.2	-0.3	-0.01	
6.2980	0.8910	1907.3	1908.6	1.3	0.07	
6.4000	0.7890	1688.2	1687.0	-1.2	-0.07	
6.5000	0.6890	1468.0	1467.5	-0.5	-0.03	
6.6020	0.5870	1241.4	1243.2	1.8	0.14	
6.7090	0.4800	1011.9	1008.8	-3.1	-0.30	
6.7980	0.3910	813.9	815.6	1.7	0.21	
6.8990	0.2900	598.2	599.2	1.0	0.17	
6.9980	0.1910	391.8	390.7	-1.1	-0.29	
7.1020	0.0870	175.5	175.9	0.4	0.25	
7.2030	-0.0140	0.0	-28.0	-28.0	*****	*

RMS DEVIATION IN HC2CAL= 1.5 GAUSS.
RMS DEV(CORRECTED FOR DEGREES OF FREEDOM)= 1.8 GAUSS.

SAMPLE H, DATA SET 3.

HC2CAL = 0.21432E+04 G (TC-T/K)**1
+ 0.26269E+02 G (TC-T/K)**2

TC= 7.198 K.

TEXP	TC-T	HC2EXP	HC2CAL	HC2CAL-HC2EXP	%DEV	
6.1040	1.0940	2376.7	2377.2	0.5	0.02	
6.2980	0.9000	1951.0	1951.0	-0.0	-0.00	
6.4000	0.7980	1726.7	1727.7	1.0	0.06	
6.5000	0.6980	1511.6	1509.3	-2.3	-0.15	
6.6020	0.5960	1289.5	1287.1	-2.4	-0.18	
6.7090	0.4890	1059.2	1054.7	-0.5	-0.05	
6.7980	0.4000	856.6	861.8	5.2	0.60	
6.8990	0.2990	643.1	643.4	0.3	0.04	
6.9980	0.2000	430.2	429.8	-0.4	-0.09	
7.1020	0.0960	207.8	206.0	-1.8	-0.85	
7.2050	-0.0070	0.0	-15.0	-15.0	*****	*

RMS DEVIATION IN HC2CAL= 2.1 GAUSS.
RMS DEV(CORRECTED FOR DEGREES OF FREEDOM)= 2.3 GAUSS.

Table X. $H_{c2}(T)$ data on Pb-Mn sample D compared with a polynomial fit.

SAMPLE D, DATA SET 1.

HC2CAL = 0.23752E+04 G (TC-T/K)**1
+ -0.36432E+02 G (TC-T/K)**2

TC= 6.286 K.

TEXP	TC-T	HC2EXP	HC2CAL	HC2CAL-HC2EXP	%DEV	
4.6420	1.6440	3817.8	3806.3	-11.5	-0.30	
4.7250	1.5610	3603.4	3618.9	15.5	0.43	
4.8090	1.4770	3425.0	3428.7	3.7	0.11	
4.8950	1.3910	3245.7	3233.4	-12.3	-0.38	
4.9800	1.3060	3039.0	3039.9	0.9	0.03	
5.0670	1.2190	2839.3	2841.2	1.9	0.07	
5.1480	1.1380	2644.4	2655.8	11.4	0.43	
5.2330	1.0530	2468.5	2460.7	-7.8	-0.32	
5.3220	0.9640	2253.3	2255.8	2.5	0.11	
5.4030	0.8830	2067.0	2068.9	1.9	0.09	
5.4910	0.7950	1872.8	1865.2	-7.6	-0.40	
5.5740	0.7120	1672.5	1672.7	0.2	0.01	
5.6600	0.6260	1474.2	1472.6	-1.6	-0.11	
5.7460	0.5400	1274.1	1272.0	-2.1	-0.17	
5.8280	0.4580	1081.0	1080.2	-0.8	-0.07	
5.9150	0.3710	866.4	876.2	9.8	1.13	
6.0000	0.2860	683.3	676.3	-7.0	-1.02	
6.0860	0.2000	468.8	473.6	4.8	1.02	
6.1690	0.1170	278.1	277.4	-0.7	-0.25	
6.2570	0.0290	107.8	68.8	-39.0	*****	*
6.3220	-0.0360	0.0	-85.6	-85.6	*****	*

RMS DEVIATION IN HC2CAL= 7.2 GAUSS.
RMS DEV(CORRECTED FOR DEGREES OF FREEDOM)= 7.6 GAUSS.

Table X. (cont.)

SAMPLE D, DATA SET 2.

HC2CAL = 0.23708E+04 G (TC-T/K)**1
+ -0.31965E+02 G (TC-T/K)**2

TC= 6.310 K.

TEXP	TC-T	HC2EXP	HC2CAL	HC2CAL-HC2EXP	%DEV	
4.6420	1.6680	3867.9	3865.6	-2.3	-0.06	
4.7250	1.5850	3675.3	3677.5	2.2	0.06	
4.8090	1.5010	3485.1	3486.6	1.5	0.04	
4.8950	1.4150	3293.7	3290.7	-3.0	-0.09	
4.9800	1.3300	3095.8	3096.7	0.9	0.03	
5.0670	1.2430	2896.1	2897.6	1.5	0.05	
5.1480	1.1620	2710.0	2711.7	1.7	0.06	
5.2330	1.0770	2516.2	2516.3	0.1	0.00	
5.3220	0.9880	2312.8	2311.2	-1.6	-0.07	
5.4030	0.9070	2125.1	2124.0	-1.1	-0.05	
5.4910	0.8190	1920.8	1920.3	-0.5	-0.03	
5.5740	0.7360	1727.2	1727.6	0.4	0.02	
5.6600	0.6500	1529.1	1527.5	-1.6	-0.10	
5.7460	0.5640	1325.2	1327.0	1.8	0.13	
6.3360	-0.0260	0.0	-61.7	-61.7	*****	*

RMS DEVIATION IN HC2CAL= 1.6 GAUSS.
RMS DEV(CORRECTED FOR DEGREES OF FREEDOM)= 1.7 GAUSS.

SAMPLE D, DATA SET 2.

HC2CAL = 0.21587E+04 G (TC-T/K)**1
+ 0.36634E+03 G (TC-T/K)**2
+ -0.22914E+03 G (TC-T/K)**3

TC= 6.324 K.

TEXP	TC-T	HC2EXP	HC2CAL	HC2CAL-HC2EXP	%DEV	
5.4910	0.8330	1920.8	1920.1	-0.7	-0.04	
5.5740	0.7500	1727.2	1728.6	1.4	0.08	
5.6600	0.6640	1529.1	1527.9	-1.2	-0.08	
5.7460	0.5780	1325.2	1326.0	0.8	0.06	
5.8280	0.4960	1132.5	1132.9	0.4	0.04	
5.9150	0.4090	926.7	928.6	1.9	0.20	
6.0000	0.3240	735.8	730.1	-5.7	-0.77	
6.0860	0.2380	530.3	531.5	1.2	0.22	
6.1690	0.1550	338.8	342.6	3.8	1.11	
6.2570	0.0670	147.8	146.2	-1.6	-1.07	
6.3360	-0.0120	0.0	-25.9	-25.9	*****	*

RMS DEVIATION IN HC2CAL= 2.4 GAUSS.
RMS DEV(CORRECTED FOR DEGREES OF FREEDOM)= 2.9 GAUSS.

Table X. (cont.)

SAMPLE D, DATA SET 3.

HC2CAL = 0.23319E+04 G (TC-T/K)**1
+ -0.80504E+00 G (TC-T/K)**5

TC= 6.341 K.

TEXP	TC-T	HC2EXP	HC2CAL	HC2CAL-HC2EXP	%DEV	
4.6420	1.6990	3947.5	3949.4	1.9	0.05	
4.7250	1.6160	3759.3	3758.6	-0.7	-0.02	
4.8090	1.5320	3566.7	3565.0	-1.7	-0.05	
4.8950	1.4460	3368.1	3366.3	-1.8	-0.05	
4.9800	1.3610	3169.5	3169.6	0.1	0.00	
5.0670	1.2740	2969.1	2967.9	-1.2	-0.04	
5.1480	1.1930	2775.6	2779.8	4.2	0.15	
5.2330	1.1080	2581.0	2582.3	1.3	0.05	
5.3220	1.0190	2375.1	2375.2	0.1	0.01	
5.4030	0.9380	2188.8	2186.7	-2.1	-0.10	
5.4910	0.8500	1982.3	1981.7	-0.6	-0.03	
5.5740	0.7670	1788.7	1788.3	-0.4	-0.02	
5.6600	0.6810	1587.7	1587.9	0.2	0.01	
5.7460	0.5950	1386.3	1387.4	1.1	0.08	
6.3390	0.0020	0.0	4.7	4.7	*****	*

RMS DEVIATION IN HC2CAL= 1.6 GAUSS.
RMS DEV(CORRECTED FOR DEGREES OF FREEDOM)= 1.8 GAUSS.

SAMPLE D, DATA SET 3.

HC2CAL = 0.22272E+04 G (TC-T/K)**1
+ 0.26617E+03 G (TC-T/K)**2
+ -0.17704E+03 G (TC-T/K)**3

TC= 6.343 K.

TEXP	TC-T	HC2EXP	HC2CAL	HC2CAL-HC2EXP	%DEV	
5.4910	0.8520	1982.3	1981.3	-1.0	-0.05	
5.5740	0.7690	1788.7	1789.6	0.9	0.05	
5.6600	0.6830	1587.7	1589.0	1.3	0.08	
5.7460	0.5970	1386.3	1386.8	0.5	0.04	
5.8280	0.5150	1194.2	1193.4	-0.8	-0.06	
5.9150	0.4280	992.9	988.1	-4.8	-0.48	
6.0000	0.3430	785.3	788.1	2.8	0.36	
6.0860	0.2570	583.7	587.0	3.3	0.56	
6.1690	0.1740	397.3	394.7	-2.6	-0.66	
6.2570	0.0860	192.9	193.4	0.5	0.26	
6.3390	0.0040	0.0	8.9	8.9	*****	*

RMS DEVIATION IN HC2CAL= 2.3 GAUSS.
RMS DEV(CORRECTED FOR DEGREES OF FREEDOM)= 2.7 GAUSS.

Table XI. $H_{c2}(T)$ data on Pb-Mn sample E compared with a polynomial fit.

SAMPLE E, DATA SET 1.

HC2CAL = 0.22734E+04 G (TC-T/K)**1
+ -0.33040E+02 G (TC-T/K)**3

TC= 4.747 K.

TEXP	TC-T	HC2EXP	HC2CAL	HC2CAL-HC2EXP	%DEV	
2.9010	1.8460	3987.8	3988.9	1.1	0.03	
3.0010	1.7460	3800.7	3793.6	-7.1	-0.19	
3.1000	1.6470	3595.0	3596.7	1.7	0.05	
3.2020	1.5450	3381.0	3390.6	9.6	0.28	
3.2990	1.4480	3191.8	3191.6	-0.2	-0.01	
3.4010	1.3460	2973.8	2979.5	5.7	0.19	
3.5010	1.2460	2732.4	2768.8	36.4	1.33	*
3.5990	1.1480	2571.9	2559.9	-12.0	-0.47	
3.6990	1.0480	2352.2	2344.5	-7.7	-0.33	
3.8000	0.9470	2128.0	2124.9	-3.1	-0.15	
3.8980	0.8490	1905.4	1909.9	4.5	0.24	
4.0000	0.7470	1685.8	1684.5	-1.3	-0.08	
4.0990	0.6480	1441.7	1464.2	22.5	1.56	*
4.2000	0.5470	1234.1	1238.2	4.1	0.33	
4.3000	0.4470	1009.1	1013.3	4.2	0.41	
4.4000	0.3470	774.4	787.5	13.1	1.69	
4.4990	0.2480	565.5	563.3	-2.2	-0.39	
4.6010	0.1460	337.2	331.8	-5.4	-1.60	
4.7010	0.0460	110.1	104.6	-5.5	-5.02	
4.7720	-0.0250	0.0	-56.8	-56.8	*****	*

RMS DEVIATION IN HC2CAL= 6.3 GAUSS.
RMS DEV(CORRECTED FOR DEGREES OF FREEDOM)= 6.8 GAUSS.

SAMPLE E, DATA SET 2.

HC2CAL = 0.22310E+04 G (TC-T/K)**1
+ -0.11306E+02 G (TC-T/K)**4

TC= 4.783 K.

TEXP	TC-T	HC2EXP	HC2CAL	HC2CAL-HC2EXP	%DEV	
2.9010	1.8820	4059.0	4058.3	-0.7	-0.02	
3.0010	1.7820	3864.6	3863.0	-1.6	-0.04	
3.1000	1.6830	3664.1	3665.3	1.2	0.03	
3.2020	1.5810	3454.3	3457.8	3.5	0.10	
3.2990	1.4840	3258.9	3257.1	-1.8	-0.06	
3.4010	1.3820	3041.2	3043.0	1.8	0.06	
3.5010	1.2820	2829.1	2830.6	1.5	0.05	
3.5990	1.1840	2622.8	2620.2	-2.6	-0.10	
3.6990	1.0840	2406.1	2403.6	-2.5	-0.10	
3.8000	0.9830	2183.4	2183.3	-0.1	-0.01	
3.8980	0.8850	1966.2	1968.2	2.0	0.10	
4.0000	0.7830	1744.6	1743.2	-1.4	-0.08	
4.0990	0.6840	1527.9	1524.0	-3.9	-0.25	
4.2000	0.5830	1297.9	1299.8	1.9	0.15	
4.3000	0.4830	1078.4	1077.3	-1.1	-0.10	
4.4000	0.3830	852.5	854.5	2.0	0.24	
4.4990	0.2840	629.1	633.7	4.6	0.74	
4.6010	0.1820	405.2	406.2	1.0	0.24	
4.7010	0.0820	184.0	183.0	-1.0	-0.54	
4.8010	-0.0180	0.0	-40.2	-40.2	*****	*

RMS DEVIATION IN HC2CAL= 2.2 GAUSS.
RMS DEV(CORRECTED FOR DEGREES OF FREEDOM)= 2.3 GAUSS.

Table XI. (cont.)

SAMPLE E, DATA SET 3.

HC2CAL = 0.22823E+04 G (TC-T/K)**1
+ -0.29817E+02 G (TC-T/K)**3

TC= 4.804 K.

TEXP	TC-T	HC2EXP	HC2CAL	HC2CAL-HC2EXP	%DEV	
2.9010	1.9030	4135.2	4137.6	2.4	0.06	
3.0010	1.8030	3944.6	3940.1	-4.5	-0.11	
3.1000	1.7040	3745.9	3741.4	-4.5	-0.12	
3.2020	1.6020	3530.3	3533.6	3.3	0.09	
3.2990	1.5050	3335.3	3333.1	-2.2	-0.06	
3.4010	1.4030	3116.0	3119.7	3.7	0.12	
3.5010	1.3030	2901.3	2907.8	6.5	0.22	
3.5990	1.2050	2694.3	2697.9	3.6	0.14	
3.6990	1.1050	2481.8	2481.7	-0.1	-0.01	
3.8000	1.0040	2261.4	2261.2	-0.2	-0.01	
3.8980	0.9060	2048.9	2045.5	-3.4	-0.16	
4.0000	0.8040	1818.7	1819.4	0.7	0.04	
4.0990	0.7050	1603.4	1598.5	-4.9	-0.30	
4.2000	0.6040	1379.5	1371.9	-7.6	-0.55	
4.3000	0.5040	1144.9	1146.4	1.5	0.13	
4.4000	0.4040	920.7	920.1	-0.6	-0.07	
4.4990	0.3050	692.8	695.2	2.4	0.35	
4.6010	0.2030	462.0	463.0	1.0	0.23	
4.7010	0.1030	232.1	235.0	2.9	1.27	
4.8050	-0.0010	0.0	-2.3	-2.3	*****	*

RMS DEVIATION IN HC2CAL= 3.6 GAUSS.
RMS DEV(CORRECTED FOR DEGREES OF FREEDOM)= 3.8 GAUSS.

Table XII. $H_{c2}(T)$ data on Pb-Mn sample F compared with a polynomial fit.

SAMPLE F, DATA SET 1.

HC2CAL = 0.21841E+04 G (TC-T/K)**1
+ -0.86211E+02 G (TC-T/K)**2

TC= 4.449 K.

TEXP	TC-T	HC2EXP	HC2CAL	HC2CAL-HC2EXP	%DEV	
2.5000	1.9490	3927.5	3929.3	1.8	0.05	
2.6000	1.8490	3747.4	3743.6	-3.8	-0.10	
2.7000	1.7490	3559.7	3556.2	-3.5	-0.10	
2.8000	1.6490	3370.2	3367.1	-3.1	-0.09	
2.9000	1.5490	3171.5	3176.3	4.8	0.15	
2.9990	1.4500	2971.3	2985.7	14.4	0.48	
3.1000	1.3490	2789.6	2789.4	-0.2	-0.01	
3.2000	1.2490	2593.9	2593.4	-0.5	-0.02	
3.3000	1.1490	2404.9	2395.7	-9.2	-0.38	
3.4000	1.0490	2205.0	2196.2	-8.8	-0.40	
3.5000	0.9490	1989.4	1995.1	5.7	0.28	
3.6000	0.8490	1793.3	1792.1	-1.2	-0.06	
3.7000	0.7490	1584.1	1587.5	3.4	0.22	
4.4660	-0.0170	0.0	-37.2	-37.2	*****	*

RMS DEVIATION IN HC2CAL= 6.0 GAUSS.
RMS DEV(CORRECTED FOR DEGREES OF FREEDOM)= 6.6 GAUSS.

SAMPLE F, DATA SET 1.

HC2CAL = 0.21390E+04 G (TC-T/K)**1
+ -0.22207E+02 G (TC-T/K)**4

TC= 4.442 K.

TEXP	TC-T	HC2EXP	HC2CAL	HC2CAL-HC2EXP	%DEV	
3.3000	1.1420	2404.9	2404.9	-0.0	-0.00	
3.4000	1.0420	2205.0	2202.6	-2.4	-0.11	
3.5000	0.9420	1989.4	1997.4	8.0	0.40	
3.6000	0.8420	1793.3	1789.9	-3.4	-0.19	
3.7000	0.7420	1584.1	1580.4	-3.7	-0.23	
3.8000	0.6420	1374.7	1369.5	-5.2	-0.38	
3.9010	0.5410	1154.5	1155.3	0.8	0.07	
4.0000	0.4420	941.0	944.6	3.6	0.38	
4.1000	0.3420	731.3	731.2	-0.1	-0.01	
4.2010	0.2410	504.6	515.4	10.8	2.15	
4.3000	0.1420	307.0	303.7	-3.3	-1.06	
4.3990	0.0430	98.0	92.0	-6.0	-6.14	
4.4660	-0.0240	0.0	-51.3	-51.3	*****	*

RMS DEVIATION IN HC2CAL= 5.0 GAUSS.
RMS DEV(CORRECTED FOR DEGREES OF FREEDOM)= 5.5 GAUSS.

Table XII. (cont.)

SAMPLE F, DATA SET 2.

HC2CAL = 0.22433E+04 G (TC-T/K)**1
+ -0.10271E+03 G (TC-T/K)**2

TC= 4.456 K.

TEXP	TC-T	HC2EXP	HC2CAL	HC2CAL-HC2EXP	%DEV	
2.5000	1.9560	3991.2	3995.0	3.8	0.10	
2.6000	1.8560	3812.5	3809.8	-2.7	-0.07	
2.7000	1.7560	3628.8	3622.6	-6.2	-0.17	
2.8000	1.6560	3429.2	3433.3	4.1	0.12	
2.9000	1.5560	3244.0	3242.0	-2.0	-0.06	
2.9290	1.4570	3047.8	3050.5	2.7	0.09	
3.1000	1.3560	2853.9	2853.1	-0.8	-0.03	
3.2000	1.2560	2651.6	2655.6	4.0	0.15	
3.3000	1.1560	2454.3	2456.0	1.7	0.07	
3.4000	1.0560	2257.6	2254.4	-3.2	-0.14	
3.5000	0.9560	2051.5	2050.8	-0.7	-0.04	
3.6000	0.8560	1849.2	1845.0	-4.2	-0.23	
3.7000	0.7560	1633.8	1637.3	3.5	0.21	
4.4080	-0.0320	0.0	-71.9	-71.9	*****	*

RMS DEVIATION IN HC2CAL= 3.4 GAUSS.
RMS DEV(CORRECTED FOR DEGREES OF FREEDOM)= 3.7 GAUSS.

SAMPLE F, DATA SET 2.

HC2CAL = 0.20552E+04 G (TC-T/K)**1
+ 0.15360E+03 G (TC-T/K)**3
+ -0.11612E+03 G (TC-T/K)**4

TC= 4.481 K.

TEXP	TC-T	HC2EXP	HC2CAL	HC2CAL-HC2EXP	%DEV	
3.3000	1.1810	2454.3	2454.3	0.0	0.00	
3.4000	1.0810	2257.6	2257.2	-0.4	-0.02	
3.5000	0.9810	2051.5	2053.6	2.1	0.10	
3.6000	0.8810	1849.2	1845.7	-3.5	-0.19	
3.7000	0.7810	1633.8	1635.1	1.3	0.08	
3.8000	0.6810	1422.4	1423.1	0.7	0.05	
3.9010	0.5800	1208.9	1208.9	-0.0	-0.00	
4.0000	0.4810	998.5	999.4	0.9	0.09	
4.1000	0.3810	791.2	789.1	-2.1	-0.27	
4.2010	0.2800	576.5	578.1	1.6	0.28	
4.3000	0.1810	374.3	372.8	-1.5	-0.41	
4.3990	0.0820	167.7	168.6	0.9	0.54	
4.4080	-0.0070	0.0	-14.4	-14.4	*****	*

RMS DEVIATION IN HC2CAL= 1.4 GAUSS.
RMS DEV(CORRECTED FOR DEGREES OF FREEDOM)= 1.8 GAUSS.

Table XII. (cont.)

SAMPLE F, DATA SET 3.

HC2CAL = 0.22377E+04 G (TC-T/K)**1
+ -0.94776E+02 G (TC-T/K)**2

TC= 4.492 K.

TEXP	TC-T	HC2EXP	HC2CAL	HC2CAL-HC2EXP	%DEV	
2.5000	1.9920	4076.3	4081.4	5.1	0.13	
2.6000	1.8920	3897.2	3894.5	-2.7	-0.07	
2.7000	1.7920	3711.2	3705.6	-5.6	-0.15	
2.8000	1.6920	3512.8	3514.9	2.1	0.06	
2.9000	1.5920	3325.9	3322.2	-3.7	-0.11	
2.9990	1.4930	3129.0	3129.6	0.6	0.02	
3.1000	1.3920	2930.5	2931.2	0.7	0.03	
3.2000	1.2920	2725.7	2732.9	7.2	0.26	
3.3000	1.1920	2533.5	2532.7	-0.8	-0.03	
3.4000	1.0920	2331.5	2330.6	-0.9	-0.04	
3.5000	0.9920	2127.0	2126.5	-0.5	-0.02	
3.6000	0.8920	1923.6	1920.6	-3.0	-0.15	
3.7000	0.7920	1711.5	1712.8	1.3	0.08	
4.4940	-0.0020	0.0	-4.5	-4.5	*****	*

RMS DEVIATION IN HC2CAL= 3.4 GAUSS.
RMS DEV(CORRECTED FOR DEGREES OF FREEDOM)= 3.7 GAUSS.

SAMPLE F, DATA SET 3.

HC2CAL = 0.20179E+04 G (TC-T/K)**1
+ 0.44853E+03 G (TC-T/K)**2
+ -0.46851E+03 G (TC-T/K)**3
+ 0.13462E+03 G (TC-T/K)**4

TC= 4.498 K.

TEXP	TC-T	HC2EXP	HC2CAL	HC2CAL-HC2EXP	%DEV	
3.3000	1.1980	2533.5	2533.0	-0.5	-0.02	
3.4000	1.0980	2331.5	2331.9	0.4	0.02	
3.5000	0.9980	2127.0	2128.5	1.5	0.07	
3.6000	0.8980	1923.6	1922.1	-1.5	-0.08	
3.7000	0.7980	1711.5	1712.4	0.9	0.05	
3.8000	0.6980	1499.7	1499.7	-0.0	-0.00	
3.9010	0.5970	1285.0	1282.0	-3.0	-0.24	
4.0000	0.4980	1066.2	1066.6	0.4	0.04	
4.1000	0.3980	845.8	848.0	2.2	0.26	
4.2010	0.2970	624.4	627.7	3.3	0.52	
4.3000	0.1980	417.5	413.7	-3.8	-0.91	
4.3990	0.0990	204.5	203.7	-0.8	-0.38	
4.4940	0.0040	0.0	8.1	8.1	*****	*

RMS DEVIATION IN HC2CAL= 2.0 GAUSS.
RMS DEV(CORRECTED FOR DEGREES OF FREEDOM)= 2.4 GAUSS.

Table XIII. $H_{c2}(T)$ data on Pb-Mn sample G compared with a polynomial fit.

SAMPLE G, DATA SET 1.

HC2CAL = 0.18138E+04 G (TC-T/K)**1
+ -0.12543E+03 G (TC-T/K)**2
+ -0.12623E+02 G (TC-T/K)**3

TC= 3.644 K.

TEXP	TC-T	HC2EXP	HC2CAL	HC2CAL-HC2EXP	%DEV	
1.0890	2.5550	3630.0	3603.4	-26.6	-0.73	*
1.3000	2.3440	3401.5	3398.6	-2.9	-0.09	
1.4000	2.2440	3291.5	3294.8	3.3	0.10	
1.5000	2.1440	3186.8	3186.8	0.0	0.00	
1.6010	2.0430	3079.0	3073.5	-5.5	-0.18	
1.7000	1.9440	2951.6	2958.5	6.9	0.23	
1.8000	1.8440	2835.9	2838.3	2.4	0.08	
1.9000	1.7440	2716.2	2714.2	-2.0	-0.07	
2.0000	1.6440	2508.7	2506.2	-2.5	-0.10	
2.1000	1.5440	2449.7	2454.5	4.8	0.20	
2.2000	1.4440	2319.7	2319.1	-0.6	-0.02	
2.3000	1.3440	2189.2	2180.2	-9.0	-0.41	
2.4000	1.2440	2032.6	2037.6	5.0	0.25	
2.5000	1.1440	1893.2	1891.6	-1.6	-0.08	
2.6000	1.0440	1737.8	1742.3	4.5	0.26	
2.7000	0.9440	1589.2	1589.6	0.4	0.03	
2.8000	0.8440	1440.3	1433.7	-6.6	-0.46	
2.9000	0.7440	1277.6	1274.7	-2.9	-0.23	
3.0000	0.6440	1111.2	1112.6	1.4	0.12	
3.1000	0.5440	948.6	947.5	-1.1	-0.12	
3.2000	0.4440	770.8	779.4	8.6	1.12	
3.3000	0.3440	604.1	608.5	4.4	0.73	
3.4000	0.2440	440.7	434.9	-5.8	-1.32	
3.5000	0.1440	259.8	258.5	-1.3	-0.49	
3.5990	0.0450	102.1	81.4	-20.7	*****	*
3.6030	-0.0390	0.0	-70.9	-70.9	*****	*

RMS DEVIATION IN HC2CAL= 4.4 GAUSS.
RMS DEV(CORRECTED FOR DEGREES OF FREEDOM)= 4.7 GAUSS.

SAMPLE G, DATA SET 2.

HC2CAL = 0.16950E+04 G (TC-T/K)**1
+ -0.66593E+02 G (TC-T/K)**3
+ 0.87432E+01 G (TC-T/K)**4

TC= 3.696 K.

TEXP	TC-T	HC2EXP	HC2CAL	HC2CAL-HC2EXP	%DEV	
1.0890	2.6070	3662.8	3644.9	-17.9	-0.49	*
1.3000	2.3960	3436.2	3435.3	-0.9	-0.03	
1.4000	2.2960	3331.8	3330.6	-1.2	-0.04	
1.5000	2.1960	3220.8	3222.1	1.3	0.04	
1.6010	2.0950	3109.4	3108.8	-0.6	-0.02	
1.7000	1.9960	2991.3	2994.1	2.8	0.09	
1.8000	1.8960	2872.9	2874.4	1.5	0.05	
1.9000	1.7960	2749.6	2750.9	1.3	0.05	
2.0000	1.6960	2624.1	2623.6	-0.5	-0.02	
2.1000	1.5960	2493.6	2492.5	-1.1	-0.04	
2.2000	1.4960	2360.9	2357.8	-3.1	-0.13	
2.3000	1.3960	2220.2	2219.4	-0.8	-0.04	
2.4000	1.2960	2079.0	2077.5	-1.5	-0.07	
2.5000	1.1960	1931.3	1932.2	0.9	0.04	
2.6000	1.0960	1785.0	1783.6	-1.4	-0.08	
2.7000	0.9960	1631.2	1631.8	0.6	0.04	
2.8000	0.8960	1477.0	1477.2	0.2	0.01	
2.9000	0.7960	1319.1	1319.8	0.7	0.05	
3.0000	0.6960	1158.9	1159.9	1.0	0.09	
3.1000	0.5960	997.7	997.7	0.0	0.00	
3.2000	0.4960	829.3	833.5	4.2	0.51	
3.3000	0.3960	666.2	667.6	1.4	0.21	
3.4000	0.2960	500.8	500.3	-0.5	-0.10	
3.5000	0.1960	337.5	331.9	-5.4	-1.60	
3.5990	0.0970	164.2	164.4	0.2	0.14	
3.7070	-0.0110	0.0	-18.7	-18.7	*****	*

RMS DEVIATION IN HC2CAL= 1.9 GAUSS.
RMS DEV(CORRECTED FOR DEGREES OF FREEDOM)= 2.0 GAUSS.

Table XIII. (cont.)

SAMPLE 6, DATA SET 3.

HC2CAL = 0.17273E+04 G (TC-T/K)**1
+ -0.77012E+02 G (TC-T/K)**3
+ 0.11780E+02 G (TC-T/K)**4

TC= 3.714 K.

TEXP	TC-T	HC2EXP	HC2CAL	HC2CAL-HC2EXP	XDEV	
1.0890	2.6250	3714.9	3700.6	-14.3	-0.39	*
1.3000	2.4140	3485.6	3486.4	0.8	0.02	
1.4000	2.3140	3382.2	3380.6	-1.6	-0.05	
1.5000	2.2140	3272.2	3271.6	-0.6	-0.02	
1.6010	2.1130	3156.3	3158.1	1.8	0.06	
1.7000	2.0140	3044.8	3043.5	-1.3	-0.04	
1.8000	1.9140	2924.7	2924.2	-0.5	-0.02	
1.9000	1.8140	2799.6	2801.2	1.6	0.06	
2.0000	1.7140	2673.3	2674.5	1.2	0.05	
2.1000	1.6140	2542.1	2544.0	1.9	0.08	
2.2000	1.5140	2411.4	2409.8	-1.6	-0.07	
2.3000	1.4140	2271.9	2271.8	-0.1	-0.00	
2.4000	1.3140	2131.9	2130.1	-1.8	-0.08	
2.5000	1.2140	1984.5	1984.8	0.3	0.01	
2.6000	1.1140	1837.8	1835.9	-1.9	-0.10	
2.7000	1.0140	1685.7	1683.7	-2.0	-0.12	
2.8000	0.9140	1526.4	1528.2	1.8	0.12	
2.9000	0.8140	1371.5	1369.7	-1.8	-0.13	
3.0000	0.7140	1204.2	1208.3	4.1	0.34	
3.1000	0.6140	1044.2	1044.4	0.2	0.02	
3.2000	0.5140	878.5	878.2	-0.3	-0.03	
3.3600	0.4140	710.4	710.0	-0.4	-0.06	
3.4000	0.3140	541.1	540.1	-1.0	-0.18	
3.5000	0.2140	369.7	368.9	-0.8	-0.21	
3.5990	0.1150	190.8	198.5	7.7	4.05	
3.7110	0.0030	0.0	5.2	5.2	*****	*

RMS DEVIATION IN HC2CAL= 2.2 GAUSS.
RMS DEV(CORRECTED FOR DEGREES OF FREEDOM)= 2.3 GAUSS.

Appendix F.

Experimental Uncertainties

In this section we discuss the sources and magnitudes of the uncertainties in the $H_{c2}(T)$ data. There were two types of uncertainties: random and systematic. The sources of random uncertainties in the data, which were responsible for scatter in the data, were different in the In-Mn samples from the Pb-Mn samples because of the different data-taking techniques used. The sources of random uncertainties are discussed separately for the two alloy systems. The sources of systematic uncertainties were the same in the In-Mn and Pb-Mn data. These are discussed after the random uncertainties.

1. In-Mn

These were the sources and magnitudes of the random uncertainties in the $H_{c2}(T)$ data taken on In-Mn:

a. The sample temperature was measured to a precision of $\pm \frac{1}{2}$ mK. The uncertainty introduced into H_{c2} by assuming the temperature to be correct was roughly

$$\pm \frac{1}{2} \text{ mK} \times \frac{dH_{c2}}{dT} \approx \pm \frac{1}{2} \text{ mK} \times \frac{1}{2} \frac{\text{kgauss}}{\text{K}} \approx \frac{1}{4} \text{ gauss} \qquad (36)$$

b. The line drawn through the linear part of the resistive transition was one of many which would have fit equally well. The uncertainty this introduced into H_{c2} was estimated to be $\pm$ 1 gauss.

c. The uncertainty in the position of the knee in the resistive transition curves was about ± 1 gauss.

d. The estimated uncertainty in converting Hall voltages into magnetic field values was about ± 1.5 gauss.

These estimates indicate that the scatter in the data should be about

$$\left[\left(\frac{1}{4}\right)^2 + 1^2 + 1.5^2 \right]^{1/2} \approx 2 \text{ gauss.} \qquad (37)$$

This compares well with the scatter actually observed in the data (see Appendix E).

2. Pb-Mn

These were the sources and magnitudes of the random uncertainties in the H_{c2} data on Pb-Mn alloys:

a. The sample temperature was measured to a precision of $\pm \frac{1}{2}$ mK. The uncertainty introduced into H_{c2} was roughly

$$\pm \frac{1}{2} \text{ mK} \times \frac{dH_{c2}}{dT} \approx 1 \text{ gauss.} \qquad (38)$$

b. The point on the resistive transition where the sample resistance became non-zero was only defined to ± 7 gauss. This applied to data set 1 only.

c. The uncertainty in the line through the linear part of the resistive transition introduced an uncertainty into H_{c2} of about ± 3 gauss. This applied to data sets 2 and 3 only.

d. The uncertainty in placing the continuous plot of the resistive transition over the discrete data points was about ± 2 gauss.

e. The uncertainty in reading exactly where the line through the linear part of the resistive transition curve intersected the R=0 and $R=R_{max}$ lines was about ± 1 gauss.

f. The uncertainty in converting the measured Hall voltages into magnetic field values was estimated to be ± 2 gauss.

These estimates indicate that the scatter in the data should be about

$$[1^2 + 7^2 + 2^2 + 2^2]^{1/2} \approx 8 \text{ gauss} \quad \text{(data set 1)} \tag{39}$$

$$[1^2 + 3^2 + 2^2 + 1^2 + 2^2]^{1/2} \approx 4 \text{ gauss (data sets 2 and 3)} \tag{40}$$

These estimates are larger than the scatter observed in the data (see Appendix E).

The sources of systematic uncertainties in the data were the same in both the In-Mn and Pb-Mn runs. They were:

a. The magnetic field was homogeneous over the sample to ± 0.1 %.

b. If the temperature given by the Ge resistor, T_{Ge}, were proportional to, but not equal to, the thermodynamic temperature, T_{th}, then the uncertainty in H_{c2} would be proportional to the uncertainty in the temperature, according to the formula

$$\Delta H_{c2} = \frac{dH_{c2}}{dT} \times \Delta T \approx \frac{dH_{c2}}{dT} \times (1-b)T, \tag{41}$$

where

$$T_{Ge} = bT_{th} . \tag{42}$$

We estimate that $b \approx 1 \pm 0.001$; dH_{c2}/dT was about 0.5 gauss/mK for In-Mn, and 2 gauss/mK for Pb-Mn. Note that this source of error in H_{c2} would not affect the temperature dependence of H_{c2} very much. Furthermore, it would affect all of the critical field data in the same way. Therefore, it would not provide evidence against additive pair-breaking.

c. Smooth oscillations of T_{Ge} about T_{th} would cause smooth oscillations of the measured H_{c2} data relative to the correct values of H_{c2}. An amplitude and period for these oscillations of 1 mK and 1 K would introduce oscillations of about $\pm \frac{1}{2}$ gauss into the In-Mn data, and about $\pm$ 2 gauss into the Pb-Mn data. The oscillations of dH_{c2}/dT for the Pb-Mn samples would be about $\pm$ 1 % over a temperature range of 0.5 K. These oscillations would depend only on T, and not on which sample was in the cryostat. Hence, they would not provide evidence against additive pair-breaking. Note that the estimated size of these oscillations would not be large enough to explain the positive curvature region in the Pb-Mn data.

Appendix G.

Alloy Fabrication Techniques

This appendix was for the most part taken directly from John Przybysz's thesis.[77] Some modifications have been made concerning the chemical analysis and concerning which alloys were used in the experiment.

Several different metallurgical techniques were used to produce the ingot mixtures of Pb-Mn and In-Mn. The techniques that were used to produce the early samples were later abandoned in favor of other methods which resulted in more predictable impurity concentrations. For each alloy system, a master mixture was prepared and chemically analyzed. Dilute alloys were made by combining pieces of the master alloy with more of the host superconducting metal.

The lead-manganese master alloy mixture was made in a radio-frequency furnace using a tantalum crucible. The phase diagram of Pb-Mn[78] indicated that all the Mn should dissolve above 800° C. Upon cooling, the lead and manganese phases should separate. Turbulence in the liquid, caused by the rf fields, should mix the phases.

A piece of tantalum foil was cut to fit as a lid for the crucible. The crucible and lid were outgassed at 825° C for ten mintues at 5×10^{-4} Torr. Pieces of 99.99 % pure lead and 99.99 % pure manganese were put in the crucible to make a 39.1 g, 2.00 at. % Mn alloy. The crucible was placed in a bell jar, and the jar was evacuated to 5×10^{-6} Torr. The rf furnace heated the crucible above 900° C for five minutes. Metal

vapors streaming out under the lid caused considerable arcing from the furnace coils to the crucible and made it impossible to sustain larger heating power. The melt was cooled by blowing a stream of helium gas past the crucible. The amount of material lost through evaporation and spillage was 7.3 g.

An ingot weighing 26.9 g was finally cut free of the tantalum crucible. After it was etched in nitric acid, it weighed 26.8 g. dc arc emission spectroscopy (ES) showed that the top of the ingot contained 60 times more Mn than the bottom.

To make the ingot homogeneous, it was rolled and folded about 40 times between sheets of tantalum. ES analysis of five pieces showed that the ingot was homogeneous and free of tantalum and other impurities. Flame emission spectroscopy (FE) showed that the mixture contained 2.04 at. % Mn.

Dilute alloys were made by encapsulating appropriate quantities of 99.999 % pure lead and the master alloy in quartz tubes, and melting the mixture in a resistance-heated furnace. Six alloys were made in this way from constituent parts intended to yield 0.048, 0.096, 0.144, 0.183, 0.240, and 0.288 at. % Mn, for dilute alloys #1 through #6, respectively.

Each alloy was sealed in a capsule made from quartz tubing with an inside diameter of 12 mm. The tubing was first heated and outgassed by a mechanical pump. Then the pieces of Pb and master alloy were inserted in the tube. The tube was constricted, pumped to $2\text{-}3\times10^{-5}$ Torr, and sealed with a torch.

The capsule was heated to a temperature high enough to dissolve all the manganese--usually 900° C. Then it was put in a furnace just above the melting point of lead. It was taken out with tongs, shaken vigorously, and then quenched in a bucket of water. The sample seemed to solidify in less than five seconds.

After ES analysis showed that alloys #1 and #2 were inhomogeneous, they were encapsulated again, melted, shaken, and quenched. The top of the quartz capsule containing alloy #1 broke off during the last shaking.

The alloys were mechanically mixed to make them homogeneous by pressing and folding them between steel blocks. Each alloy received between 15 and 20 folds. ES analysis showed that they did not pick up any iron impurities from the blocks, and no other transition metal impurities were detected.

The alloys were dissolved in nitric acid for the flame emission analysis. Alloys #2 and #4 were analyzed twice. Detected concentrations of Mn for alloys #1 to #6 were 0.012, 0.056 and 0.058, 0.102, 0.124 and 0.132, 0.16, and 0.20 at. %, respectively. The Mn concentrations in the alloys were consistently below the intended value by about 0.05 at. %. Either Mn was lost in the process or it reacted to form an oxide which is insoluble in nitric acid.

Pb-Mn alloys #2, #4, #5, and #6 were used to make samples D, E, F, and G respectively. Samples C and H were made from 99.999 % pure lead.

The indium-manganese master alloy was made by melting 99.999 % pure In and 99.99 % pure Mn in a Vycor capsule. The constituents should have yielded a 60.3 g ingot of 0.107 at. %. After melting, shaking,

and quenching in water, the ingot was mechanically mixed by pressing and folding about 20 times. The sample was sandwiched between sheets of ten mil Mylar to keep the indium from sticking to the steel blocks. FE analysis showed that the resulting master alloy contained 0.116 at. % Mn.

Four dilute alloys were made by mechanically mixing 99.999 % pure indium with a piece of the master alloy. The expected concentrations of Mn in the In-Mn alloys #1 to #4 were 0.0214, 0.0325, 0.0396, and 0.0466 at. %. The measured concentrations were 0.020, 0.030, 0.039, and 0.047 at. %. The measurements were done spectrophotometrically, and the estimated accuracy was $\pm$ 5 %. ES analysis showed that the samples were homogeneous.

Samples 5 and 7 were made from 99.999 % pure indium. Samples 13 and 19 were made from In-Mn alloys #2 and #3.

Appendix H.

Calibration of Cryocal Germanium Resistors #3133, #3659, #2246, #2243

Introduction

Three Cryocal germanium resistors, serial no. 2243, 2246, and 3659, were calibrated against a fourth Cryocal germanium resistor serial no. 3133. Resistor #3133 came from Cryocal with calibration data from 1.5 K to 20 K. In 1973, H. R. Kerchner, another graduate student in this group, made a table of resistance vs. temperature for #3133 from Cryocal's data. We checked Kerchner's table against the He^4 vapor-pressure temperature, T_{58}, to see that resistor #3133 was still calibrated. Resistance-vs.-temperature data for all four resistors were taken first in a glass dewar cryostat and then in a metal cryostat. This was done because the glass dewar cryostat could only obtain temperatures less than 4.2 K. The metal cryostat was used to obtain temperatures from 1.2 K to 8.3 K. The resistance-vs.-temperature data obtained for resistors #2243, #2246, and #3659 were fitted with functions of the form:

$$\ln(T) = \sum_{i=0}^{N} C_i \ln(R)^{-i}$$

by using Brian Gibson's computer program GIBORTH. Tables of R vs. T were generated for these resistors by using 9th order fits to the data taken in the metal cryostat. The cryocal data on #3133, with an additional point at 1.23 K taken by calibrating #3133 with T_{58}, were fitted with a 12th order polynomial, and a table of R vs. T was generated.

The precision of the calibration was ~ .01 %. The accuracy was limited by the accuracy of the calibration of #3133, and was ~ .1 %.

Glass Dewar Cryostat Calibration

The glass dewar cryostat consisted of a metal insert designed by R. A. Anderson, a former member of this group, in a vacuum-insulated glass dewar which sat inside a larger dewar. The outer dewar was for liquid nitrogen (LN), and the inner dewar was for liquid helium (LHe). The bottom of a brass cryostat head was attached to, and made a vacuum seal with, the inner dewar. The side of the cryostat head had a port, through which to pump on the LHe bath. As usual, the insulating vacuum jacket around the LHe dewar was not sealed off; there was a nozzle on it through which it could be pumped out. The insert which contained the resistors to be calibrated made a vacuum seal with the top of the cryostat head. The insert had a port, through which a transfer tube or pressure probe could be placed into the LHe dewar.

The resistors were soldered to copper wires which were thermally grounded to the bottom of a thick copper disk on the lower end of the insert. Around the resistors were two cylindrical brass cans, one inside the other, which both made vacuum seals with the bottom of the copper disk. The inner can contained the resistors, and was filled with 1 atmosphere of He gas at 300 K for heat exchange. The space between the brass cans was evacuated. The outer can and copper disk were submerged in the LHe bath. A heater and a carbon resistor had been glued to the copper disk to use with an electronic temperature regulator.

Resistance measurements were four-terminal d.c. measurements, made with the circuit sketched in Figure 38. The voltage across the 10 kΩ standard resistor indicated the current through the germanium resistor. This voltage and the voltage across the germanium resistor were read with a six-digit Dana Digital Multimeter (DMM),[79] which had a sensitivity of 1 μV. The dotted lines in Figure 38 show where the circuit was grounded when the DMM was making one of these measurements.

A problem with the circuit arose at the beginning of the data taking. When the current was reversed or the position of the DMM in the circuit was changed, the reading on the DMM jumped to some number, and then drifted approximately exponentially to the correct reading. It took about 5 minutes to settle down sometimes, and up to twenty minutes other times. The problem was traced to a corroded insulator in the battery clip. This apparently introduced an erratic effective capacitance and resistance in series to ground from the negative end of the battery. This is indicated by the dashed line in Figure 38. When the current was reversed or the position of the DMM in the circuit was changed, this capacitor would charge or discharge as necessary through part of the circuit. Insulating the battery clip from ground solved the problem. The correct reading was obtained in about 5 seconds after switching.

The vapor pressure above the LHe bath was measured with a Hg manometer when the bath temperature was above the lambda temperature (T_λ = 2.18 K), and with an oil manometer when the bath was below T_λ. The manometers consisted of Hg and oil in U-tubes. One side of each tube was connected to a mechanical vacuum pump and pumped down to ~ 1 μ.

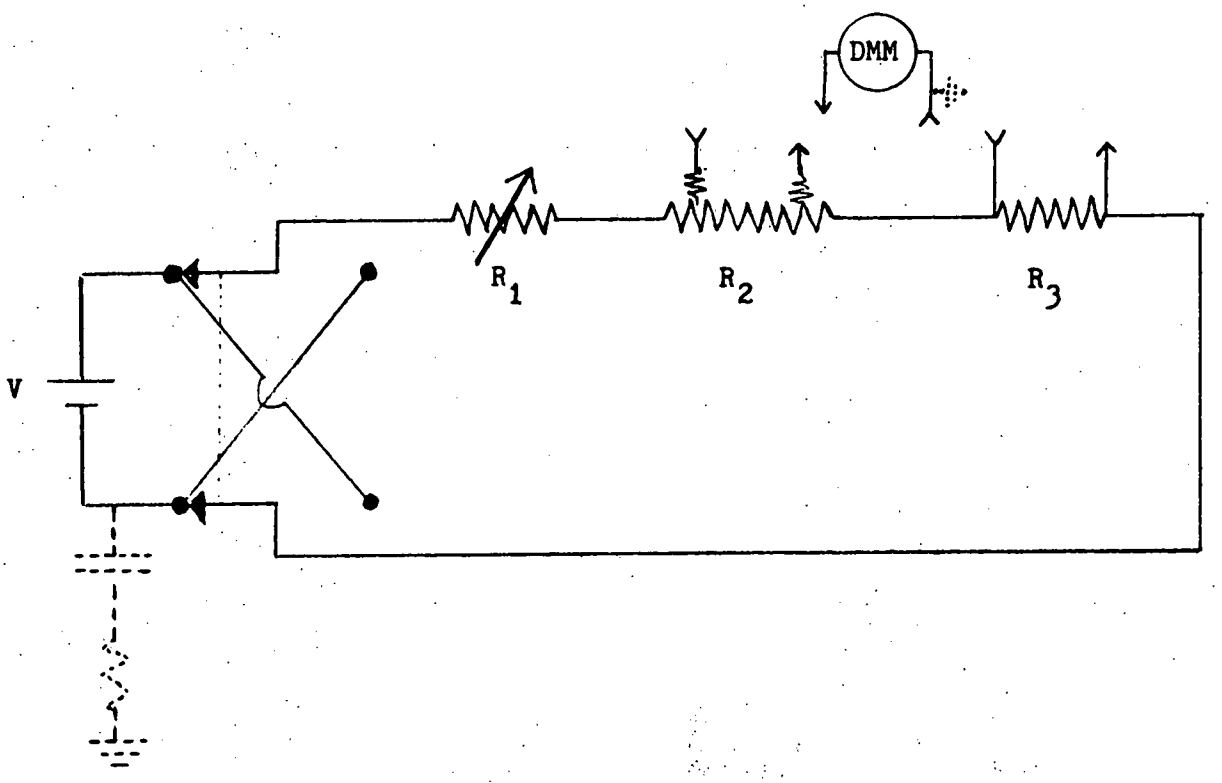

Figure 38. Circuit used to make four-terminal d.c. measurements of the resistance of the Cryocal germanium resistors when they were calibrated.

R_1 = Current regulating resistor; 12 values from 0 to 10 M .
R_2 = Cryocal germanium resistor.
R_3 = 10 kΩ standard resistor.
V = Two 1.35 volt Hg batteries in series.

The other side of the U-tube was connected to the pressure probe in the space above the LHe bath. The pressure probe was a $\frac{1}{4}$" diameter tube, and its tip was from 1 cm to 15 cm above the LHe surface. The height of the Hg or oil in the tubes was measured with a cathetometer to ~ 1/50 mm. This uncertainty caused uncertainties in the vapor pressure temperature of <.2 mK.

This was the procedure used to cool the cryostat from 300 K to 4.2 K. The LHe vacuum jacket was flushed with air to get rid of any He gas, and then pumped out to 5 torr. The residual gas in the jacket helped the LN bath cool the LHe dewar. When the LHe dewar was filled with LHe this residual gas froze, leaving an insulating vacuum in the jacket. The air was pumped out of the LHe dewar and replaced with dry N_2 gas. The LN dewar was then filled slowly with LN (about 0.5 psi pushing the LN into the dewar). Then a small amount of LN was put into the LHe dewar to cool it and the insert. (Care was taken to try to not put in so much LN that some remained when the dewar reached 77 K, for then it took hours for the rest of the LN to evaporate.) After this, even with a puddle of LN remaining, the LHe dewar was evacuated and then filled with He gas. Any residual LN, if its level was below the bottom of the insert, caused no problem because it froze when the LHe dewar was evacuated and remained frozen until the LHe was transferred. The LHe transfer tube was cooled and inserted into the LHe dewar, and the He recovery line was opened. The LHe was transferred slowly (at about 0.2 psi) to minimize boil off. Four to five liters were normally required to initially fill the cryostat. Two liters

were sufficient to refill the cold cryostat. After the transfer, the transfer tube port was plugged, and the cryostat was allowed at least 45 minutes to thermally equilibrate. (Data taken too soon after LHe transfer were always bad.) Then the pressure tube was inserted. Finally the He recovery line was closed off, the manostat was opened to the LHe bath, and data taking was begun. The LN dewar was refilled every 4 hours, and the LHe dewar was refilled every 12 hours.

The temperature was regulated by the manostat. The stability of the temperature was monitored by connecting the carbon resistor in the copper disk to the electronic temperature regulating circuit and watching the output of the a.c. bridge on an oscilloscope. Temperature fluctuations were smaller than 0.1 mK. During a run the temperature was lowered in 0.25 K steps by opening the needle valve between the ballast tank in the manostat and the pump line. When the voltage across resistor #3133 indicated the desired temperature, the valve was closed. It took about 15 mintues to change the temperature and start taking data again.

Data taken at each temperature included the voltages across the germanium and 10 kΩ standard resistors for both current directions, the vapor pressure above the LHe bath, the height of the LHe surface above the joint between the brass cans and the copper disk (for $T>T_\lambda$ only), and room temperature.

The resistance of the germanium resistors was determined as

$$R = \frac{|V^+| + |V^-|}{|I^+| + |I^-|} \tag{43}$$

where ± refers to the current direction. This separate averaging of V and I eliminated d.c. thermal emf's. The temperature of the resistors was determined from the resistance of #3133 by using a table of R vs. T for that resistor, calculated by Kerchner from the data supplied by Cryocal.

The vapor pressure temperature was determined from the T_{58} scale.[80] The T_{58} table in reference 80 gives temperature vs. pressure in mm of Hg at 20° C with g = 980.665 cm/s^2. Hence the pressure data, taken at room temperature here in Urbana where[81] g = 980.139 cm/s^2, were corrected. Above T_λ the additional pressure of the LHe above the copper disk had to be added to the vapor pressure to obtain the temperature of the disk. The pressure of the LHe in mm of Hg was calculated to be:

$$P_{LHe} = h_{LHe} \frac{\rho_{LHe}(T)}{\rho_{Hg}(20°C)} \frac{980.139}{980.665} \quad , \tag{44}$$

where ρ_{LHe} = (density of LHe at T, See reference 82), $\rho_{Hg}(20°C)$ = 13.546 gm/cm^3, and h_{LHe} = (depth of LHe). This pressure was added to the vapor pressure, and the corresponding temperature was found in T_{58}.

Below T_λ the oil manometer was used. The density of the oil was measured relative to the density of Hg, and was found to be $\rho_{oil}(25°C) = \rho_{Hg}(20°C)/14.873 \pm .01$. The thermal expansion coefficient of the oil was .00078 ± .0001°C^{-1}. The pressure P_{RT}, measured in mm of oil at room temperature, was converted to pressure P_{20} expressed in mm Hg at 20° C and g = 980.665 cm/s^2:

$$P_{20} = P_{RT} [1. + 0.00078(25°C - T_{room})] \frac{1}{14.873} \times \frac{980.139}{980.665} \quad . \tag{45}$$

This pressure was used to find T from the T_{58} table. There was no pressure correction of P_{20} for the weight of the LHe below T_λ because of the high thermal conductivity of superfluid LHe.

A graph of $(T_{3133} - T_{58})$ vs. T_{58} is shown in Figure 39. It has the expected[83] form above 2K. The resistor had been calibrated against T_{58} below 2K, so $(T_{3133} - T_{58})$ was expected to be 0. The results showed that resistor #3133 was still calibrated. The other three resistors were then calibrated against resistor #3133. The R-vs.-T_{3133} data for these three resistors were then taken to use later in checking the data taken in the metal cryostat.

Metal Cryostat Calibration

Since we could not obtain temperatures above 4.2 K in the glass cryostat, the resistors were all recalibrated in the same metal cryostat which was used for taking the critical field data. The resistors #2243, #2246, and #3659 were calibrated against resistor #3133 from 1.2 K to 8.3 K. Resistor #3133 was rechecked against T_{58} from 1.2 K to 3.6 K.

The resistor leads were soldered to #36 Formvar-insulated copper wires. These wires had been thermally grounded by varnishing them through cigarette paper to a copper heat sink. The resistor casings were inserted into individual holes in the copper. Also attached to the copper were a heater and a carbon resistor, which were used for electronic temperature regulation. To keep the thermometer leads from touching the surrounding 4 K heat shield, the shield was loosely lined with 5-mil Mylar. A pressure sensing tube was built of a 29 inch long piece of $\frac{1}{4}$" diameter tubing ending with a 1-1/2" piece of 1/16"

diameter tubing. This was inserted into the LHe reservoir through the LHe transfer port. The same electronics were used as for the calibration in the glass dewar cryostat.

Since the manostat would only regulate the temperature below 3.6 K, resistor #3133 was checked against T_{58} from 1.2 K to 3.6 K. The copper walls of the LHe reservoir made temperature corrections due to the additional pressure of the LHe negligible. The results are shown in Figure 39. They confirm the calibration of resistor #3133. Note that T_{3133} was determined from Kerchner's table.

The calibration of resistors #2243, #2246, and #3659 was done from 1.2 K to 8.3 K. Data below 4.2 K were taken by lowering the temperature in 0.25 K steps with the manostat, and then regulating the temperature electronically. The quality of data deteriorated with increasing heater power. That is, when the electronic temperature regulator maintained the carbon resistor at temperature T, and the manostat maintained the LHe bath at $T-\Delta T$, the resistances of the germanium resistors increased with increasing ΔT. This was caused by insufficient thermal grounding of the resistor leads to the copper heat sink.

The resistance of each resistor was calculated from the data as described above. In doing this, the temperature T_{3133} was not taken from Kerchner's table; instead, a 13th order fit to Cryocal's data (with an additional point at 1.23 K taken from the check of #3133 against T_{58}) was made. A table of R-vs.-T, generated from this fit, was used to determine T_{3133} from R_{3133} for the calibration of resistors #2246, #2243, and #3659. The R-vs.-T data for these three resistors were fitted with a 9th order polynomial of the form:

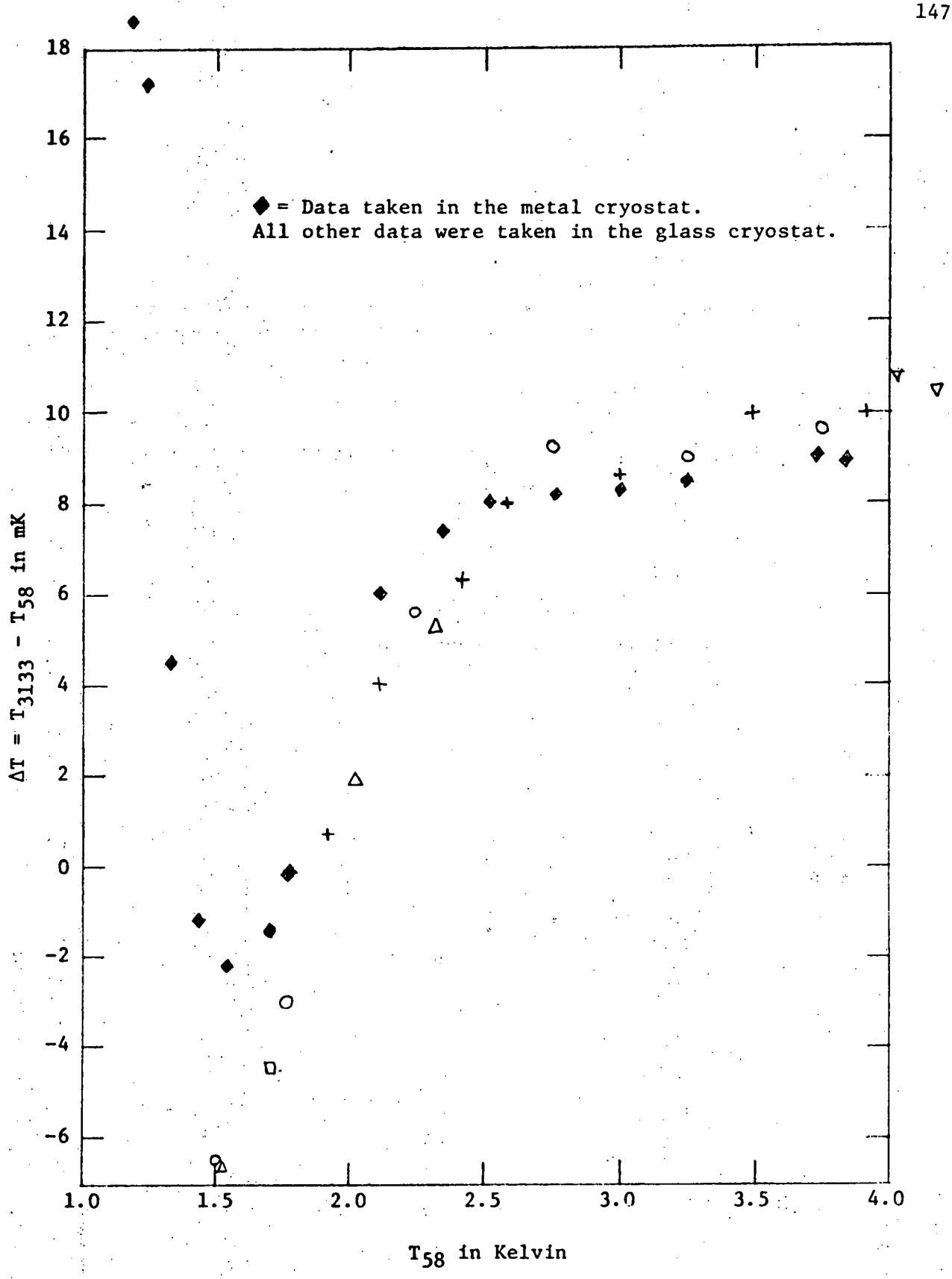

Figure 39. Deviation of the calibration of resistor #3133 from the T_{58} scale. Kerchner's table was used to obtain T_{3133} from R_{3133}.

$$\ln(T) = \sum_{i=0}^{9} C_i \ln(R)^i \quad . \tag{46}$$

Tables of R-vs.-T were generated from 1.2 K to 8.4 K. The data taken in the glass dewar cryostat were checked against these tables and were found to be consistent. The orders of all fits were determined to be the one which minimized $\sigma_{RMS}/[M-(N+1)]^{1/2}$ where σ_{RMS} is the RMS deviation of the data from the fit, M is the number of data points, and N is the order of the fit.[76]

REFERENCES

1. A. W. Bjerkaas, D. M. Ginsberg, and B. J. Mrstik, Phys. Rev. B 5, 854 (1971).

2. B. J. Mrstik and D. M. Ginsberg, Phys. Rev. B 7, 4844 (1973).

3. D. M. Ginsberg and B. J. Mrstik in Low Temperature Physics-LT 13, edited by K. D. Timmerhaus, W. J. Sullivan, and E. F. Hammel (Plenum Publishing Corp., New York, 1974), Vol. III, p. 767.

4. D. M. Ginsberg, Phys. Rev. B 10, 4044 (1974).

5. D. M. Ginsberg, Phys. Rev. B 13, 2895 (1976).

6. J. X. Przybysz and D. M. Ginsberg, Phys. Rev. B 14, 1039 (1976).

7. J. X. Przybysz and D. M. Ginsberg, Phys. Rev. B 15, 2835 (1977).

8. T. R. Lemberger and D. M. Ginsberg, Phys. Rev. B 14, 1785 (1976).

9. D. M. Ginsberg, Phys. Rev. B 15, 1315 (1977).

10. J. W. Thomasson and D. M. Ginsberg, Phys. Rev. B 15, 4270 (1977).

11. A. W. Buckel and R. Hilsch, Z. Phys. 128, 324 (1950).

12. B. T. Matthias, H. Suhl, and E. Corenzwit, Phys. Rev. Lett. 1, 92 (1958).

13. C. Herring, Physica 24, S184 (1958).

14. A. A. Abrikosov and L. P. Gor'kov, Zh. Eksp. Teor. Fiz. 39, 1781 (1960) [Sov. Phys. JETP 12, 1243 (1961)].

15. S. Skalski, O. Betbeder-Matibet, and P. R. Weiss, Phys. Rev. 136, A1500 (1964).

16. V. Ambegaokar and A. Griffin, Phys. Rev. 137, A1151 (1965).

17. A review of the development of the AG theory is given by K. Maki in Superconductivity, edited by R. D. Parks (Dekker, New York, 1969), p. 1035.

18. M. A. Woolf and F. Reif, Phys. Rev. 137, A557 (1965).

19. D. K. Finnemore, D. L. Johnson, J. E. Ostenson, F. H. Spedding, and B. D. Beaudry, Phys. Rev. 137, A550 (1965).

20. R. D. Parks, in Superconductivity, edited by P. R. Wallace (Gordon and Breach, N. Y., 1969), Vol. II, p. 625.

21. G. J. Dick and F. Reif, Phys. Rev. 181, 774 (1969).

22. H. Shiba, Prog. Theor. Phys. 40, 435 (1968).

23. A. N. Chaba and A. D. S. Nagi, Nuovo Cimento Lett. 4, 794 (1972).

24. A. N. Chaba and A. D. S. Nagi, Can. J. Phys. 50, 1736 (1972).

25. E. Müller-Hartmann, in Magnetism, edited by H. Suhl (Academic Press, New York, 1973), Vol. V, p. 353.

26. B. Schuh and E. Müller-Hartmann, Z. Phys. B 29, 39 (1978).

27. S. Takayanagi and T. Sugawara, J. Phys. Soc. Jap. 38, 718 (1975).

28. P. Fulde and K. Maki, Phys. Rev. 141, 275 (1966).

29. K. Maki, J. Low Temp. Phys. 6, 505 (1972).

30. O. Fischer and M. Peter, in Magnetism, edited by H. Suhl (Academic Press, New York, 1973), Vol. V, p. 327.

31. K. H. Bennemann, in Superconductivity, edited by P. R. Wallace (Gordon and Breach, New York, 1969), Vol. I, p. 3.

32. K. Maki, Physics 1, 21 (1964).

33. D. Rainer and G. Bergmann, J. Low Temp. Phys. 14, 501 (1974).

34. M. B. Maple, in Magnetism, edited by H. Suhl (Academic Press, New York, 1973), Vol. V, p. 289.

35. N. Barth, H. E. Hoening, and P. Fulde, Sol. St. Comm. 5, 459 (1967).

36. G. Bergmann, Z. Phys. 267, 287 (1974).

37. R. Koepke and G. Bergmann, Z. Phys. 242, 31 (1971).

38. L. Holland, Vacuum Deposition of Thin Films (John Wiley and Sons, New York, 1958), p. 111.

39. W. Opitz, Z. Phys. 141, 263 (1955).

40. N. Barth, Z. Phys. 148, 646 (1957).

41. S. Tolansky, Multiple-Beam Interferometry of Surfaces and Films (Oxford University Press, London and New York, 1948).

42. Teledeltos conducting paper can be obtained from the Western Union Telegraph Co., Upper Saddle River, New Jersey.

43. B. B. Goodman, IBM J. Res. Dev. 6, 63 (1962).

44. L. P. Gor'kov, Zh. Eksp. Teor. Fiz. 37, 1407 (1959) [Sov. Phys.-JETP 10, 998 (1960).].

45. D. K. Finnemore and D. E. Mapother, Phys. Rev. 140, A507 (1965).

46. J. Feder and D. S. McLachlan, Phys. Rev. 177, 763 (1969).

47. K. R. Lyall and J. F. Cochran, Phys. Rev. 159, 517 (1967).

48. R. A. Anderson and D. M. Ginsberg, Phys. Rev. B 5, 4421 (1972).

49. J. Bardeen, L. N. Cooper, and J. R. Schrieffer, Phys. Rev. 108, 1175 (1957).

50. G. Bergmann, Z. Phys. 228, 25 (1969).

51. American Institute of Physics Handbook, 3rd ed., edited by D. E. Gray (McGraw-Hill, New York, 1963).

52. D. Rainer and G. Bergmann, private communication.

53. K. Knorr and N. Barth, J. Low Temp. Phys. 4, 469 (1971).

54. D. Rainer, G. Bergmann, and U. Eckhardt, Phys. Rev. B 8, 5324 (1973).

55. The substrates were obtained from the Valpey Corp., Holliston, Mass.

56. Apiezon N grease is manufactured by Associated Electrical Industries Ltd. for Apiezon Products Ltd., England.

57. Kimwipes are manufactured by the Kimberly-Clark Corp., Neenah, Wisc.

58. The silver paint is manufactured by Micro-Circuits Co., New Buffalo, Michigan.

59. Consolidated Vacuum Corporation, Rochester, New York.

60. The oil used was DC 704 supplied by Dow Corning Corp., Midland, Michigan.

61. Variac W20M Autotransformer manufactured by General Radio Co., Concord, Mass.

62. Leeds and Northrup, Philadelphia, Pennsylvania.

63. Cryocal, Inc., Riviera Beach, Florida.

64. L. J. Neuringer and Y. Shapira, Rev. Sci. Instrum. 40, 1314 (1969).

65. Varian Associates, Palo Alto, California.

66. Model HA-11 Hall generator, manufactured by American Aerospace Controls, Inc., Farmingdale, New York.

67. Princeton Applied Research Corp., Princeton, New Jersey.

68. Rawson-Lush Instrument Co., Inc., Acton, Massachusetts.

69. Welch Scientific Co., Chicago, Illinois.

70. Scientific Instruments and Equipment Division, Bendix Corp., Rochester, New York.

71 GE 7031 varnish is manufactured by the Insulating Materials Department of General Electric Corporation, Schenectady, N. Y.

72. Model 148 Nanovoltmeter manufactured by Keithley Instruments, Inc., Cleveland, Ohio.

73. Model 2DR-2 X-Y Chart Recorder manufactured by F. L. Moseley Co., Pasadena, Cal., a subsidiary of Hewlett-Packard Co., Palo Alto, California.

74. J. A. Cape, Phys. Rev. 166, 432 (1968).

75. R. E. Miller and G. D. Cody, Phys. Rev. 173, 494 (1968).

76. P. R. Bevington, Data Reduction and Error Analysis for the Physical Sciences (McGraw-Hill, New York, 1969), p. 187.

77. J. X. Przybysz, Ph.D. Thesis, University of Illinois, 1976 (unpublished).

78. M. Hansen, Constitution of Binary Alloys (McGraw-Hill, N. Y., 1958), p. 943.

79. Model 5370, Dana Laboratories, Inc., Irvine, California.

80. A table of T_{58} can be found in Experimental Cryophysics, edited by F. E. Hoare, L. C. Jackson, and N. Kurti (Butterworth, London, 1961).

81. W. W. Merrymon, Masters Thesis, University of Illinois, 1917 (unpublished).

82. K. R. Akins, Liquid Helium (Cambridge University Press, 1959), p. 37.

83. B. J. Mrstik, Ph.D. Thesis, University of Illinois, 1973 (unpublished).

VITA

Thomas Richard Lemberger was [redacted] He attended schools in Madison until he graduated from James Madison Memorial High School in 1969. He attended the University of Illinois at Chicago Circle for two years before entering the University of Illinois at Urbana-Champaign. He received the degree of Bachelor of Science in Physics with High Honors in 1973, and the degree of Master of Science in Physics in 1975, both from the University of Illinois at Urbana-Champaign. During the course of his graduate career, he held teaching and research assistantships.

He is a member of the American Physical Society and the American Association for the Advancement of Science.